CENTER FOR THE SIMULATION OF ACCIDENTAL FIRES & EXPLOSIONS

-VALIDATION TEAM-

FAST COOKOFF TESTS REPORT

Prepared by

William Ciro

Revised by

Eric Eddings & Adel Sarofim

Salt Lake City, October 28, 2003

TABLE OF CONTENTS

NOMENCLATURE

A .....Area of the cylinder in m^2 or Compound A

B .....Compound B

C .....Compound C

C_p .....Heat capacity, J/Kg K

D .....Compound D

E_a .....Energy of activation, J/kg K

K .....Thermal conductivity, W/m K

k .....Rate constant, 1/s.

L_{Air}.....Air gap width, m

m .....Mass fraction of A, B, C or D.

n.....Dummy variable in Eq. (3.10) and (3.11).

Q .....Heat of reaction per unit mass, J/kg

q .....Heat flux, W/m^2

R_H .....Resistance of the heater, Ohms

R_g .....Universal constant for gases, J/mol K

R_E .....Temperature measurement location, m

R_i .....Inner radius of the PBX-9501 pellet, m

R_{PBX} .....Outer radius of the PBX-9501 pellet, m

$R_{Steel,}$.....Outer radius of the steel pipe, m

r .....Radial position, m

r_E .....Thermocouple location, m

S .....Rate of heat generation per unit volume, W/m^3

s .....Dummy variable in Eq. (3.2)

T .....Temperature, K

t .....Time, s.

V .....Voltage, Volts.

Z .....Pre-exponential factor, s^{-1}

Greek symbols

α .....Thermal diffusivity, m^2/s

α_1 .....Thermal expansion coefficients of steel, 1/K

α_2 .....Thermal expansion coefficients of steel, $1/K^2$

β_1 .....Thermal expansion coefficient of PBX-9501, 1/K

ρ ..... Density, Kg/m^3

Subscripts

Air ..... Air

E .....Temperature Measurement location

g .....Gas

I .....Inner radius

i .....Spatial index

j ..... Reaction number

o .....Initial condition

PBX .....PBX material

s .....Solid

Steel .....Steel material

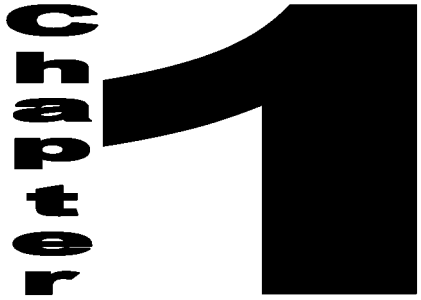

INTRODUCTION

The Center for the Simulation of Accidental Fires and Explosions (C-SAFE) at the University of Utah is focused on providing science-based tools for the numerical simulation of accident scenarios involving fires and high-energy devices (Pershing, 2000).

The initial computational efforts are concentrated in a well-defined scenario in which a steel pipe filled with conventional explosives is exposed to a hydrocarbon fire. An example of this would be a high explosive material within a bomb or missile engulfed in an intense jet-fuel fire after an airplane crash. This is a complex combination of processes for which there is limited detailed information available on the coupled processes for use in validating a computer simulation. The CSAFE validation efforts are focused on those processes in which more physical understanding is needed (Eddings and Sarofim, 1999).

One of the validation tasks is concerned with the thermal behavior of high-energy devices engulfed in a pool fire. This scenario, better known as cookoff, will be studied in conjunction with Thiokol Corporation.

This report will provide detailed information on the efforts and accomplishments of the CSAFE Validation team.

Chapter 2

EXPERIMENTAL

A good description of the cookoff experiments is presented.

CSAFE COOKOFF EXPERIMENTS

The University of Utah contracted Thiokol Propulsion Company to run some experimental work regarding fires and explosions. For this purpose, a series of fast cookoff experiments were carried out considering two experimental conditions. The first one was the typical fuel fire cook off (i.e. variable heat flux). The fuel was propane and it will be referred in this report as the fire test. The second condition consisted of supplying a constant heat flux on the surface of the container. This will be referred as the electrical test.

This chapter is based on the information provided by Thiokol Propulsion Company in reports TR11996 and TR12646.

2.1 FIRE COOKOFF TEST - TR11566 NOVEMBER 1998

This section is based on the information provided by Thiokol Propulsion Company in Report TR11566, C-SAFE Cook-Off Test #1.

2.1.1 TEST DESCRIPTION

The requirements of this test were rather arbitrary at first and the final design was a consensus of opinions of both the University of Utah and Thiokol. We decided that a cylindrical container would be used containing an HMX formulation. The fire box would be rectangular and the flame provided by propane burners. The HMX formulation would be PBXC-123 and the weight would be 8 lbs. It was decided to make the container out of Schedule 40 steel pipe 4 in. in diameter and 12 in. long. Threaded end caps would also be supplied. The explosive material would be cast in the pipe with a 1.5 in. diameter air

core. The weight of the material was 7.6 lbs. The test was conducted at Hazards Testing Team's T-75 facility.

2.1.2 EXPLOSIVE MATERIAL

The explosive formulation used in the C-SAFE cook-off test is designated as C-SAFE-7 and is described in Table 2.1. The safety properties of the cured and uncured explosive are listed in Table 2.2 and show that the formulation is relatively insensitive to impact, friction, ESD (electrostatic discharge), and heat. This 83% HMX castable formulation used a liquid HTPB (hydroxyl terminated polybutadiene) polymer (R-45M) that was crosslinked during an elevated-temperature cure by the IPDI (isophorone diisocyanate), with the TPB (triphenyl bismuth) cure catalyst to speed the cure reactions. The DOA plasticizer and lecithin were used to aid processing.

This formulation is similar to the military formulation PBXC-123, but has a higher level of DOA with respect to R-45M polymer as well as the added lecithin to enhance processing. The original plan was to make the PBXC-123 formulation, but the specified HMX particle sizes were not available at Thiokol to do this. The HMX particle sizes that were used in the final formulation were chosen from available lots, and the particle size distribution was selected by varying the ratio of different HMX lots in a series of small mixes to find the combination that produced the best processing. Even with this work and the additional plasticizer and lecithin, the formulation had a high mix viscosity.

After processing the formulation in ¼ pint and pint mixes and characterizing the safety, cure and processing characteristics of the formulation, the formulation was made in a one-gallon mix for casting into the test article. Because of the high viscosity, the one-gallon mix was not cast under vacuum through a slit plate as is normally done to remove entrapped air. Instead, the explosive was packed by hand into the test article. With vibration, the explosive flowed easily around the thermocouple wires. Because of the time constraint for conducting the cook-off test, an accelerated cure was used with the cure temperature being set to 341 K (155 °F) for one day and 347 K (165 °F) for two days, significantly higher than the normal cure temperature of 330 K (135 °F). After 3 days of cure, the test article was removed from the oven and allowed to cool before the removal of the Teflon core. The explosive was not fully cured after the three-day cure

and was quite soft, although hard enough to retain its shape and not tear during the core removal. The data from the small mixes show that 5 to 7 days were required for a full cure.

Table 2.1. C-SAFE-7 Explosive Formulation and Theoretical Performance

Ingredient	Percent Weight
HMX (Coarse)	55.00
HMX (57 micron)	15.00
HMX (5 micron)	13.00
R-45M	7.52
DOA	8.12
Lecithin	0.70
IPDI	0.62
TPB	0.04
Theoretical Performance	
Density (g/cc)	1.623
Detonation Velocity (km/s)	7.33
CJ Pressure (kbar)	2.14
Total Cylinder Expansion Energy (kJ/cc)	8.30

Table 2.2. Safety Data for C-SAFE-7 Explosive Formulation

Safety Test	Uncured	Cured
ABL Impact (cm)	80	80
TC Impact (in)	>46	>46
ABL Friction (psi)	800 @ 8 ft/sec	800 @ 8 ft/sec
TC Friction (lb)	>64	63
TC ESD (J)	7.19	>8
SBAT (simulated bulk autoignition) onset (°C)	154	157

2.1.3 STEEL CONTAINER

Four-inch Schedule 40 steel pipe was used for the container. The air core of the explosive was 1.5 in., leaving the 1.75-in. explosive web. The length of the container

was chosen to be 12 in. The ends of the pipe were threaded and threaded end caps were machined to fit. The end caps each had a hole drilled in the center to allow for a pressure port/vent and access for the thermocouples. A pressure port was also installed in the center of the cylinder. The design of the cylinder is shown in Figures 2.1 and 2.2.

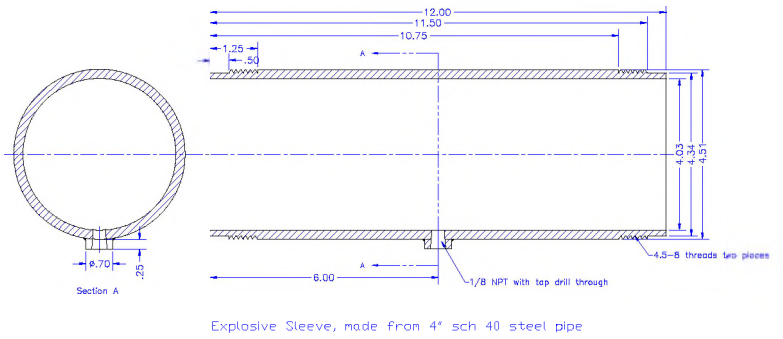

Figure 2.1 Explosive Cylinder

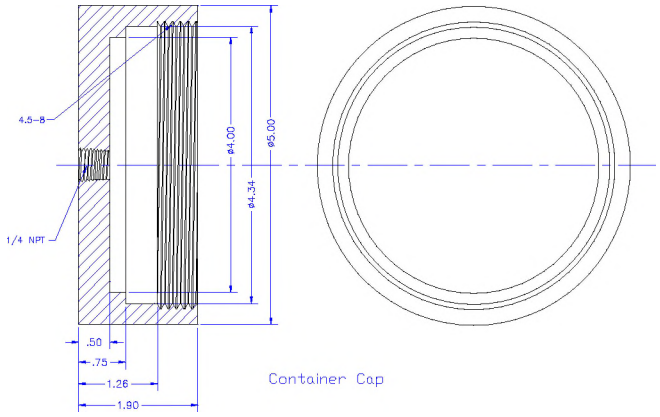

Figure 2.2 Explosive Cylinder End Caps

2.1.4 TEST CONFIGURATION

The test configuration is shown schematically in Figure 2.3. The cylindrical container was suspended from an A-frame with chains with six propane burners positioned beneath. The burners were surrounded by thin aluminum sheet metal about two in. off the ground which acted as a wind break and air intake. The thermocouple wires were all bundled together and wrapped with RTV tape exiting one end of the cylinder. The other end of the cylinder was connected by a tee to ¼-in. stainless tubing on one side, and a vent on the other side of the tee. The tubing was connected to a pressure transducer which measured the pressure in the core of the explosive. The port in the middle of the cylinder was also connected to a pressure transducer by ¼-in. tubing and measured the pressure of the explosive/case interface. The propane gas supply pressure was adjusted to 5 psi. At this pressure, temperature on the outside of the cylinder was 755 to 811 K (900 to 1000 °F).

2.1.5 INSTRUMENTATION

The cook-off test was instrumented with two 1000 psi Taber model 206 pressure transducers and 14 type K thermocouples. The pressure transducers measured the pressure in the air space in the middle of the explosive and at the interface of the explosive steel case. The air space was not sealed as it vented to the outside atmosphere. The thermocouples were placed according to Figure 2.4. Four were spot welded to the outside of the case, four were spot welded to the inside of the case, four were placed at various points in the explosive itself, and two were placed in the air space in the center of the explosive. X-rays were taken of the cylinder loaded with the explosive and instrumentation prior to the test to verify the exact location of the thermocouples. In the process of loading the explosive we were concerned that the thermocouples may have been misplaced from their intended location. Table 2.3 summarizes the measurements. Originally, we planned to have four more thermocouples placed in the propane flame on the outside of the cylinder, but there weren't enough data collection channels to accommodate these extra thermocouples and they were not used. The pressure data and thermocouple data were acquired digitally and the twelve thermocouples were backed up

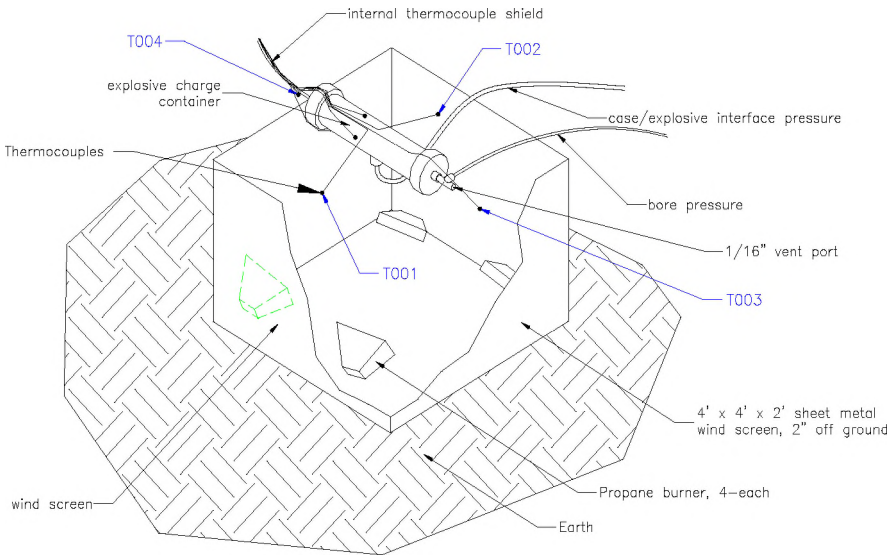

Figure 2.3 Test configuration

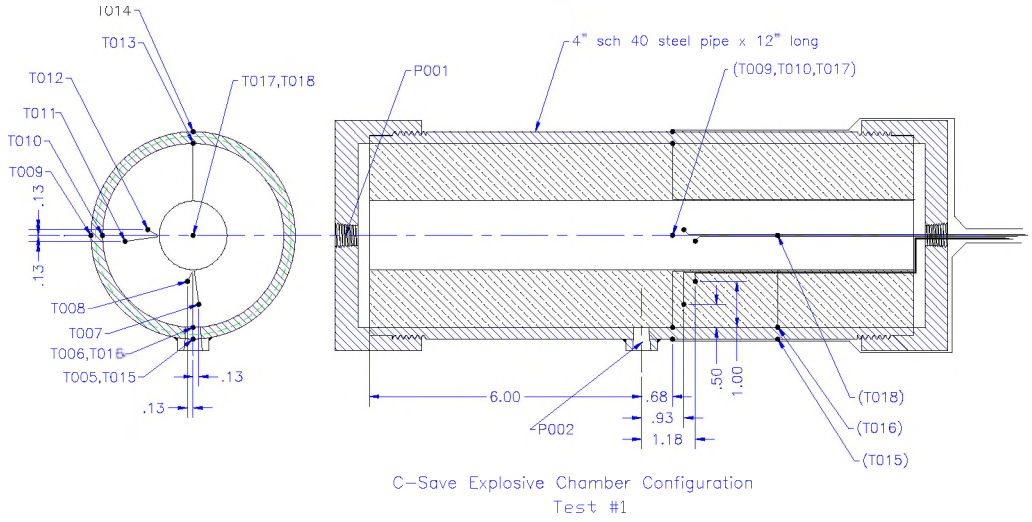

Figure 2.4 Thermocouple Locations in Explosive Cylinder

Table 2.3 C-SAFE Instrumentation List, Test #1

Identifier	Description	Location	Range
T001	Thermocouple	4" from chamber and same elevation as chamber axis in flame	0-2000°F
T002	Thermocouple	4" from chamber and same elevation as chamber axis in flame (opposite side from T001)	0-2000°F
T003	Thermocouple	4" from chamber on pressure tap end	0-2000°F
T004	Thermocouple	4" from chamber on instrumentation feed-through end	0-2000°F
T005	Thermocouple	Outside bottom of chamber as shown on Drawing I10-98022	0-1000°F
T006	Thermocouple	Inside bottom of chamber as shown on Drawing I10-98022	0-1000°F
T007	Thermocouple	In explosive on bottom side of chamber as shown in Drawing I10-98022	0-1000°F
T008	Thermocouple	In explosive on bottom side of chamber as shown in Drawing I10-98022	0-1000°F
T009	Thermocouple	Outside side of chamber as shown on Drawing I10-98022	0-1000°F
T010	Thermocouple	Inside side of chamber as shown on Drawing I10-98022	0-1000°F
T011	Thermocouple	In explosive on side of chamber as shown in Drawing I10-98022	0-1000°F
T012	Thermocouple	In explosive on side of chamber as shown in Drawing I10-98022	0-1000°F
T013	Thermocouple	Outside top of chamber as shown on Drawing I10-98022	0-1000°F
T014	Thermocouple	Inside top of chamber as shown on Drawing I10-98022	0-1000°F
T015	Thermocouple	Outside bottom of chamber as shown on Drawing I10-98022	0-1000°F
T016	Thermocouple	Inside bottom of chamber as shown on Drawing I10-98022	0-1000°F
T017	Thermocouple	Bore, on axis in line with T005	0-1000°F
T018	Thermocouple	Bore, on axis in line with T015	0-1000°F
P001	Pressure Transducer	Pressure in explosive bore	0-1000 psi
P002	Pressure Transducer	Pressure at explosive/case interface	0-1000 psi
Camera 1	IR Image	Side with chamber just filling view	0-1000°F
Camera 2	Test Monitor	End view of chamber covering 20 feet side-to-side	
Camera 3	Test Monitor	Side view of chamber covering 20 feet side-to-side	

with an FM Wideband I tape recorder. The thermocouples were conditioned with Analog Devices amplifiers. In addition to the instrumentation described above, an IR camera was used to monitor the infrared emission of the test. Video recordings of the cook-off were made from two different angles.

2.1.6 DISCUSSION

The cook-off test was set up as described above. The weather conditions at the time of the test were:

Ambient temperature – 59 °F Relative Humidity – 48%

Wind was from the West at 7 mph

The propane valve was opened and the propane was ignited using a nichrome wire heated by electrical current to ignite a small piece of solid rocket propellant. At approximately 106 s into the burn, the explosive ignited and the steel cylinder exploded. The cylinder ruptured uniformly along a line opposite the seam and peeled back around the end caps. The cylinder held by the chains made one revolution around the cross arm of the A-frame. Explosive material was ejected from the cylinder and scattered on the ground around the test site. We estimated that about one third of the material ignited in the cylinder, one third burned on the ground, and the rest was not burned.

Data from the instrumentation were collected at a rate of 50 Hz. One of the thermocouples, T006, located on the inside of the steel cylinder near the center, failed 20 s into the run. The pressure transducers were arranged to monitor the inside bore and the explosive/case interface. Both were ranged to 1000 psi. They both recorded no pressure increase until the explosive ignited and then both overranged in excess of 1000 psi.

The thermocouple measurements showed some interesting results. Those in the explosive material ranged from 294 K (70°F) to 297 K (75°F) just prior to the ignition. This is an average of ten measurements of 200 ms just prior to ignition. These are thermocouples T007, T008, T011, and T012. This shows that inside the explosive material the temperatures were not elevated.

The two thermocouples inside the bore showed a significant difference. Thermocouple T017, at the center of the cylinder, remained at about 300 K (80°F) until near the end and then the last 200 ms averaged 348 K (167°F) and was increasing to a maximum of 398 K (258°F) just prior to the ignition. T018, about one-fourth of the way from the end remained between 300 K (80°F) and 310 K (100°F) until near the end and then the last

200 ms averaged 438 K (330°F) and was increasing to a maximum for 522 K (481°F) just prior to the ignition.

The four thermocouples on the outside of the cylinder were also significantly different. T005, on the bottom, in the center of the cylinder, averaged 653 K (716°F) just prior to the ignition. T009, on the side, in the center of the cylinder, averaged 500 K (442°F) just prior to the ignition. T014, on the top center of the cylinder, averaged 758 K (905°F) just prior to ignition. T015, on the bottom, ¼-in from the end, averaged 667 K (741°F) just prior to ignition, which agreed well with T005, the other bottom thermocouple. It is interesting to note that the highest temperature was at the top of the cylinder and the side temperature was between the top and bottom temperatures.

The three remaining thermocouples were on the inside of the cylinder between the case and the explosive. T010, on the side, in the center of the cylinder averaged 583 K (591°F) just prior to ignition. T013, on the top center, averaged 444 K (340°F) just prior to ignition. T016, on the bottom, ¼-in from the end, averaged 430 K (314°F) just prior to ignition.

Another interesting result to note is that the outside, side, center measurement was 500 K (442°F) while the inside, side, center measurement was 583 K (591°F). This could possibly have been the effect of the wind blowing from the side.

Some of the differences noted in the thermocouple measurements could be caused by the thermocouple not being in the location where it was placed. Movement could have occurred when the explosive was cast in the cylinder. X-rays taken of the cylinder prior to the test were not definitive. It was very difficult to see the small wires behind the ¼-in wall of the cylinder.

The IR camera was positioned about 100 yards away from the test setup and focused on the top of the cylinder. Because of the distance and the uncertainty in emissivity of the cylinder the measurement was not as accurate as one would want. However, there was a fairly good agreement with the thermocouple measurements assuming an emissivity of 0.6.

2.2. FIRE COOKOFF TESTS – TR11996 OCTOBER 1999

Five fast cookoff tests were carried out in 1999, one with an inert material and the other four with explosive material. Six propane burners supplied the heat to ignite the materials.

2.2.1. TEST MATERIALS

The materials were prepared by Los Alamos National Laboratory. The materials were machined into pellets of 4-inches in diameter and 4-inches thick with a 1-inch diameter hole through the center. The pellet dimensions are shown in Figure 2.5. The composition of the inert material and explosive are shown in Table 2.4 and Table 2.5 respectively.

Table 2.4. Composition of Inert Material

Material	Analysis, %	Nominal, %
Barium Nitrate	45.28	44.65
Pentek	48.93	49.35
Estane	2.86	3.00
BDNPA/F	2.93	3.00

Table 2.5. Composition of the Explosive

Material	Percent Weight
HMX	95.00
Estane	2.50
BDNPA/F	2.50

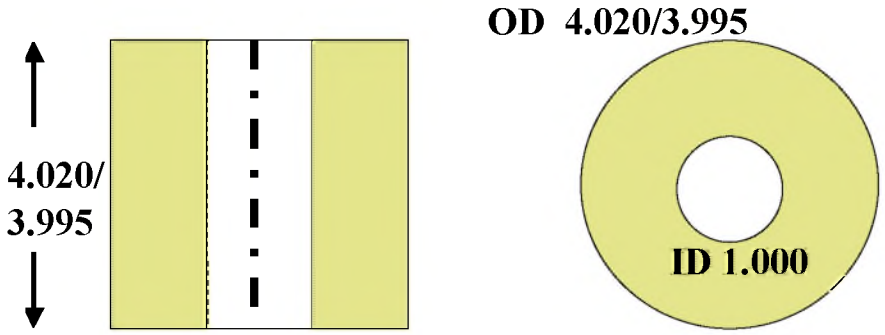

Figure 2.5. Drawing of test material pellets (all dimensions in inches).

Three pellets were used for each test, making the overall material 4 inches in diameter and 12 inches long. For both materials, Estane and BDNPA/F were used as binder to hold the material together. These same binder materials were used to cement the pellets together before they were inserted into the cylindrical container.

2.2.2. STEEL CONTAINER

Four-inch, Schedule 40 steel pipe was used for the container. The length of the container was chosen to be 12 inches. The ends of the pipe were threaded, and threaded end caps were machined to fit. One end cap was solid, and the other end cap had a hole drilled in the center to allow the instrumentation wires to exit the container. A 1/2-inch diameter stainless steel tube, about 4 feet long, was connected to the end cap. The instrumentation wires coming from the inside of the cylinder passed through the tube, and the outside wires were tied to the tube.

2.2.3. TEST CONFIGURATION

Photographs of the test configuration are shown in Figures 2.6 and 2.7. For each test, the cylindrical container was suspended from an A-frame over chains with six propane burners positioned beneath. The burners were surrounded by thin aluminum sheet metal 18 inches high and about 2 inches off the ground that acted as a wind break and air

intake. The propane gas supply pressure was adjusted to 12 psi. We attempted to measure the actual flow rate of the propane but could not find a suitable flow meter.

Figure 2.6. Photograph of the test configuration

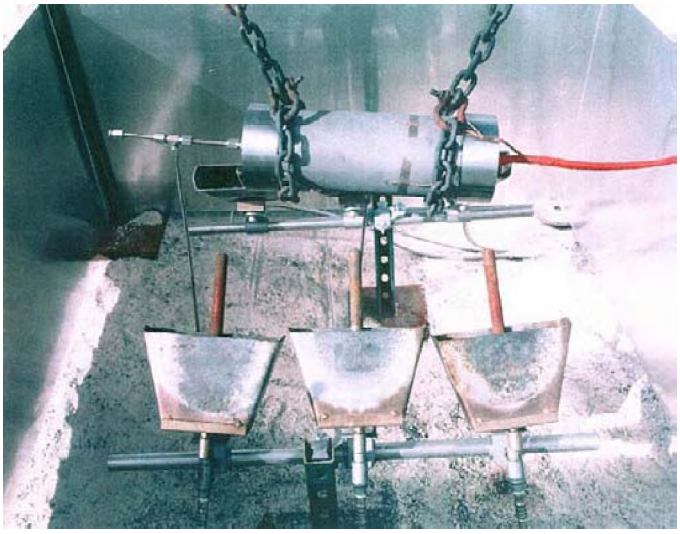

Figure 2.7. Close up photograph of container, burners and wind screen

2.2.4. INSTRUMENTATION

The first test was instrumented with 24 type-K thermocouples, 12 on the inside and 12 on the outside. The thermocouples were placed according to Figure 2.8. The inside thermocouples were 30 AWG and were placed at the interface of the test material and the

inner wall. They were not welded to the metal case. The thermocouples were placed at the interfaces between the three pellets. Grooves were made from the center hole to the outside of the pellet as channels for the thermocouple and wire to lie in. The wires were then run down the center hole, through the opening; and the end cap, and through the stainless steel tube. The outside of the tube was wrapped with RTV tape to try to protect the wires from heat from the propane burners. The outside thermocouples were made of.30 AWG insulated metal sheathed wire. They were placed at the appropriate locations and wired, not welded, to the outside of the container. Measurement parameters are summarized in Table 2.6. The data were acquired digitally for 16 channels and all channels were recorded on an FM tape recorder as back up. Unfortunately, three channels on the FM tape deck quit working during the test, and these channels were not recorded digitally. Therefore, the data for TC12, TC 13, and TC 15 were lost for test 1.

The explosive tests (Tests 2-5) were set up essentially the same as the inert test, with the exception that thermocouple TC11 was replaced with a pressure transducer, PO1. It was an Entran model EPB-C02-5K psi-C/Z4 miniature pressure transducer.

Measurements were taken as given in Table 2.6. Adjustments were made, so that between the 16 channel digitizing system and the FM tape recorder, all the channels were successfully recorded.

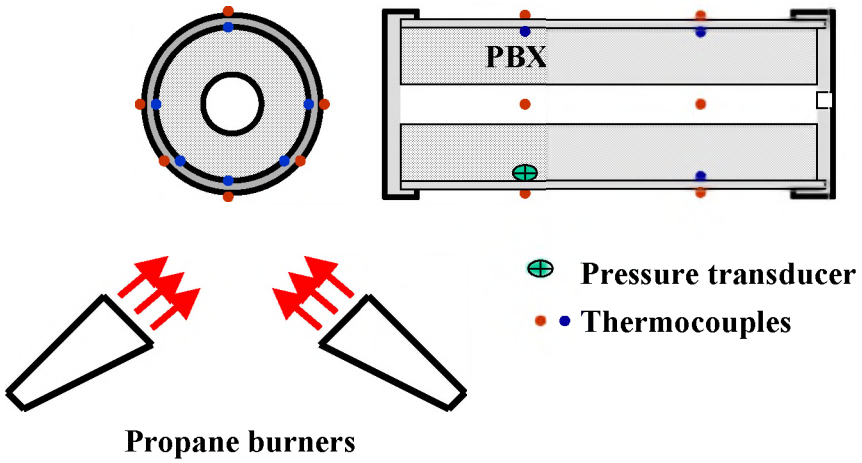

Figure 2.8. Measurement locations in explosive cylinder

Table 2.6. C-SAFE 1999 Instrumentation List

TC #	Description	Location
T01	Thermocouple	Metal-Explosive Interface, Top, First Third
T02	Thermocouple	Metal-Explosive Interface, Top, Second Third
T03	Thermocouple	Metal-Explosive Interface, Left Middle, First Third
T04	Thermocouple	Metal-Explosive Interface, Left Middle, Second Third
T05	Thermocouple	Metal-Explosive Interface, Right Middle, First Third
T06	Thermocouple	Metal-Explosive Interface, Right Middle, Second Third
T07	Thermocouple	Metal-Explosive Interface, Lower Left, First Third
T08	Thermocouple	Metal-Explosive Interface, Lower Left, Second Third
T09	Thermocouple	Metal-Explosive Interface, Lower Right, First Third
T10	Thermocouple	Metal-Explosive Interface, Lower Right, Second Third
T11	Thermocouple	Metal-Explosive Interface, Bottom, First Third
T12	Thermocouple	Metal-Explosive Interface, Bottom, Second Third
T13	Thermocouple	Steel Surface, Top, First Third
T14	Thermocouple	Steel Surface, Top, Second Third
T15	Thermocouple	Steel Surface, Left Middle, First Third
T16	Thermocouple	Steel Surface, Left Middle, Second Third
T17	Thermocouple	Steel Surface, Right Middle, First Third
T18	Thermocouple	Steel Surface, Right Middle, Second Third
T19	Thermocouple	Steel Surface, Lower Left, First Third
T20	Thermocouple	Steel Surface, Lower Left, Second Third
T21	Thermocouple	Steel Surface, Lower Right, First Third
T22	Thermocouple	Steel Surface, Lower Right, Second Third
T23	Thermocouple	Steel Surface, Bottom, First Third
T24	Thermocouple	Steel Surface, Bottom, Second Third
Camera 1	IR Image	Side View, Container Filling view (30 fps)
Camera 2	High Speed	Side View, Covering 10 Ft side to side (2000 fps)
Camera 3	Video	Side View, Covering 20 Ft side to side (30 fps)
Camera 4	Video	Side View, Covering 20 Ft side to side (30 fps
Camera 5	Video	Side View, Close Up, Covering 5 Ft (30 fps)
Camera 6	Video	Side View, Close Up, Covering 20 Ft (30 fps)

For Tests 2 and 3 no attempt was made to seal the container. The end caps were just screwed on, and the instrumentation leads exited the container as described above for the first test. Grooves were cut in the end faces of two of the pellets to accommodate the wires. The pellets were glued together using the Estane-BNDPA/F binder. The explosive material was not bonded to the steel cylinder. Test 3 duplicated Test 2 to determine the repeatability of the tests.

For Test 4, we tried to seal the cylindrical container to force the pressure inside to increase. An O-ring was placed between each end of the cylinder and the end cap. In addition, Dow Corning 90-006 aerospace sealant was used to coat the threads before the end caps were screwed into place. Some of the sealant was also forced down the stainless steel tubing around the instrumentation wires. The explosive pellets were prepared and instrumented as before and were not bonded to the cylinder wall.

For Test 5, we again sealed the cylindrical container, as in Test 4, but put much more aerospace sealant in the stainless steel tubing than before. The sealant was applied from both ends of the tube. Also we bonded the explosive pellets to the inside of the cylinder wall using the binder material.

The data acquisition system worked well for Tests 2-5, and all of the data were collected without any problems. In addition to the thermocouples and pressure transducer, an IR camera was used to monitor the infrared emission of all of the tests. Four standard-speed video cameras recorded the test from different angles. A NAC Memrecam high-speed color video camera was rented for this series of tests. The high-speed camera was run at 2000 fps at 1/4 frame and a shutter speed of 1/6000 second. The camera was able to record and digitally store 4.2 s worth of data. The camera was set to run continuously and to trigger on an end pulse, so that when the test exploded, the trigger was applied, and the 4 previous seconds were saved.

2.2.5. EXPERIMENTAL RESULTS

The weather conditions were not recorded for the first test but were recorded for subsequent tests. The propane valve was opened and the propane was ignited using a burn pit igniter that consists of a nichrome wire imbedded in a small piece of solid rocket propellant. This was done remotely and was repeated for all the tests.

2.2.5.1. TEST 1, INERT MATERIAL, OCTOBER 4, 1999

The weather conditions for this test were not recorded, but it was cold, windy and threatening rain. Wind was gusting to 25-30 mph. The test was nearly called off because of the weather, but it was decided to proceed. The inert material, consisting of 6.3 pounds of barium nitrate/Pentek was heated with the propane burners. The steel cylinder containing the inert material did not explode but the material began to burn and emit smoke. After about 10 minutes, the smoke diminished and the data acquisition was terminated. Data from the thermocouples were collected at a rate of 50 Hz. A digital data acquisition system was used for sixteen channels and an FM tape recorder was used to record all the channels including those recorded digitally. During the test four channels in the FM recorder stopped working but one of them was also recorded digitally. However, data from T12, T13, and T15 were lost.

For the thermocouples on the inside top of the container (T01 and T02), there was a temperature rise to around 402 K (265 °F), taking in excess of 100 seconds. The temperatures remained in this range until about 400 s and then rose to 549 K (530 °F) for TO1 and 444 K (340 °F) for T02.

The four inside-middle thermocouples went up to between 533 K (500 °F) and 588 K (600 °F). T03 took over 400 s to reach 533 K (500 °F), T05 and T06 reached 533 K (500 °F) between 300 and 400 s, and T04 reached 533 K (500 °F) in 260 seconds. T05 experienced a couple of dips in the data that are not explainable.

All of the lower inside thermocouples were quite erratic with many hills and valleys, although they show some similarities. T09 and T10 dropped at about 350 °F sand stayed at about 449 K (350 °F) for the rest of the test. T07 also dropped at that time but then rose again. T08 continued at a high temperature, between 533 K (500 °F) and 588 K (600 °F).

For the inside bottom thermocouples, T11 showed similar characteristics to T09 and T10. T12 data was lost. T14 (outside, top) showed fluctuations from 577 K (580°F) to 766 K (920°F), probably caused by wind gusts. T13 data was lost.

The outside middle thermocouples ranged from 644 K (700°F) to over 977 K (1300°F) with many fluctuations. T16 and T18 were generally higher than T17. T15 data was lost.

For the outside lower thermocouples, T19 and T21 were high initially then dropped. T19 rose to 1310 K (1900°F) then dropped to around 922 K (1200°F) and T21 rose to almost 1033 K (1400°F) then dropped to between 755 K – 810 K (900 °F – 1000 °F). T20 averaged between 810 K (1000°F) and 922 K (1200°F). T22 averaged between 755 K (900 °F) and 866 K (1100 °F).

For the outside bottom thermocouples, T23 was generally lower than T24. T23 ranged between 700 K (800 °F) and 810 K (1000 °F). T24 rose to 1255 K (1800°F) initially and then dropped to between 922 K (1200 °F) and 1144 K (1600 °F) for the majority of the time.

The data for this test shows that the heating of the container was not very uniform or stable, with the variability probably due to the wind.

2.2.5.2. TEST 2, EXPLOSIVE MATERIAL, OCTOBER 7, 1999

Weather conditions for Test 2 were as follows: Temperature: 61 F; Relative Humidity: 33%, and Wind Speed: 5 -12 mph out of the North. The container exploded at 133 s into the burn. The end caps separated completely from the pipe, leaving the threaded part of the pipe still in the end caps. The end cap with the exit hole for the instrumentation wires lost the end of the cap leaving just a ring. The pipe part of the container was not found. Pictures of the container after the test are shown in Figure 2.9 and 2.10. Following the test, 1361 g (3.0 pounds) of explosive material were gathered up from the site. This was 32% of the total material. The material that was found may not be all the material ejected from the container due to the explosion.

For this test T11 was not used. It was replaced with a pressure transducer PO1, at the inside bottom, first third position. All of the data channels were recorded properly. The pressure inside the container at the explosive/wall interface remained low for about 70 s and then rose to over 250 psi. Then the pressure fluctuated up and down, generally decreasing until just prior to the explosion when it rose again to nearly 250 psi.

Temperatures at the inside top (TO1 and T02) rose slowly and uniformly to between 316 K (110°F) and 322 K (120°F) before the explosion. Temperatures at the inside middle (T03, T04, T05, and T06) also rose slowly and fairly uniformly to between 366 K (200

°F) and 394 K (250 °F). Temperatures at the inside lower positions (TC07, TC08, TC09, and TC10) rose slowly but not as uniformly as the top and middle. They all reached a temperature of about 405 K (270°F) before the explosion. The one temperature at the inside bottom (TC12) was similar to the inside lower position temperatures.

Figure 2.9. Test 2 hardware after explosion

Figure 2.10. Test 2 hardware after explosion

Temperatures on the outside were much more variable than those on the inside. The top temperatures (TC 13 and TC 14) were the lowest, reaching 477 K (400°F) to 505 K (450°F) before the explosion. Temperatures at the outside middle reached 810 K

(1000°F) to 866 K (1100°F). TC15 and TC 16 on the right side were more consistent and than TC 17 and TC 18. The latter two had much wider fluctuations, perhaps because of the wind. The outside lower temperatures varied widely and did not agree well with each other. TC 19 barely reached 755 K (900° F), TC20 and TC22 reached 922 K (1200°F) to 1033 K (1400° F), while TC 21 reached 1255 K (1800° F). The outside bottom temperatures were below those at the middle and lower positions. They reached around 810 K (1000°F) before the explosion.

From the data, the highest temperatures inside the container were at the lower positions, reaching about 405 K (270°F) at the time of the explosion. It was also evident from the video recordings that when the pressure began to rise, gases were expelled from the container along the threads in the end caps. These gases ignited and burned and may be the cause of the pressure rising and then falling inside the container.

2.2.5.3. TEST 3, EXPLOSIVE MATERIAL, OCTOBER 7, 1999

Test 3 was conducted with essentially the same configuration as Test 2. This was done to determine the variability of the data. The weather conditions at the time of the test were s follows: Temperature: 294 K (70°F); Relative Humidity: 26%; Wind Speed: 0 to 5 mph with he direction variable. The container exploded at 106 s into the burn. The end caps separated completely from the pipe, leaving the threaded part of the pipe still in the end caps. Both end caps were bulged but did not separate. The pipe part of the container split open and then folded back on itself. Pictures of the container after the test are shown in Figures 2.11and 2.12. Following the test, 2845 g (6.3 pounds) of explosive material were gathered up from the site. This was 66 % of the total material. The scattered material may not have been completely recovered.

A pressure transducer, P01, was again used in place of T11. All of the data channels were recorded properly. The pressure inside the container at the steel/explosive interface remained low for about 40 s then rose to about 500 psi. The pressure then decreased to about 60 psi at the explosion.

Figure 2.11. Test 3 hardware after explosion

Figure 2.12. Test 3 hardware after explosion

Temperatures at the inside top (TO1 and T02) rose slowly and uniformly to 349 K (170°F) for T01 and 333 K (140°F) for T02 before the explosion. Temperatures at the middle rose slowly and fairly uniformly but their maximums were not consistent. T03 and T05 rose to 283 K (50 °F) to 405 K (270 °F) while T04 and T05 rose to 349 K (170°F) to 366 K (200°F). The higher temperatures were on opposite sides of the same end of the container. Temperatures at the inside lower positions also rose slowly and uniformly but were quite different in the maximums. T07 and T09 reached about 477 K (400°F) while T08 reached just over 422 K (300 °F) and T10 reached 383 K (230 °F). The higher temperatures were on opposite sides at the same end of the container in agreement with the middle temperatures. The temperature at the inside bottom (T12) agreed pretty well with T10, reaching a maximum of 383 K (230 °F) before the explosion.

The outside temperatures for this test were much more variable than those on the inside. The outside top thermocouples (T13 and T14) varied considerably and reached a maximum of between 588 K (600°F) and 644 K (700°F). The outside middle temperatures varied widely and did not agree well at all. Maximums varied from 810 K (1000°F) for T18 to 1310 K (1900°F) for T15. The outside lower temperatures also varied considerably. Maximums ranged from 922 K (1200°F) for T20 to almost 1422 K (2100°F) for T22. T19 and T21 had maximums around 1144 K (1600°F). The outside bottom temperatures were below those at the middle and lower positions at about 755 K (900°F). The data for T23 was very erratic.

The highest temperatures inside the container were at the lower positions, reaching 422 K (300°F) and 477 K (400 °F) respectively, at the time of the explosion. The videos showed that gases also escaped from the container and burned.

2.2.5.4. TEST 4, EXPLOSIVE MATERIAL, OCTOBER 25, 1999

Because we had gases escaping from the container, we decided to try to seal the end caps to the pipe. An O-ring was placed between the ends of the pipe and the end caps. The threads were coated with Dow Corning 90-006 aerospace sealant. Some of the sealant was also forced down the stainless steel tubing that housed the instrumentation wires. Other than these changes, the other test parameters were the same as before.

Weather conditions for Test 4 were as follows: Temperature: 62 F, Relative humidity 19%, Wind Speed: 6 to 8 mph out of the East. The container exploded at 141 s into the burn. The end caps separated completely from the pipe, leaving the threaded part of the pipe still in the end caps. Both end caps lost their ends but only one was recovered. The pipe came apart into at least 3 pieces. Pictures of the container after the test are shown in Figure 2.13 and 2.14. Following the test, 2655 g (5.9 pounds) of explosive material were gathered up from the site. This was 62 % of the total material.

The pressure trace for this test was definitely different from previous tests. The pressure started to rise uniformly almost front the beginning and reached a maximum of 400 psi at about 68 seconds. Then, it decreased with some variability, going negative at about 97 s and remained negative until the explosion. The cause of the negative reading is not known.

Figure 2.13. Test 4 hardware after explosion

Figure 2.14. Test 4 hardware after explosion

Temperatures at the inside top rose slowly and uniformly to a maximum of 383 K (230˚F) for TO1 and 372 K (210˚F) for T02. Temperatures at the inside middle were well behaved and rose to a maximum of 388 K (240˚F) to 400 K (260˚F) for T03, T05, and T06. T04 was lower at a maximum temperature of 366 K (200˚F). Temperatures at the inside lower positions were well behaved but differed in their maximums. T07 reached about 416 K (290˚F), T08 and T09 both reached about 366 K (200˚F), and T10 reached about 360 K (190˚F.) The inside bottom temperature, T12, reached about 372 K (210˚F).

The outside temperatures varied considerable and did not agree well with each other. At the top, T13 fluctuated widely and reached a maximum of just rover 810 K (1000˚F). T14 behaved better but only reached a maximum of around 477 K (400˚F). The outside middle temperatures were very different. T15 reach a maximum of 1422 K (2100˚F), T16 went to just over 810 K (1000˚F), T17 reached 1033 K (1400˚F), and T18 reached about 1200 K (1700˚F). The Outside lower temperature did not correlate well either. There were great fluctuations in the data and the maximum ranged from 672 K (750˚F) to over 977 K (1300˚F). The outside bottom temperatures reached a maximum of nearly 1255 K (1800˚F) for T23 and only 616 K (650˚F) for T24.

The highest temperature inside was at the lower position at 416 K (290°F). The video showed that we were successful in stopping the gases from escaping from around the threads but not through the steel tubing.

2.2.5.5. TEST 5, EXPLOSIVE MATERIAL, OCTOBER 28, 1999

Test 5 was similar to test 4 except that more aerospace sealant was used to try to seal the stainless steel tubing housing the instrumentation wires. The sealant was forced into both ends of the tubing. In addition, the explosive pellets were bonded to the cylinder wall using the Estane/BNDPA/F binder. The weather conditions were as follows: Temperature: 285 K (54°F), Relative Humidity: 62 %, Wind Speed: 10 mph out of the Northwest. The container exploded at 98 s into the burn. The end cap without the hole in it, separated completely from the pipe, and the other end cap was minimally attached. Both end caps were bulged but did not lose their ends. The threaded part of the pipe remained in the end caps. The pipe split open along a line opposite the weld seam and flattened out. Pictures of the container after the test are shown in Figure 2.15 and 2.16. Following the test, 1773 g (3.9 pounds) of explosive material were gathered up from the site. This was 41 % of the total material.

Figure 2.15. Test 5 hardware after the explosion

Figure 2.16. Test 5 hardware after the explosion

The pressure reading inside: the container remained low for about 30 s, then rose to a maximum of nearly 1400 psi at 60 seconds. After reaching the maximum, the pressure dropped off but stayed between 700 psi to 1100 psi until the explosion.

The temperatures at the inside top (T01 and T02) rose slowly and uniformly to almost 366 K (200˚F) for T01 and about 350 K (170˚F) for T02. Temperatures at the inside middle were quite different from each other. T03 and T05 rose more slowly than the other two and reached a maximum of 388 K (240˚F) to 405 K (270˚F). T04 and T06 started out slowly, and then at about 60 s, increased rapidly. T04 reached a maximum of about 460 K (370˚F) and T06 reached a maximum of about 394 K (250˚F). The inside lower position temperatures were also quite different from each other. T07 and T08 were similar in their maximum temperatures, 366 K (200˚F) and 372 K (210˚F), respectively, but their profiles were very different. T07 rose slowly and uniformly while T08 rose slowly at first and then increased rapidly at about 80 seconds. T09 rose slowly until about 50 s and then increased rapidly to a maximum of almost 444 K (340˚F). T10 rose slowly and uniformly to a maximum of about 394 K (250˚F). The inside bottom temperature rose slowly at first and then at about 60 s increased rapidly to a maximum of 427 K (310˚F).

The outside temperatures were not consistent with each other. T13 fluctuated considerably but generally increased with time to a maximum of about 572 K (570°F). T14 reach a maximum of 866 K (1100°F) in just over 20 s and then dropped to an average level of 672 K (750°F) until the explosion. The outside middle temperatures were quite similar. They all rose quickly during the first 30 s and then fluctuated at levels around 922 K (1200°F) to 977 K (1300°F). The outside lower position temperatures were similar to the middle temperatures. They rose quickly and then leveled off. T19 and T20 reached highs of 977 K (1300°F) and 1088 K (1500°F) respectively. T21 and T22 only went to 810 K (1000°F) and 866 K (1100°F) respectively. The outside bottom temperatures also rose quickly at the beginning but then T23 dropped from a high of 950 K (1250°F) to an average around 810 K (1000°F). T24 quickly rose to 755 K (900°F) and then continued upward to nearly 922 K (1200°F) at the end.

The highest temperature inside the container was at the middle position and was 275 K (370°F). However, one of the lower position temperatures reached 444 K (340°F). The videos did not reveal escaping gas and the pressure was considerably higher for this test than the others. We do not know whether that was because the container was sealed better, or whether it was because the explosive material was bonded to the cylinder wall. The outside temperatures continue to be widely variable and difficult to analyze. Sometimes the hot spots are on the same side of the cylinder at a location, and then at another location, they are on the same end of the cylinder.

2.3 ELECTRICAL COOKOFF TESTS

This report is based on the information provided by Thiokol Propulsion Company in Report TR12646, C-SAFE TESTS, Phase III.

2.3.1 INTRODUCTION

A new container was designed to hold only one 4" diameter x 4" thick pellet of PBX9501 explosive. The previous design held three of the pellets. The container was changed from schedule 80 pipe with Marman-type V-band clamps to a ¼" thick container with thickened ends, and the end plugs were sealed with o-rings and snap rings. This container was designed to withstand pressures up to about 7500 psi on the sidewall and

end plugs. A hydrostatic pressure test was conducted of the empty container to determine the pressure at which it would burst.

2.3.2 DISCUSSION

The tests specified for this contract were a hydrostatic pressure test of the container, a pressure transducer characterization test, a burn rate test of the PBX-9501 material, and up to six cook-off tests depending on the time and budget. The container must first be assembled and the hydrostatic pressure test performed before the other tests could proceed.

The original design for the container for the cook-off tests was to be a 4-inch inside diameter schedule-80 pipe with a Marman-type V-band clamp on each end to hold the end caps. Flanges with an o-ring groove were welded to each end of the pipe. The end caps were machined so that their edges matched the flange design. The pipe was to be 12 inches long to hold three, 4-inch diameter x 4-inch thick explosive pellets. The container was to be surrounded by an 11-inch wide band heater.

Because of the long lead-time to procure the Marman clamps and flanges, the tests were delayed until after January 2001. At that time the University of Utah personnel decided to change the design of the container to hold one pellet instead of three pellets. This would make the computer modeling of the test much easier. Also at that time it was decided to change the container design and use and engineered design with an o-ring and snap ring instead of the schedule 80 pipe with end caps held in place by Marman-type V-band clamps. The container was designed to be able to withstand about 7500 psi on the sidewalls and end plugs. A picture of this container is shown in Figure 2.17.

Figure 2.17. Steel container used in the electrical cookoff tests

2.3.3 HYDROSTATIC PRESSURE TEST

After the design was completed, two containers were fabricated. The first container was used for a hydrostatic pressure test. The objective of this test was to determine the pressure at which the container would burst. A hole was drilled in one of the end caps and a fitting was attached to connect to the pressurized water system. The end with the pressure fitting was designated the top of the container. Strain gages were mounted on the container, axially and circumferentially, at eight locations, making sixteen total. Strain gages were mounted at the top and bottom at 0°, 90°, 180°, and 270°.

Pressure was applied in small increments starting about 20 seconds into the test. At about 110 seconds into the test and a pressure of 7541 psi, the container started to leak. The snap-ring grooves gave way and the pressure forced the snap ring to deform allowing the end plugs to move causing the leak. The container did not burst. However, the sidewalls were bulged making the container look like a small potbelly stove.

2.3.4 PRESSURE TRANSDUCER CHARACTERIZATION

Entran Model EPB-C02-5KP-/C/Z4 pressure transducers were purchased to use in this year's testing. These pressure transducers have a range of 5000 psi (not to exceed 10,000 psi) and have an operating temperature range of 233 to 394 K (-40 to 250°F). They are

temperature compensated between 310 and 366 K (100 and 200°F). Since the temperature conditions of the tests were going to exceed these operating conditions, we wanted to know the response of the pressure readings as a function of temperature.

One of the previously designed containers was used for this characterization test. The Entran pressure transducer and a type K thermocouple were installed inside the container. A pressure port was installed in one of the end caps to connect to the pressurized-air line. A Conax connector was installed in the other end cap allowing the leads from the Entran pressure transducer and thermocouple to exit the container without causing a pressure leak. A Taber Model 207 pressure transducer was installed on the pressure supply line just outside of the container. The Taber transducer was maintained at ambient temperature and was used to record the pressure inside the container to compare with the Entran transducer reading. An 11-inch wide band heater surrounded the container. The pressure line was connected to a tank of compressed air. The pressure valves and voltage to the band heater were operated remotely for personnel safety.

Several runs were made to determine how the setup operated and the response of the pressurized system. For the actual test, the compressed air tank regulator was set to 350 psi. The data acquisition system recorded the temperature and both pressure readings at a rate of 1 sample per second. The pressure valves were opened and the voltage was applied to the band heater and data were recorded for 1 hour and 13 minutes. The regulator on the pressure tank was not able to keep the pressure at 350 psi, allowing it to drop to 310 psi over a period of time. The initial temperature inside the container was 287 K (57°F).

The actual pressure measured by the Taber transducer went up and down as the regulator tried to stabilize. The Entran transducer increased in pressure as the temperature increased.

2.3.5 HYDROBURST TEST #1 – 2002

We have completed closed ballistic bomb testing of pelletized PBX-9501 explosive from 50 to 7,000 psi. This memo summarizes those findings.

2.3.5.1 INSTRUMENTATION BACKGROUND

The closed ballistic bomb is a one-liter cylindrical high-pressure vessel instrumented with a pressure transducer, thermocouple, nitrogen gas supply lines, a data acquisition system and an ignition system. The bomb is jacketed in a liquid-filled conditioning collar for temperature control. It is used to determine the burn rate and ignitability of propellants, gas generants and other materials from sub-ambient to 14,000 psi over a broad range of temperatures. The samples may be pressed pellets, extruded or cored slugs, or other shapes as required.

2.3.5.2 EXPERIMENTAL

The samples were weighed on an analytical balance reading to the tenth of a milligram. The samples were measured dimensionally in inches using a dial caliper. This data was entered into the data acquisition program prior to testing.

The pellets were adhered to the sticky side of masking tape that in turn was stuck onto cardboard. The samples were then sprayed with 3 coats of Krylon Ignition sealer as an inhibiter so only the top of the pellet would burn. A small amount of ignition powder was placed on top of the pellet as an ignition aid. The ignition powder was kept in place during bomb closure by means of a 3/8" strip of masking tape wrapped around the pellet at the uninhibited (ignition) end.

The prepared samples were loaded into the M-9 1-liter closed bomb by placing them onto the sample plate and a lift/sacrificial plate, with a short length of Parr bomb ignition wire pulled taught over the ignition aid coated part of the pellet through slits in the tape and secured to the electrical posts. The bomb closure (which carries the sample holder) was loaded into the bomb, and the ignition circuit was then connected. The system was then pressurized with nitrogen to the test pressure. The data acquisition system was used to trigger ignition and record the resultant pressure rise as well as perform various other calculations.

2.3.5.3 OBSERVATIONS

The pellets burned well with no problems or loss of inhibition (as would be shown by a break to a steeper pressure rise trace). There was no combustion residue except with the

samples tested below about 500 psi when carbon dust was evident (which is typical of similar materials). The sample tested at 20-psi did not ignite.

The raw data files were stored on a CD. Each trace consists of four segments of information per burn. They are respectively the conditioning pressure, the ignition, the pressure rise from burning and the cool down. Three additional pellets were burned with a 60 second record time to show data for the cool down.

There is about 40 psi of generated gas independent of the test pressure. Also, there is a pressure rise increase associated with higher starting pressures. Consequently 7000 psi was the highest initial starting pressure used in order to keep from overshooting the gauge maximum of 15,000 psi. Similarly, the psi/g data is used as a figure of merit in gas generant data analysis and increases quite dramatically for PBX-9501. These values are some of the largest ever seen in our lab.

2.3.5.4 RESULTS AND CONCLUSIONS

The burn rate exponent for PBX-9501 is 0.86 and is quite linear between the pressure ranges of 50 to 7000 psi.

2.3.6 TEST 6, ELECTRICAL, JULY 2001

The first cook-off test was conducted on July 3, 2001. The container used is shown in Figure 2.17. The explosive material was PBX-9501, the same material that was used in previous years. It is described in previous years' reports. Conax connectors were installed in each end cap of the container. They were used to seal the wires against a pressure leak. The pressure transducer leads came out one of the ends, and the thermocouple leads came out the other end. The band heater was 4.5-inches inside diameter x 4-inches long with a mineral insulated construction. Its output was 35 W/sq in and was supplied by Entherm. The band heater was split so that it could be placed around the container.

Since only one pellet was used, it was cut in half to allow instruments to be placed in the middle of the pellet. The cutting was done on a lathe using a 1/16-inch parting tool. The outside thermocouples were placed between the container and the band heater. Their locations are described in Table 2.7, along with the data acquisition setup parameters. A

2-inch layer of pipe insulation was wrapped around the outside of the band heater. A voltage of 110 volts was applied to the band heater. The container was placed on the ground with the 0° mark down and the split in the band heater was placed at about the 45° mark.

Our LeCroy data acquisition system was set up for 16 channels and recorded the inside thermocouples, the pressure transducer channels, and 5 of the outside thermocouples. Our Nicolet system recorded the rest of the outside thermocouple channels. One inside thermocouple, TC07 was damaged in the assembly and did not respond in the final checkout. Therefore, it was not connected to the data acquisition system.

Because the LeCroy system only has 512 K of memory and must be divided equally among the 4 channels, the acquisition time was only 10.9 minutes. This was a concern because we did not know how long the material would heat until it exploded. Personnel at the University of Utah conducted some experiments with the band heater and calculated that the time to explosion would be 2 to 3 minutes. In actuality, the time to explosion was 31 minutes. This meant that the digitizers timed out and were re-armed and triggered two more times. In the third segment of data collection we noticed that the second and third LeCroy digitizers, which were recording thermocouples TC06 and TC08 – TC14 had stopped recording data. The dilemma we faced was whether to continue recording, in which case we would lose those channels of data, or to stop the acquisition, re-boot the system, and start over. If we chose the latter option, the explosion could occur during the time for the restart and we would lose all of the data recorded by the LeCroy system. The decision was made to restart the system. During the restart, the explosion occurred and the pressure transducer data along with thermocouple data up through TC14 were lost. The only data acquired were thermocouple channels TC150TC20 and only for the last ten minutes of the test.

The explosion that took place was very complete. The container disintegrated and only four small pieces of metal material were found. One of these looked like it came from the band heater. No explosive material was found. The high-speed video of the event showed the container exploding and quite small pieces of material flying away.

Table 2.7 C-SAFE 2001 Instrumentation List

Name	Description	Location
TC01	Thermocouple	Inside Container, End #1, 0°
TC02	Thermocouple	Inside Container, End #1, 180°
TC03	Thermocouple	Inside Container, Middle of Pellet, 0°
TC04	Thermocouple	Inside Container, Middle of Pellet, 90°
TC05	Thermocouple	Inside Container, Middle of Pellet, 180°
TC06	Thermocouple	Inside Container, Middle of Pellet, 270°
TC07	Thermocouple	Inside Container, End #2, 0°
TC08	Thermocouple	Inside Container, End #2, 180°
TC09	Thermocouple	Outside Container, End #1, 0°
TC10	Thermocouple	Outside Container, End #1, 90°
TC11	Thermocouple	Outside Container, End #1, 180°
TC12	Thermocouple	Outside Container, End #1, 270°
TC13	Thermocouple	Outside Container, Middle, 0°
TC14	Thermocouple	Outside Container, Middle, 90°
TC15	Thermocouple	Outside Container, Middle, 180°
TC16	Thermocouple	Outside Container, Middle, 270°
TC17	Thermocouple	Outside Container, End #2, 0°
TC18	Thermocouple	Outside Container, End #2, 90°
TC19	Thermocouple	Outside Container, End #2, 180°
TC20	Thermocouple	Outside Container, End #2, 270°
P001	Pressure Transducer	Inside Container, End #1, 0°, 1/16" from edge
P002	Pressure Transducer	Inside Container, Middle, 0°, 1/16" from edge
P003	Pressure Transducer	Inside Container, In the bore of the pellet
Camera 1	High Speed Video	Side View, Covering 5 feet to the side
Camera 2	Video Monitor	Side View, Covering 20 feet to the side
Camera 3	Video Monitor	End View, Covering 20 feet side to side

2.3.7 TEST 7, ELECTRICAL, AUGUST 2001

The second cook-off test was conducted on August 6, 2001. Because of the loss of data in the first cook-off test, the decision was made to duplicate the first test with the

exception of the voltage applied to the band heater. In the first test we used 110 volts and for the second test we used 220 volts. The pressure transducers and thermocouples were placed the same as for the first test. However, the data acquisition systems were changed from the first test. The pressure transducers were set up on channels 1-3 of the LeCroy system at a sampling rate of 100 samples per second. This gave a recording time of almost 22 minutes. The pressure transducers were also set up on channels 5-7 at a sampling rate of 10,000 samples per second with a manual trigger. The data to be recorded was all pre-trigger data for a period of time of about 13 seconds. The manual trigger was applied when the explosion took place. This set up was designed so that we could record data from the beginning at a slow rate and then record the explosion at a much faster rate for the ten seconds or so, just before the explosion. The inside thermocouples were recorded on channels 8-16 of the LeCroy system at a rate of 100 samples per second. The outside thermocouples were recorded on an Iotech LabBook 16 channel data acquisition system at a sampling rate of 200 samples per second. The LabBook has enough memory that the recording time was 40 minutes at this sampling rate.

The explosion occurred at 3 minutes and 12 seconds after the voltage was applied to the band heaters. The explosion was not as violent as the first test. One side of the container was blown out and peeled back leaving the rest of the container intact. A picture of the container is shown in Figure 2.18. The explosive material was not all consumed and about 2 pounds of the 3 pounds total was recovered from the site. A picture of some of the material is shown in Figure 2.19.

All of the data were recovered from the first test. The data showed that the pressure near the interface of the material and container reached about 50 psi (uncorrected) until just prior to the event and then there was a sharp spike in the data up to about 130 psi and then the explosion took place. The bore pressure remained near zero until just prior to the test and then a spike in the data occurred up to 57 psi just before the explosion. Transducer P002 went negative until just a few seconds before the explosion took place. We can't explain the reason for this negative excursion.

Figure 2.18. Container after test

Figure 2.19. Fragments of explosive material after test

The thermocouple data also showed the spike in the data just before the explosion. Temperature inside the container ranged from 340 K (154˚F) to 443 K (338˚F). The ends were lower as expected. The middle thermocouples ranged from 392 K (247˚F) to 443 K (338˚F). The highest temperature was at the 90˚ position. The outside thermocouples ranged from 490 K (423˚F) to 766 K (920˚F). Middle thermocouples TC14-TC16 exceeded their range and recorded only to 920˚F.

2.3.8 TEST 8, ELECTRICAL, SEPTEMBER 2002

The third electrical test was conducted on September 30, 2002. The voltage applied to this test was 110 Volts. The experimental setup is similar to that described for tests 6 and 7 with the exception that some additional pressure transducers were placed around the test site (i.e. the surrounding of the ordnance) to measure the overpressure. The arrangement of the transducers is shown in Figure 2.20. This test was intended to duplicate test 6 in which most data were lost. The explosion occurred after 1520 seconds (25.3 minutes). Very few metallic pieces were gathered from the test site (see Figure 2.21).

The experimental results (Temperature and pressure) are plotted in Appendices A and B and discussed in chapter 4.

Figure 2.20 Pressure transducers arrangement

Figure 2.21 Pressure transducers arrangement

2.3.9 TEST 9, ELECTRICAL, NOVEMBER 2002

Test 9 consisted of two tests distinguished in this report as test 9A and test 9B. The main goal for test 9 was to explore the cookoff behavior (i.e. reaction violence) of HMX-based explosives in the low-heat flux regime (i.e. lower compared to test 6 and 8). The voltage was reduced by half, that is. 55 Volts, and so the applied heat flux at the steel pipe was reduced by a factor of 4 compared to test 8. No ignition resulted after 3 hours. The heating was suspended and the ordnance was cooled down. This corresponds to test 9A in this report. The same setup and instrumented container were used in test 9B. The voltage was increased to 110 Volts and the ignition occurred at 1520 seconds (25 minutes). Figure 2.22 shows some of the metallic pieces gathered from the test site.

The experimental temperatures and pressures are plotted in appendices A and B. Analysis of these results is presented in chapter 4.

Figure 2.22. Metallic pieces found after test 9B.

2.3.10 TEST 10, ELECTRICAL, NOVEMBER 2002

The main goal of test 10 was to explore the effects of no having an air core in the explosive pellet. The voltage applied to this test was 110 Volts. The explosion occurred after 1634 seconds (27.2 minutes), and was very comparable with test 6, 8, and 9B; although, the explosion was not nearly as violent. Pictures of the container and explosive material are shown in Figures 2.23 to 2.26.

The experimental temperatures and pressures are plotted in appendices A and B. Analysis of these results is presented in chapter 4.

Figure 2.23. Container after test.

Figure 2.24. Container after test.

Figure 2.25. Heater pieces gathered from the test site.

Figure 2.26. Explosive material after test.

Chapter 3

NUMERICAL ANALYSIS

The heat transfer phenomena and the associated numerical methods are specified in detail.

DATA ANALYSIS

Three different numerical methods were developed to study the thermal behavior of confined PBX-9501 when heated by a fire and electricity. The experiments were presented in detail in Chapter 2. For times to explosion up to 3 minutes in the present studies, the thermal penetration depth is approximately 4.7 mm, much smaller than the thickness of the explosive material. This implies that the system can be treated as a semi-infinite and therefore, the temperature distribution within the solid can be accurately described using a one-dimensional (1-D) heat flow equation.

The first method consisted of applying the Duhamel superposition integral to the surface temperature in order to get the surface heat flux. The second method used Inverse Heat Conduction (IHC) equations and temperature measurement within the solid to calculate the thermal boundary at the surface. The third method used a finite difference based, thermal-reaction model to investigate the boundaries of the overall system.

3.1. DUHAMEL SUPERPOSITION INTEGRAL

The measured interface temperature and the Duhamel's superposition technique were used to obtain the heat flux at the explosive surface. Considering the explosive part of the system and assuming constant thermophysical properties, the formulation of the problem for the unsteady temperature distribution $T(r,t)$ is given by

$$\frac{\partial T(r,t)}{\partial t} = \alpha_{PBX} \cdot \frac{\partial^2 T(r,t)}{\partial r^2} + \frac{1}{r}\frac{\partial T}{\partial r} \qquad (3.1)$$

An approximate solution for the surface heat flux is, (Buttsworth and Jones, 1997)

$$q = \frac{K_{PBX}}{\sqrt{\pi \cdot \alpha_{PBX}}} \cdot \left\{ \left[\frac{T(t) - To}{\sqrt{t}} \right] + \frac{1}{2} \int_0^t \frac{T(t) - T(s)}{\sqrt{(t-s)^3}} \cdot ds \right\} - \frac{K_{PBX}}{2 \cdot R_{PBX}} \left(T(t) - To \right) \qquad (3.2)$$

Equation (3.2) is accurate to better than 1 % for typical transient heat transfer configurations in which $\frac{\alpha \cdot t}{R^2} \leq 0.06$.

Equation (3.2) has a singularity when t = s. There are several numerical techniques that can be used to get a reasonable solution [Diller, 1996]. One of the most widely used consist of using a piecewise linear representation of the temperature trace [Cook and Felderman, 1966].

$$q(t_n) = \frac{2 \cdot K_{PBX}}{\sqrt{\pi \cdot \alpha_{PBX}}} \cdot \sum_{j=1}^{n} \left(\frac{T_j - T_{j-1}}{\sqrt{t_n - t_j} + \sqrt{t_n + t_{j-1}}} \right) + \frac{K_{PBX}}{2 \cdot R_{PBX}} \left(T_j - T_o \right) \qquad (3.3)$$

3.2. INVERSE HEAT CONDUCTION METHOD

Inverse heat conduction equations can be used to calculate the temperature and the heat flux on the surface of a solid from transient temperature measurements made within at one or more locations [Hills and Hensel, 1986]. Consider the infinite long cylinder illustrated in Figure 3.1. Initially, the cylinder is at uniform temperature. The temperature measurement is taken at point $r=r_E$. In addition, let the boundary condition be known at the interior of the cylinder or $r=r_1$. The heat flux and the temperature at the surface of the cylinder ($r=r_M$) can be calculated by dividing the problem into two parts. The first part consist of solving the direct problem, that is, the region between $r=r_1$and $r=r_E$. This would provide the temperature and heat flux needed to solve the second part, that is, the inverse region between $r=r_E$ and the surface $r=r_M$.

The direct problem can be solved using a finite difference technique such as the Crank-Nicholson method. The inverse heat conduction problem can be solved using a space-marching technique. The governing equation for the inverse problem is

$$\rho \cdot Cp(T) \cdot \frac{\partial T(r,t)}{\partial t} = \frac{1}{r} \cdot \frac{\partial}{\partial r}\left[r \cdot K(T) \cdot \frac{\partial T(r,t)}{\partial r} \right] \tag{3.4}$$

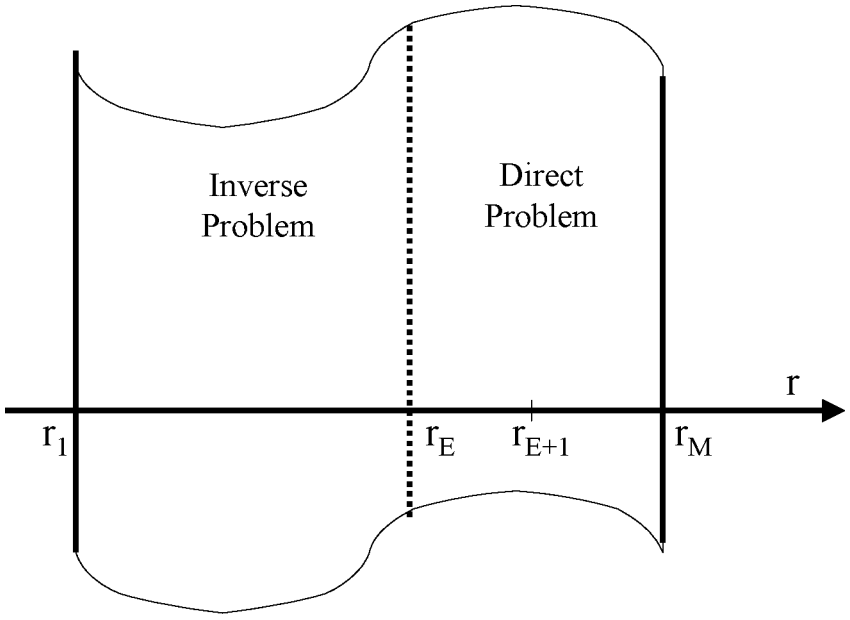

Figure 3.1. One-dimensional representation of an infinite long cylinder

If the heat flux definition is introduced in the right hand side term, Eq. 3.4 can be written as two simultaneous first-order equations

$$q = -K_{PBX}(T) \cdot \frac{\partial T(r,t)}{\partial r} \tag{3.5}$$

$$\rho_{PBX} \cdot Cp_{PBX}(T) \cdot \frac{\partial T(r,t)}{\partial t} = -\frac{\partial}{\partial r} \cdot [r \cdot q] \tag{3.6}$$

The numerical solution of Eqs (3.5) and (3.6) consisted of replacing the derivatives for finite difference approximations. A first-order forward and a first-order backward difference were used for the spatial and the time derivative respectively. After rearranging, the equations to solve are

$$T_{i+1}^{n} = -\frac{\Delta r}{K_i} q_{i+1}^{n} + T_i^{n} \tag{3.7}$$

$$q_{i+1}^{n} = -\frac{r_i}{r_{i+1}} \cdot q_i^{n} + \frac{r_i}{r_{i+1}} \cdot \frac{\Delta r \cdot \rho \cdot Cp}{\Delta t} \cdot \left(T_i^{n-1} - T_i^{n} \right) \tag{3.8}$$

Using Eq. (3.8) in Eq. (3.7) leads to

$$T_{i+1}^{n} = -\frac{r_i}{r_{i+1}} \cdot \frac{\Delta r \cdot q_i^n}{K_i} + T_i^{n-1} \cdot \left(-\frac{r_i}{r_{i+1}} \cdot \frac{\Delta r^2 \cdot \rho \cdot Cp}{K_i \cdot \Delta t} \right) + T_i^n \cdot \left(1 + \frac{r_i}{r_{i+1}} \cdot \frac{\Delta r^2 \cdot \rho \cdot Cp}{K_i \cdot \Delta t} \right) \quad (3.9)$$

Equations (3.8) and (3.9) can be used to calculate the heat flux and the temperature in the inverse region ($r_E < r < r_M$).

Analytical solutions for the inverse heat conduction problem in a semi-infinite solid are well known [Burggraf, 1964 and Beck et al, 1985]. For a slab, the temperature and the heat flux at the surface of the explosive are given by

$$T_{rM}^{t} = T_{rE}^{t} + \sum_{n=1}^{\infty} \frac{r_E^{2n}}{(2n)!} \cdot \frac{1}{\alpha^n} \cdot \frac{d^n T_{rE}}{dt^n} + \frac{r_E}{K_{PBX}} \left[q_E^t + \sum_{n=1}^{\infty} \frac{r_E^{2n}}{(2n+1)!} \cdot \frac{d^n q_E}{dt^n} \right] \quad (3.10)$$

$$q_{rM}^{t} = q_E^t + K_{PBX} \cdot \sum_{n=1}^{\infty} \frac{r_E^{2n-1}}{(2n-1)!} \cdot \frac{1}{\alpha^n} \cdot \frac{d^n T_{rE}}{dt^n} + \sum_{n=1}^{\infty} \frac{r_E^{2n}}{(2n)!} \cdot \frac{d^n q_{rE}}{dt^n} \quad (3.11)$$

The results given by the numerical and the analytical solutions were very similar. This implies that curvature effects were not important and so the 1-D planar solution can be safely used to describe the thermal behavior of high-energy materials during fast cookoff.

3.3. THERMAL REACTION MODEL

All energetic materials are, to some degree, sensitive to heat: They suffer degradation, decomposition, and ultimately ignition. In general, mechanisms and kinetics are proposed according to induction times that are obtained during slow thermal decomposition experiments with different rates of heating. The prediction of the time to explosion for HMX-based explosives has been successfully obtained by using a reduced 3-step Arrhenius scheme [McGuire and Tarver, 1981]. The scheme is based on experimental data and involves the following reactions:

$$HMX_{(s)} \Rightarrow H_2C = N - NO_{2(s)} \quad \text{(R-1)}$$

$$H_2C = N - NO_{2(s)} \Rightarrow CH_2O_{(g)} + N_2O_{(g)} \quad \text{(R-2)}$$

$$CH_2O_{(g)} + N_2O_{(g)} \Rightarrow H_2O_{(g)} + N_{2(g)} + CO_{(g)} + CO_{2(g)} \quad \text{(R-3)}$$

The first reaction represents the endothermic breaking of C-N bonds in the ring forming H_2C=N-NO_2. The second step is the exothermic rearrangement of H_2C=N-NO_2 into

CH_2O and N_2O. The final reaction is the very exothermic gas phase decomposition of CH_2O and N_2O into the stable gaseous products such as H_2O, N_2, CO and CO_2. The heat of reaction and kinetic parameters are listed in Table 3.1.

For modeling purposes, the reactions R-1 to R-3 can be conveniently represented as

$$A \xrightarrow{1} B \xrightarrow{2} 2C \xrightarrow{3} D \qquad \text{(R-4)}$$

Where A represents HMX, B represents H_2C=N-NO_2, C represents CH_2O and N_2O, and D represents the final products such as H_2O, N_2, CO and CO_2.

Table 3.1. Kinetic parameters for the thermal decomposition of HMX. (After McGuire and Tarver).

	Reaction 1	**Reaction 2**	**Reaction 3**
Heat of reaction, kJ/kg	-4.18	1.25	5.02
Activation energy, kJ/mole	220	185	143
Frequency factor, s^{-1}	$1.41*10^{21}$	$1.58*10^{16}$	$1.60*10^{12}$

Consider the sketch of the 1-D problem in Figure 3.2. When the thermal conductivity (K) and specific heat (Cp) are temperature dependant, the radial temperature distribution T(r,t) for t>0 can be obtained by solving the following

For $R_i < r < R_{PBX}$

$$\rho_{PBX} \cdot Cp_{PBX}(T) \cdot \frac{\partial T(r,t)}{\partial t} = \frac{\partial}{\partial r} \cdot \left[K_{PBX}(T) \cdot \frac{\partial T(r,t)}{\partial r} \right] + \frac{K_{PBX}(T)}{r} \cdot \frac{\partial T(r,t)}{\partial r} + S \qquad (3.12)$$

Where S represents the heat source due to the chemical decomposition of the explosive.

Based on the simplified mechanism described by reaction R-4, S is given by

$$S = m_A \cdot Q_1 \cdot Z_1 \cdot e^{\left(\frac{-Ea_1}{R_g \cdot T}\right)} + m_B \cdot Q_2 \cdot Z_2 \cdot e^{\left(\frac{-Ea_2}{R_g \cdot T}\right)} + m_C{}^2 \cdot Q_3 \cdot Z_3 \cdot e^{\left(\frac{-Ea_3}{R_g \cdot T}\right)} \qquad (3.13)$$

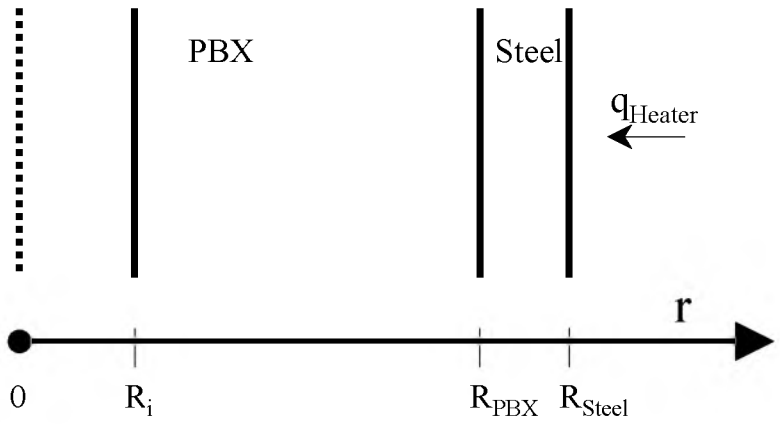

Figure 3.2 One-dimensional representation of the system

Here, m_A, m_B, m_C and m_D are the mass fraction of A, B, C and D. As the decomposition proceeds, the concentration of each of the species is described by the following rate equations

$$\frac{dA}{dt} = -k_A \cdot A \tag{3.14}$$

$$\frac{dB}{dt} = k_A \cdot A - k_B \cdot B \tag{3.15}$$

$$\frac{dC}{dt} = k_B \cdot B - k_C \cdot C^2 \tag{3.16}$$

$$\frac{dD}{dt} = k_C \cdot C^2 \tag{3.17}$$

The rate constants k_i for i=A, B, C and D and for j reactions (R1 to R4) are given by

$$k_{i,j} = Z_j \cdot e^{\left(-\frac{Eaj}{Rg \cdot T}\right)} \tag{3.18}$$

For $R_{PBX} < r < R_{steel}$

$$\rho_{Steel} \cdot Cp_{Steel}(T) \cdot \frac{\partial T(r,t)}{\partial t} = \frac{\partial}{\partial r} \cdot \left[K_{Steel}(T) \cdot \frac{\partial T(r,t)}{\partial r} \right] + \frac{K_{Steel}(T)}{r} \cdot \frac{\partial T(r,t)}{\partial r} \tag{3.19}$$

The initial condition is given by

$$T(r,0) = To \tag{3.20}$$

The boundary conditions for the electrical test case are defined as

$$-K_{Steel}(T)\frac{\partial T(R_{steel},t)}{\partial r} = \frac{V}{A \cdot R_H^2} = q_s \tag{3.21}$$

$$\frac{\partial T(R_{PBX},t)}{\partial r} = 0 \tag{3.22}$$

At the interface between the two materials, the rate of heat flow must be continuous, that is,

$$-K_{PBX} \cdot \frac{\partial T(R^+_{PBX},t)}{\partial r} = -K_{steel} \cdot \frac{\partial T(R^-_{PBX},t)}{\partial r} \tag{3.23}$$

When two unpolished surfaces are brought into contact, they actually touch only at a limited number of points, the total of which is usually only a small fraction of the apparent contact area. The remainder of the space between the surfaces may be filled with air or another fluid. When heat flows from one solid to the other, heat flow paths converge toward the actual contact spots, since the thermal conductivities of solids are generally greater than those of fluids. This creates an additional resistance to the heat flow at the interface [Kakac and Yener, 1993]. The gap may be filled with a gas and could increase even more due to the thermal expansion of the materials and the generation of gas from the exothermic combustion of the explosive. Assuming that this gap is filled with air, the new energy balance at the interface becomes

$$-K_{PBX}(T) \cdot \frac{\partial T(R^-_{PBX},t)}{\partial r} = h \cdot (T_{steel} - T_{PBX}) \tag{3.24}$$

And

$$h \cdot (T_{steel} - T_{PBX}) = -K_{Steel}(T) \cdot \frac{\partial T(R^+_{PBX},t)}{\partial r} \tag{3.25}$$

Where h is the total heat transfer coefficient at the interface. Although, h may include conduction, convection and radiation through the gap, it has been reported that

conduction is the dominant mechanism for small gaps and not too high temperatures. Therefore, h may be expressed as

$$h = \frac{K_{Air}}{L_{Air}} \tag{3.26}$$

The length of the air gap for some preliminary experiments was found to be proportional to the difference in the thermal expansion of the steel and the PBX.

$$L_{air} = \Delta R_{Steel}[\alpha_1 \cdot T_{steel} + \alpha_2 \cdot T_{steel}^{\ 2}] + \Delta R_{PBX}[\beta_1 \cdot T_{PBX}] \tag{3.27}$$

It is important to mention that the calculated air gap width was in the range of the measurement tolerance and therefore conclusions cannot be made yet based on Eq. (3.27).

Equations (3.12) through (3.19) were solved numerically by using finite difference approximations. The numerical solution of the discretized equations is performed using the well-known Crank-Nicholson procedure, which is second order accurate in space and time [Carnahan et al, 1969].

3.4. THERMOPHYSICAL PROPERTIES

The thermal properties of steel, PBX-9501 and air are relatively strong function of temperature. The accuracy of the data is a crucial factor in the analysis of experimental heat transfer data. In the following sections, the material properties required in the heat transfer models are presented.

3.4.1. STEEL

The thermal properties of steel were obtained from an online database (www.matweb.com).

$$\rho = 7860 \cdot \left\langle \frac{Kg}{m^3} \right\rangle \tag{3.28}$$

The measured heat capacity for steel 1025 at different temperatures is presented in Figure 3.3 In general, the heat capacity of steel increases in a nearly linear fashion until about 998 K. At this temperature, the heat capacity presents an endothermic peak due to a solid

phase change. The data is fitted to a curve without the point at 998 K. The value of Cp at 998 K can be easily incorporated in the model as an "if loop".

$$C_p = 5522.16883 - 0.33772 \cdot T + 7.12416E-4 \cdot T^2 \left\langle \frac{J}{kg \cdot K} \right\rangle \quad (3.29)$$

Exception: at 998 K, Cp=1432 J/ Kg K

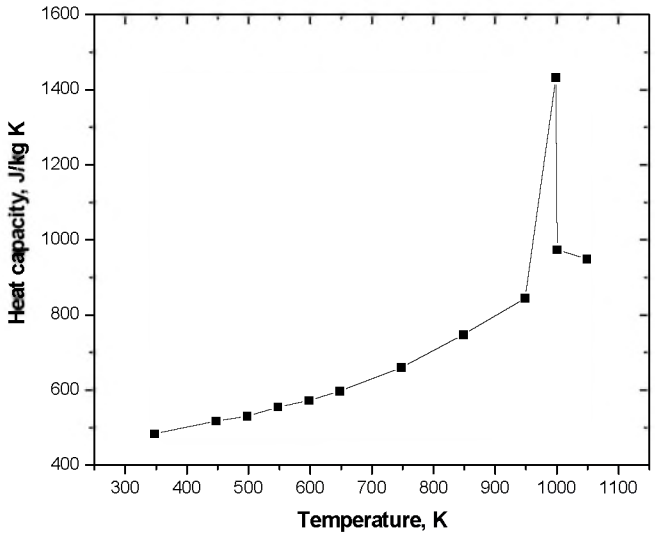

Figure 3.3. Heat capacity of steel 1026 (After http://www.matweb.com/)

Thermal conductivity of steel 1026 decreases with temperature. The measured data is presented in Figure 3.4. The data were fitted to the following equation

$$K = 54.27601 - 7.61593E-4 \cdot T - 2.35498E-5 \cdot T^2 \left\langle \frac{W}{m \cdot K} \right\rangle \quad (3.30)$$

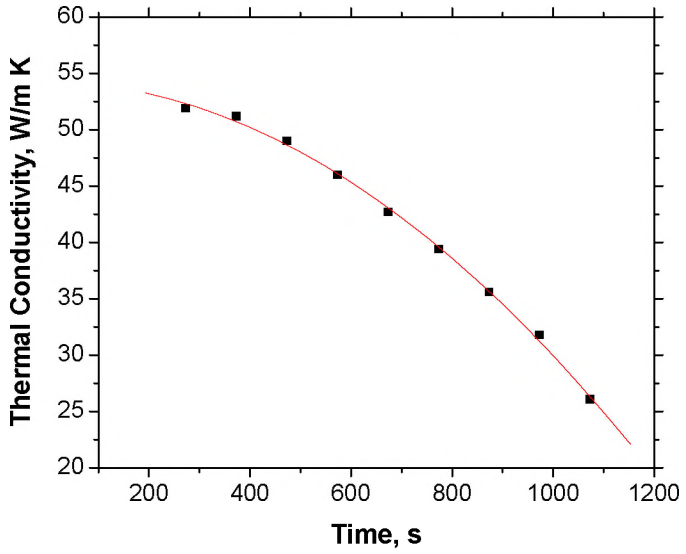

Figure 3.4. Thermal conductivity of steel 1026 (After www.matweb.com)

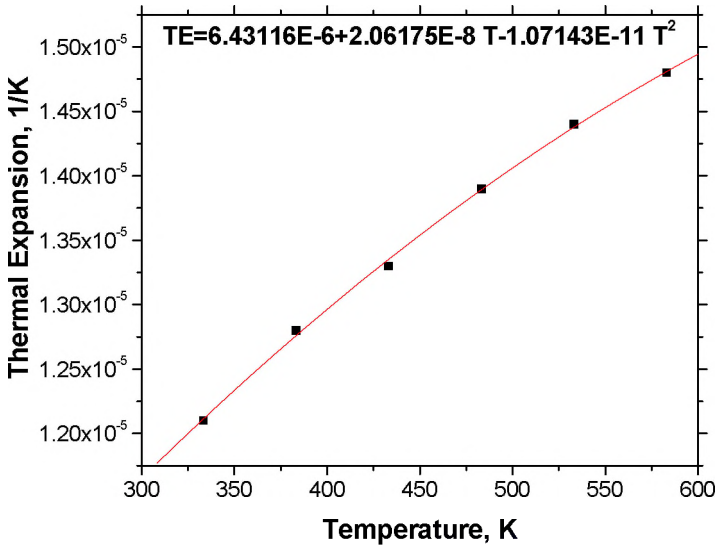

Figure 3.5. Thermal expansion of steel 1026 (After www.matweb.com)

3.4.2. PBX-9501

The thermal properties of PBX-9501 were taken from Gibbs and Popolato, 1980 and also from Menikoff and Sewell, 2001. The given polynomials were converted to standard SI units.

$$\rho = 1860 \left\langle \frac{kg}{m^3} \right\rangle \tag{3.31}$$

$$Cp = 93.575 + 3.305 \cdot T \left\langle \frac{J}{kg \cdot K} \right\rangle \tag{3.32}$$

Which is valid between 278 and 448 K.

Menikoff and Sewell, 2001, reported the thermal conductivity for HMX at temperatures between 298 and 700 K as

$$K = 7.131\text{E-}07 \cdot T^2 - 1.193\text{E-}03 \cdot \text{T} + 0.7458 \left\langle \frac{W}{m \cdot K} \right\rangle \tag{3.33}$$

The coefficient of thermal expansion was taken from Gibbs and Popolato, 1980. A constant value of 4.91 E-6/ K is valid between 300 and 350 K.

3.4.3. AIR

The thermal properties of air were taken from DiNenno, 1995. The data along with the curve fit and the equations are presented in Figures 3.6 to 3.9.

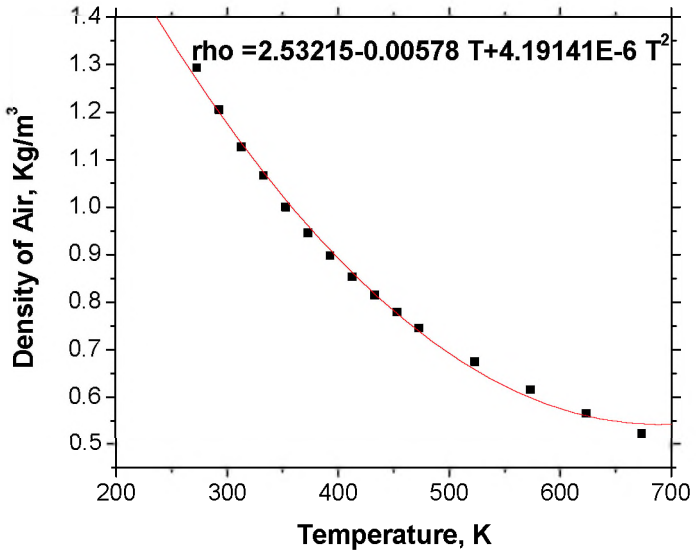

Figure 3.6. Density of air (After Dinenno, 1995)

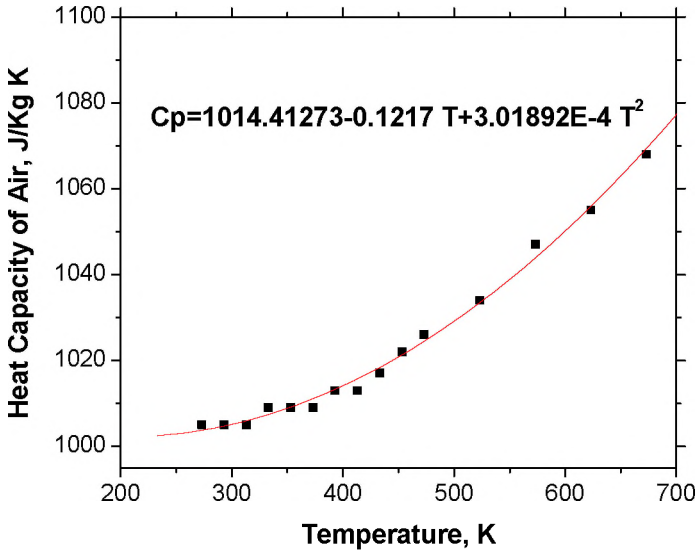

Figure 3.7. Heat Capacity of air (After Dinenno, 1995)

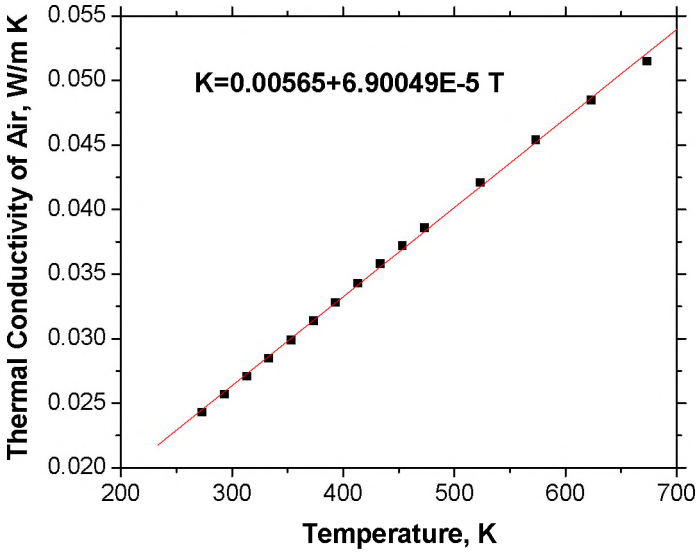

Figure 3.8. Thermal conductivity of air (After Dinenno, 1995)

Chapter 4

RESULTS AND DISCUSSION

A more in-depth analysis of the experimental data is presented. A comparison of the performance of the numerical methods is also included.

4.1. FIRE TESTS

A complete list of temperature and pressure plots for all tests is included in the CD.

In this section, the thermal analysis of each test is described. In addition, separate sections will be included to compare the experimental ignition times with those given by the ignition model for HMX-based explosives proposed by Beckstead in 1994.

4.1.1. TEST 1, EXPLOSIVE MATERIAL, NOVEMBER 1998

The correct measurement of steel temperature was one of the main difficulties found while carrying out the fire tests. The attached thermocouples are exposed to the fire and they could not give the proper temperature rise of the steel pipe. Instead, the experimental temperature profile seemed to correspond to that of a flame.

Assuming that the steel surface temperature is not too far from those represented in Figure 4.1, and having into account that the steel wall is nearly isothermal, then the temperature at the steel/PBX interface would be close to that represented by *Tpbx, side* in the abovementioned Figure. This is in agreement with the fact that the thermocouples were spot welded to the inner steel wall. Though, it is uncertain that this is the true temperature of the PBX surface since some of the thermocouples may not have been touching the PBX either because of an imperfect contact between the surfaces or a displacement of the thermocouples when the PBX was placed in the pipe.

The measured interface temperature (*T10 or Tpbx, side*) and the Duhamel superposition method were used to calculate the heat flux at the explosive surface as shown in Figure 4.2. The average heat flux was 19.8 kW/m^2 while Beckstead ignition model predicted

16.4 kW/m2. These values are presented in Figure 4.3. Even though, the values are in good agreement (18 %), it is important to mention that the ignition model assumes constant heat flux at the PBX surface and chemical reactions at atmospheric pressure.

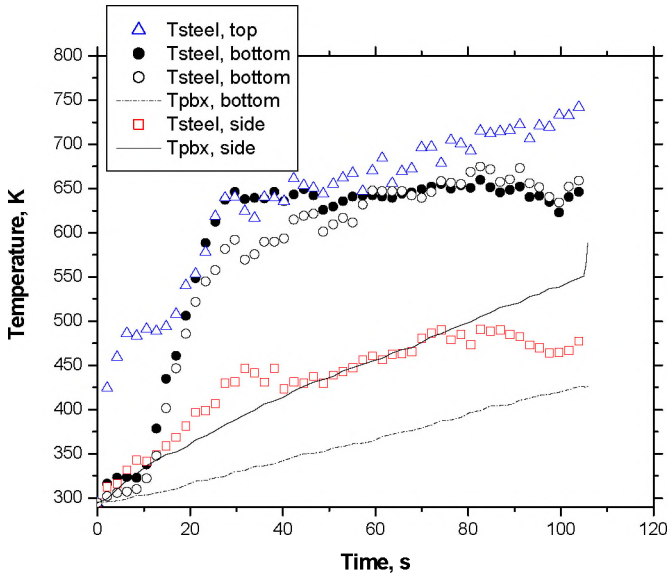

Figure 4.1. Experimental temperatures for test 1, fire, 1998

The thermal behavior of the complete system was also studied using the thermal- reaction model described in chapter 3. Some of the advantages of this model include prediction of ignition time, analysis of the temperature profile throughout the solid and also validation of the assumptions (i.e. semi-infinite condition).

The boundary condition at the steel surface was adjusted to give the inner wall temperature (*T10 or Tpbx, side*). This boundary consisted of radiative and convective heat flux and the adjustment parameters were the flame temperature and the convective heat transfer coefficient.

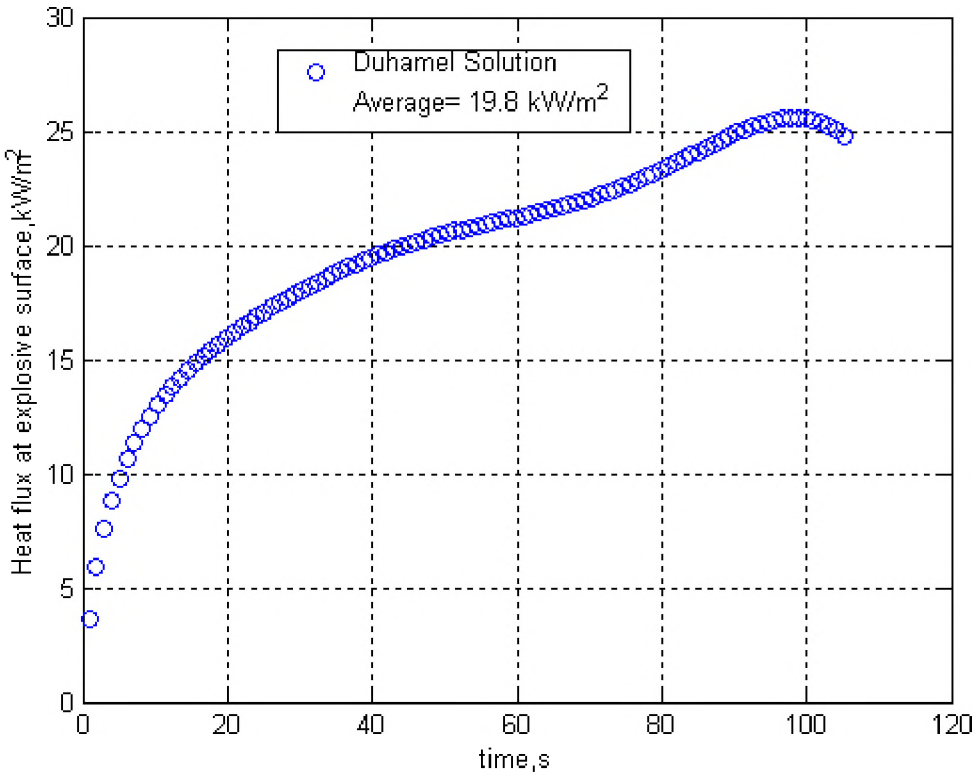

Figure 4.2 Heat flux at the PBX surface for test 1, fire, 1998

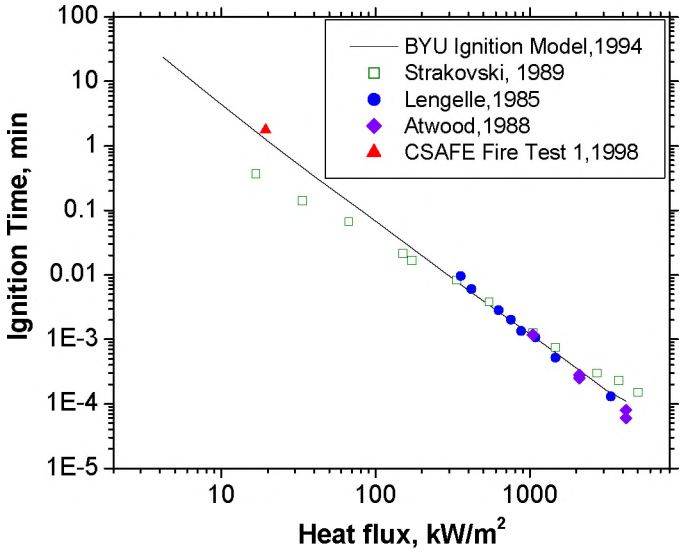

Figure 4.3. Ignition model for HMX-based explosives (After Beckstead, 1994)

All the calculations were based assuming that T10 was the true PBX temperature. The argument emphasized isothermal conditions for the steel wall. Indeed, this was a valid assumption as can be seen clearly in Figure 4.4.

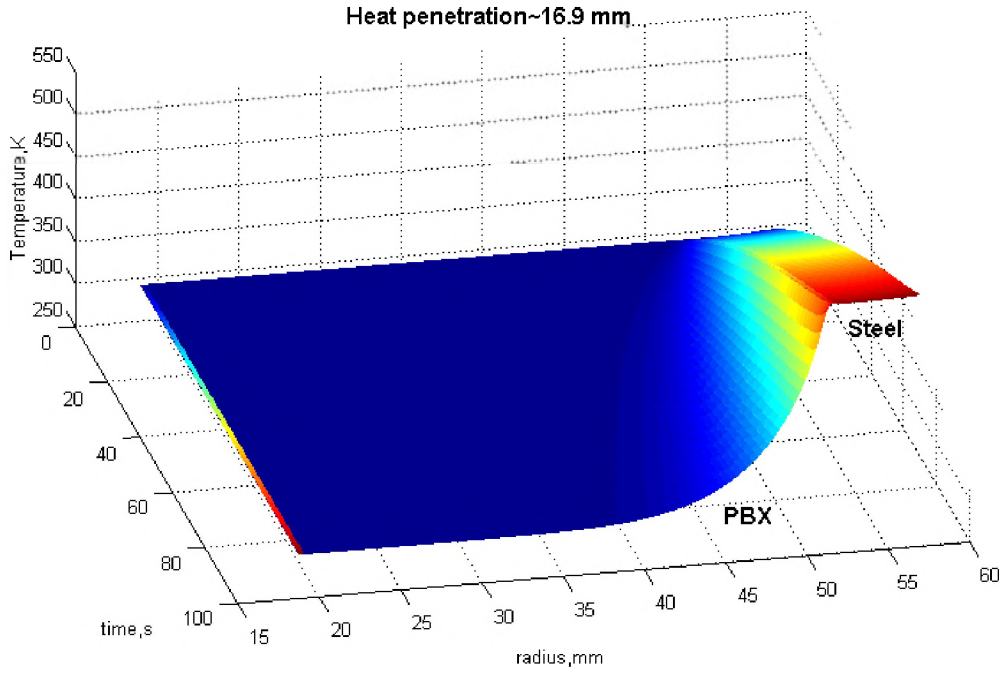

Figure 4.4. Temperature profile for test 1, fire, 1998.

The thermal-reaction model assumed also semi-infinite conditions to reduce the problem to a 1-D geometry. The penetration of heat was around 17 mm as can be seen in Figure 4.4, which is only 30 % of the explosive length. Therefore, for heat transfer calculations, the system may be treated as a semi-infinite solid.

The heat flux profile at the surface of the explosive was similar to that obtained by Duhamel and presented in Figure 4.2. An average of 19.5 kW/m^2 was computed. The model predicted an ignition time of 98 seconds, which is only 6 % sooner than the experimental time. These results are also in good agreement with the ignition model proposed by Beckstead in 1994.

4.1.2. TEST 2, EXPLOSIVE MATERIAL, OCTOBER 1999

The uncertainties in measuring the steel surface temperature are more significant for this test mainly because the thermocouples were not spot welded to neither the outer nor the

inner wall of the pipe. Figure 4.5 shows some of the measured temperatures at three different locations for both the steel and the PBX surfaces. From the Figure, it is clear that the PBX temperature is relatively low to the expected value under nearly isothermal conditions for the steel wall as was discussed and demonstrated for the fire test 1 in the last section. Again, this may be due to either the displacement of the thermocouples while placing the explosive inside the tube or some sort of air gap created at the interface between the materials. This uncertainty added to the unknown boundary condition at the steel wall difficult a proper analysis of the overall system. Fortunately, the Duhamel superposition method and the PBX surface temperatures can be used together to calculate the heat flux to which the explosive is exposed. In addition, the thermal-reaction model can be applied to the explosive to evaluate the effects on the heat flux of the thermal decomposition of the explosive and the temperature-dependent properties. As shown in Figure 4.6, the two methods present a fairly good agreement. Thus, chemical reactions and temperature dependent properties do not contribute significantly to the heat flux to which the explosive is exposed. The average heat flux (6.9 kW/m^2) for this test and the ignition model will be discussed later with the other fire tests.

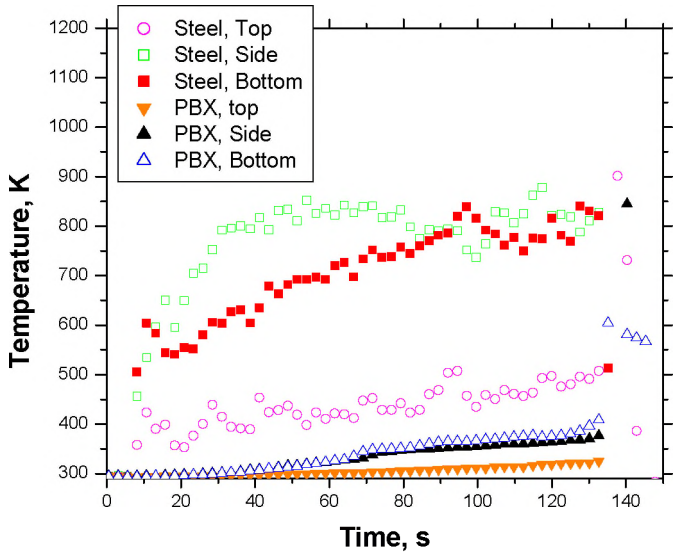

Figure 4.5. Measured temperatures for test 2, fire, 1999.

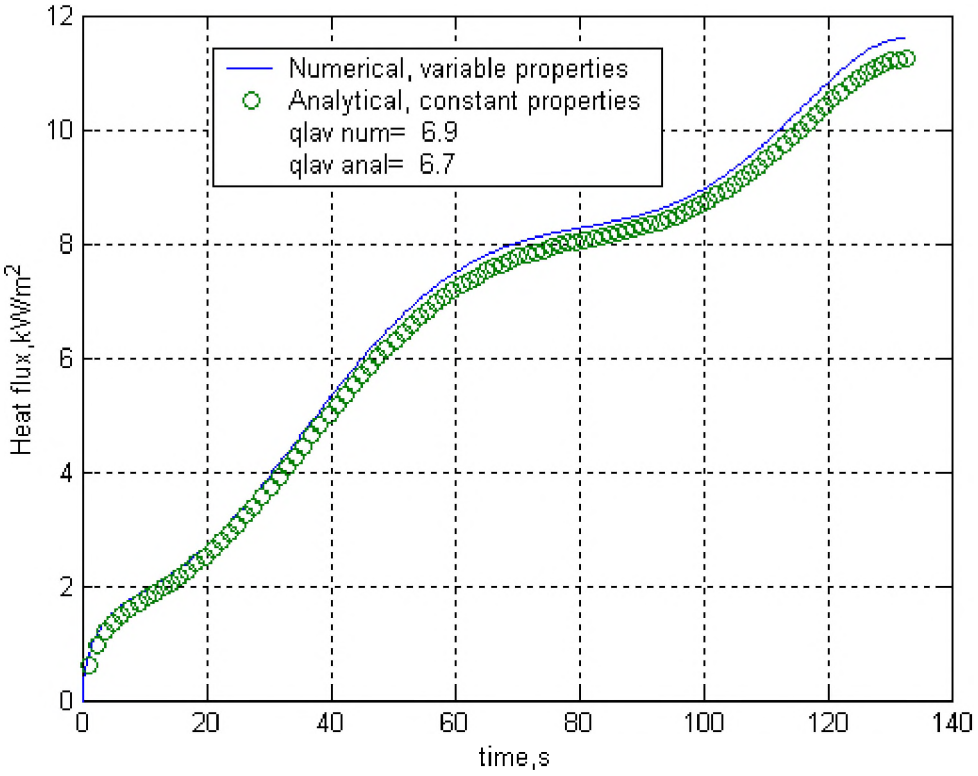

Figure 4.6. Heat flux at PBX surface for test 2, fire, 1999

4.1.3. TEST 3, EXPLOSIVE MATERIAL, OCTOBER 1999

The thermal analysis discussed in the last section for fire test 2 applies to this test. This test was indeed, intended to study the reproducibility of these fire tests, particularly fire test 2.

The measured steel and PBX surface temperatures are presented in Figure 4.7. It can be seen that the heating of the pipe was not uniform. In general, the temperature at the lower half of the pipe was consistently higher than that at the upper part. In addition, the temperature at the PBX surface was consistently lower than the expected values considering the steel temperatures.

An average of the interface temperature at the lower part of the pipe was used to calculate the heat flux to which the explosive is exposed (see Figure 4.8). An average heat flux of 6.3 kW/m^2 was computed. This value is only 9% less than that obtained for fire test 2.

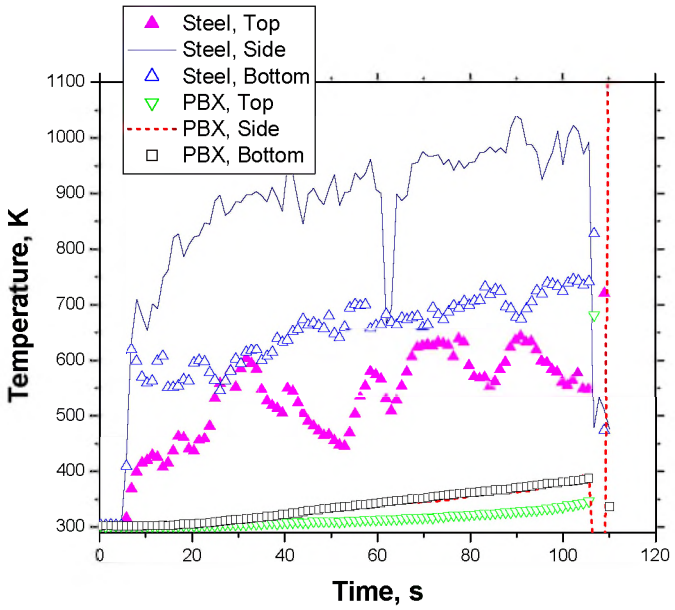

Figure 4.7. Temperatures at the steel and PBX surfaces for test 3, fire, 1999

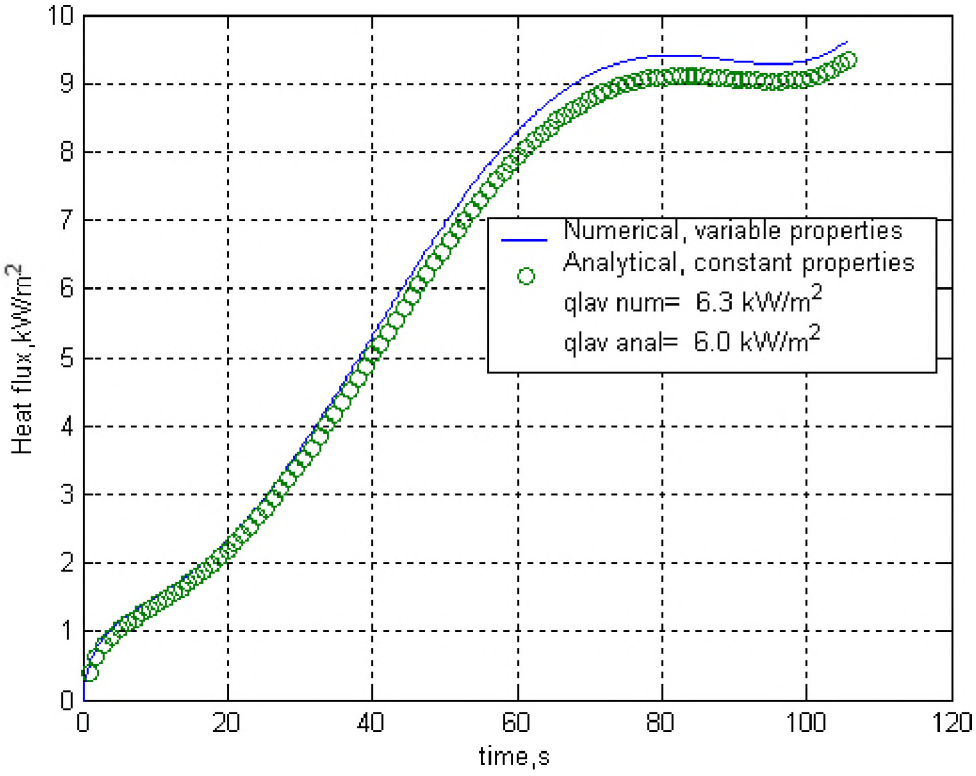

Figure 4.8. Heat flux at the PBX surface for test 3, fire, 1999.

4.1.4. TEST 4, EXPLOSIVE MATERIAL, OCTOBER 1999

This test was intended to explore the effects of sealing the pipe on the cookoff behavior of PBX-9501. It was expected that the sealing would prevent the combustion gases from escaping and thus a major pressurization would occur.

The measured steel and PBX surface temperatures are presented in Figure 4.9. Again, it is clear that the steel temperatures were not properly measured and that the interface temperatures were significantly lower than those at the steel surface.

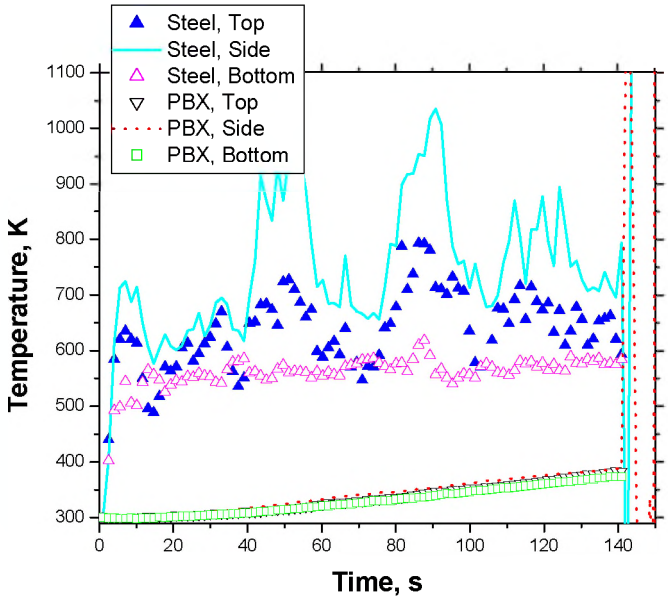

Figure 4.9. Temperatures at Steel and PBX surfaces for test 4, fire, 1999.

The heat flux at the explosive surface was calculated as described in the last section (see Figure 4.10). An average of 7.3 kW/m2 was computed. This value is around 5 % higher than that of test 2 and therefore sealing the pipe did not seem to affect the heat flux reaching the explosive.

4.1.5. TEST 5, EXPLOSIVE MATERIAL, OCTOBER 9, 1999

This test was intended to explore the effects of both sealing the pipe and bonding the explosive on the cookoff behavior of PBX-9501. In addition to that discussed in the last section, it was expected that bonding of the explosive to the inner wall would improve the

heat transfer at the interface. However, as can be seen in Figure 4.11 and 4.12, the thermal behavior of this test was similar to those discussed in the last three sections. For instance, an average heat flux of 6.4 kW/m^2 was computed, which of the same level of those found for tests 2 and 3 and around 12% lower than that of test 4. This suggests that sealing the steel pipe and bonding the explosive to the inner wall did not have a significant impact on the amount of heat flux reaching the explosive.

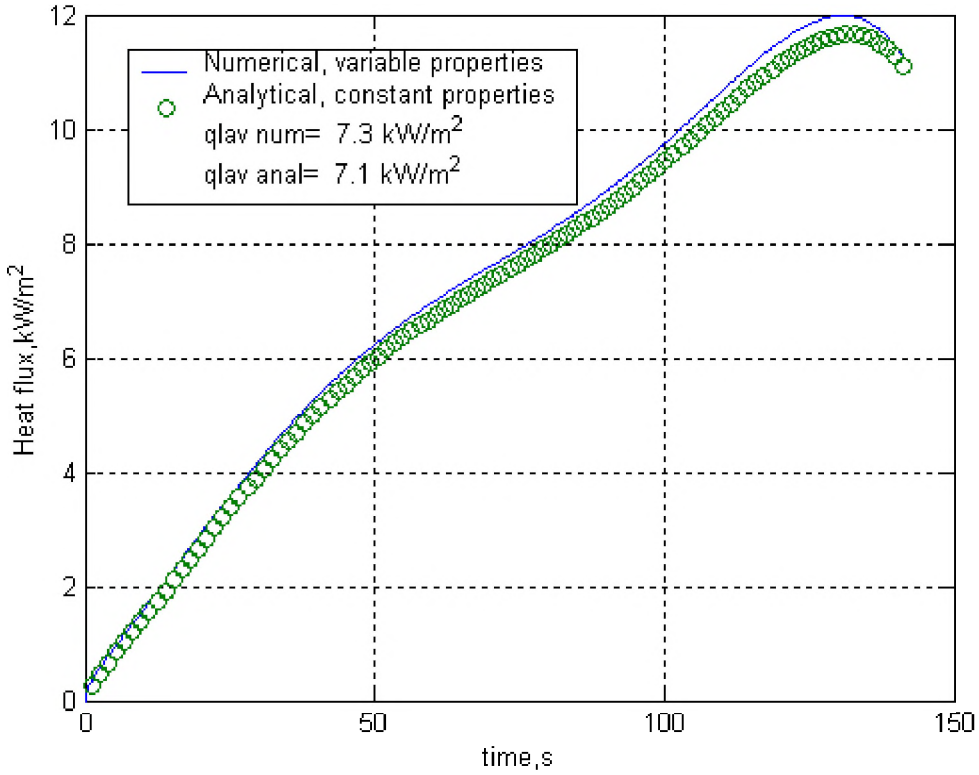

Figure 4.10. Heat flux at the explosive surface for test 4, fire, 1999.

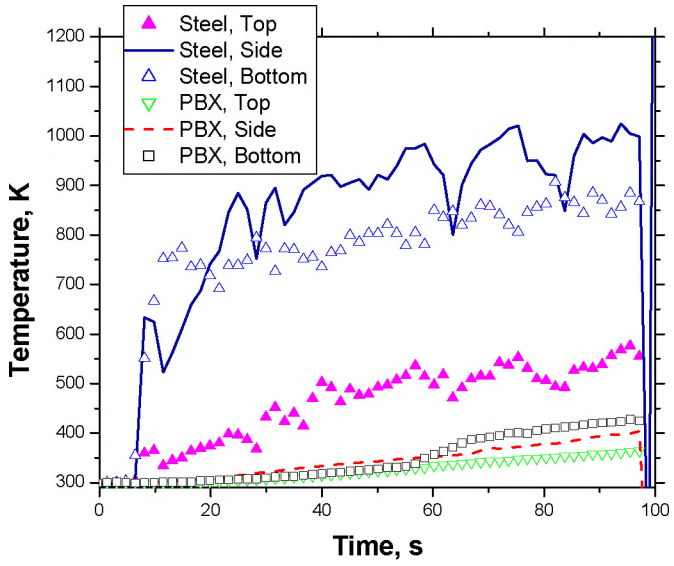

Figure 4.11. Temperatures at the Steel and PBX surfaces for test 5, fire, 1999.

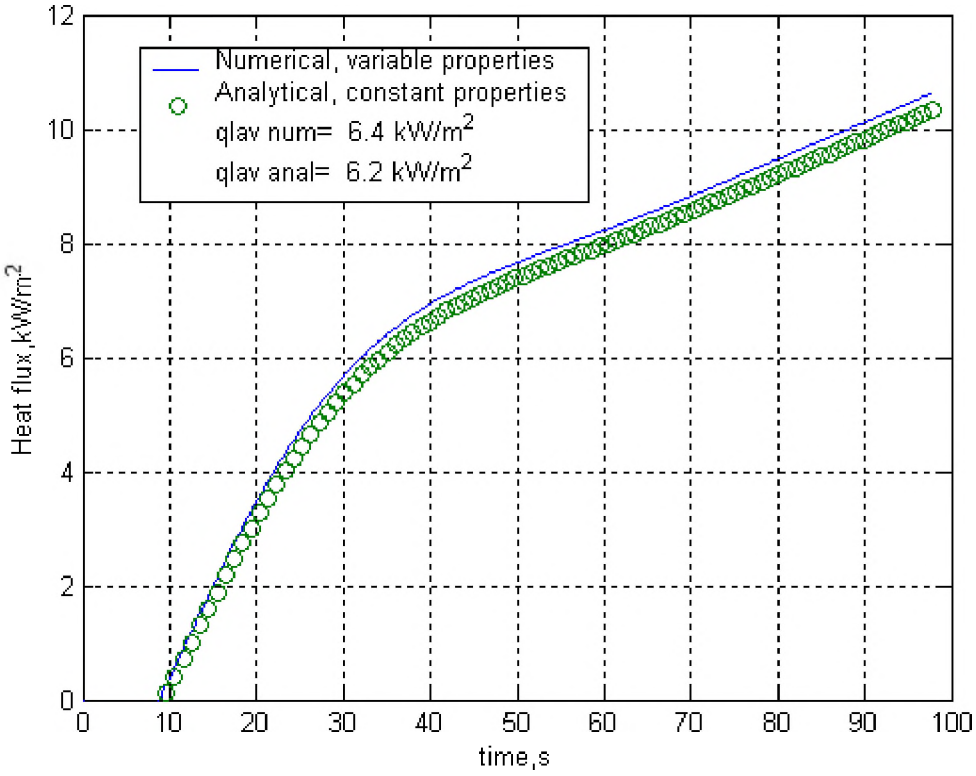

Figure 4.12. Heat flux at the explosive surface test 4, for fire, 1999.

4.1.6. THE FIRE TESTS AND THE IGNITION MODEL

The experimental times to ignition are compared to those given by the ignition model for HMX-based explosives (Beckstead, 1994). The model combines many of the physical and chemical mechanisms needed to describe the ignition process of HMX and predicts that the ignition time should decrease with increasing heat flux. It is important to mention that the model assumes that the explosive is exposed to a constant heat flux and that the reactions occur at atmospheric pressure. In this work it was shown that the heat flux presents a transient behavior (i.e. Heat flux on Figures 4.2, 4.6, 4.8, 4.10 and 4.12) and also that pressures are typical of highly confined systems (i.e., experimental pressures up 7500 psi, see for example Figures in Appendix B).

The average heat flux and the experimental ignition times for the fire tests are presented in Table 4.1. For comparison purposes, the average heat flux values are used in the ignition model to read the theoretical time from the ignition model and the values are also included in Table 4.1.These values are also compared graphically in the ignition plot in Figure 4.13. It can be seen that this work represents the only experimental data in the low heat flux regime of the ignition model plot. The trend of the data is consistent with the experimental work of Strakovski et al, 1989. Even though a direct comparison cannot be made with the ignition model, it is clear that there is a lack of understanding and further research is needed in the heating rate regime present in typical fire environments.

Table 4.1. Ignition times for the fire cookoff tests

Test #	Container Characteristics	Heat Flux, KW/m2	Experimental Ignition Time	Ignition Time Beckstead Model	Error, %
1*	N/A	19.8	1.75	1.28	-26
2	Unbounded, Unsealed	6.9	2.21	9.1	310
3	Unbounded, Unsealed	6.3	1.72	10.6	500
4	Unbounded, Sealed	7.3	2.35	8.0	240
5	Bonded, Sealed	6.4	1.63	10.3	530

*Test 1 used PBC-123 (85% HMX) while tests 2,3,4 and 5 used PBX-9501 (95% HMX)

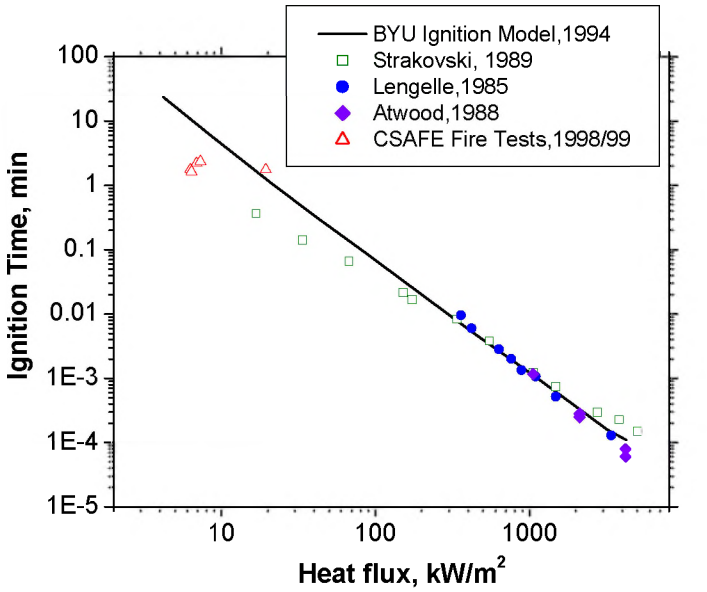

Figure 4.13. Experimental and numerical ignition times (After Beckstead, 1994)

4.2. ELECTRICAL TESTS

It was concluded in the last section that a big gap exists in the understanding of the thermal behavior of HMX-based explosives exposed to heating rates present in fires. The main uncertainty found in the fire cookoff experiments was measuring the steel surface temperature. As discussed in chapter 2, it was identified that electrical heaters could provide a well-defined boundary condition at the steel surface.

4.2.1. TEST 6, ELECTRICAL, JULY 2001

The ignition for this test took place at approximately 31 minutes. Because of the uncertainty in the time to explosion, only some thermocouple data was recovered. The temperature at the steel surface at the moment of the explosion was around 700 K. This was a very violent explosion and almost all the container and the explosive material were consumed, only four small pieces were found. Some comments on the thermal analysis of this test will be included in section 4.4. In addition, the data and some of the pictures for this test can be found in the appendices B and C included in the CD.

4.2.2. TEST 7, ELECTRICAL, AUGUST 2001

The voltage applied to this test was 220 Volts corresponding to a constant output of 76 kW/m^2. This heat flux is in the range of that found in fires. The explosion occurred after 189 seconds but the event was not nearly as violent as in test 6. About 70% of the explosive material was recovered from the test site.

The measured steel and PBX temperatures are presented in Figure 4.14. This electrical test shows a more uniform heating around the container than that of the fire tests described in section 4.1. As discussed in chapter 2, the PBX temperature was measured by thermocouples placed inside the explosive at 1.58 mm from the interface. This was intended not only to avoid interferences at the interface caused by the thermocouples but also, to have a more accurate location of them.

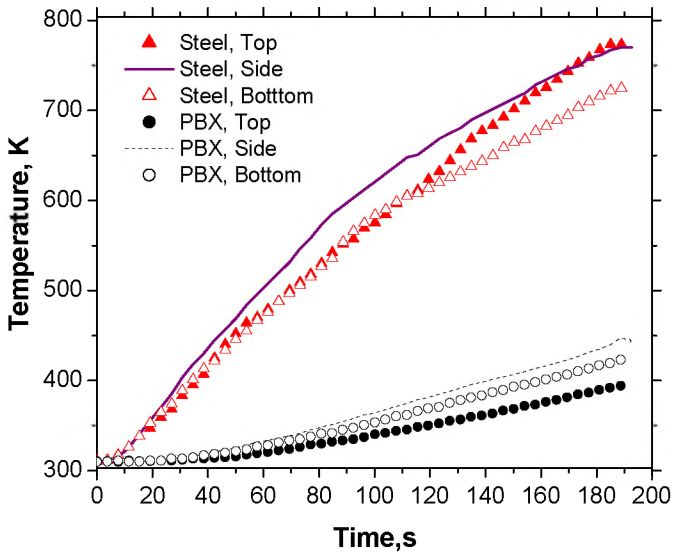

Figure 4.14. Measured temperatures for test 8, electrical, 2001.

Three numerical methods described in chapter 3 were used to calculate the heat flux at the explosive surface. The results are presented in Figure 4.15. In the legend, "Model" refers to the thermal-reaction model, "Duhamel" to the Duhamel superposition method and "IHC" to the Inverse Heat Conduction method.

The IHC and the Duhamel methods are based on the experimental temperatures and, therefore, the calculated heat flux is expected to be as accurate as directly measured

values. It is important to note that the thermal-reaction model is validated by agreeing not only with the experimental surface and interface temperatures (see Figure 4.16), but also with the heat flux given by the other methods (see Figure 4.15). A mathematical average of 9.4 kW/m^2 was obtained for the heat flux at the PBX surface. This value represents only 12 % of the total heat flux supplied by the electrical heater (at the steel pipe surface).

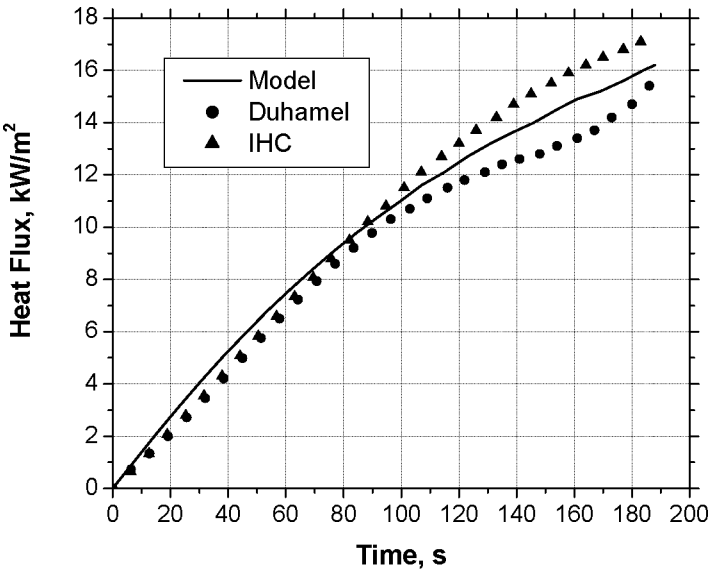

Figure 4.15. Heat Flux at the PBX surface for test 8, electrical, 2001.

The model predictions and the experimental values for the temperature of the steel and the explosive surface are presented in Figure 4.16. The good agreement confirms the existence of a contact resistance (or air gap) at the container/explosive interface. According to Figures 4.15 and 4.16, this gap seems to be the controlling mechanism of heat transfer across the interface. First at all, the inclusion of a contact resistance in the thermal-reaction model was strictly necessary to be able to match the experimental temperatures. An average of 0.6 mm was enough to drop the temperature at the interface by nearly 40%. On the other hand, revisiting Figure 4.15, the net difference between the thermal-reaction model and the other methods is the air gap definition. The thermal decomposition was not the controlling mechanism because of the similarity between Duhamel method and the thermal-reaction model.

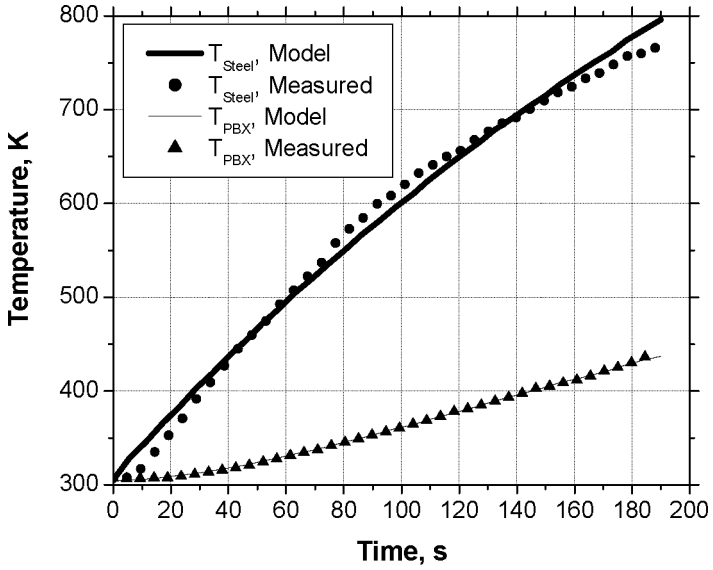

Figure 4.16. Numerical vs experimental for test 8, electrical, 2001.

4.2.3. TEST 8, ELECTRICAL, SEPTEMBER 2002

The voltage applied to this test was 110 Volts corresponding to a constant output of 19 kW/m^2. The explosion occurred after 1520 seconds (25.3 minutes), and was very comparable with test 6 in which most data was lost. The event was more violent than test 7. Very few metallic pieces were gathered from the test site (see chapter 2).

The measured steel and PBX temperatures were also very uniform around the container for this test, as presented in Figure 4.17. Even though, the ignition time for this test was almost 10 times the time for test 7, the temperatures at the PBX at the moment of the explosion were very comparable.

The inverse heat conduction method was used to evaluate the thermal conditions (i.e. Temperature and heat flux) at the PBX surface corresponding to the internally measured temperatures. This condition was then compared in Figure 4.18 to that given by the Thermal-reaction model and the Duhamel method. Very good agreement was found

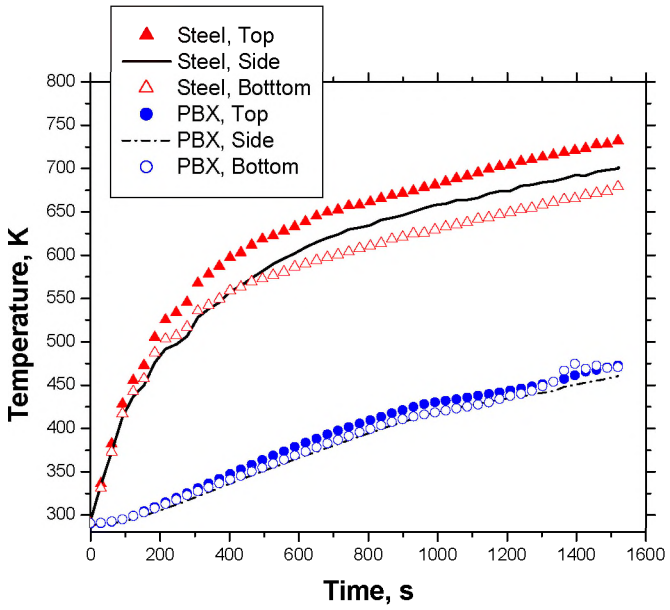

Figure 4.17. Measured temperatures for test 8, electrical, 2002

among the three methods. An average heat flux of 3.6 kW/m^2 was computed for the three methods. This value represents only 19 % of the total heat flux supplied by the electrical heater (at the steel pipe surface).

4.2.4. TEST 9, ELECTRICAL, NOVEMBER, 2002

Test 9 consisted of two tests distinguished in this report as test 9A and test 9B. The main goal for test 9 was to explore the cookoff behavior of HMX-based explosives in the low-heat flux regime in the ignition model (see Figure 4.13). The voltage was reduced by half (i.e. 55 Volts) and so the applied heat flux at the steel pipe was reduced by a factor of 4 compared to test 8. This was around 4.7 kW/m^2. This low heat flux (which, again, was intended to be low!) and the cold weather in November 2002 resulted in no ignition after 3 hours. The heating was suspended and the ordnance was cooled down. This corresponds to test 9A in this report. The same setup and instrumented container were used in test 9B. The voltage was increased to 110 Volts and the ignition occurred at 1520 seconds (25 minutes).

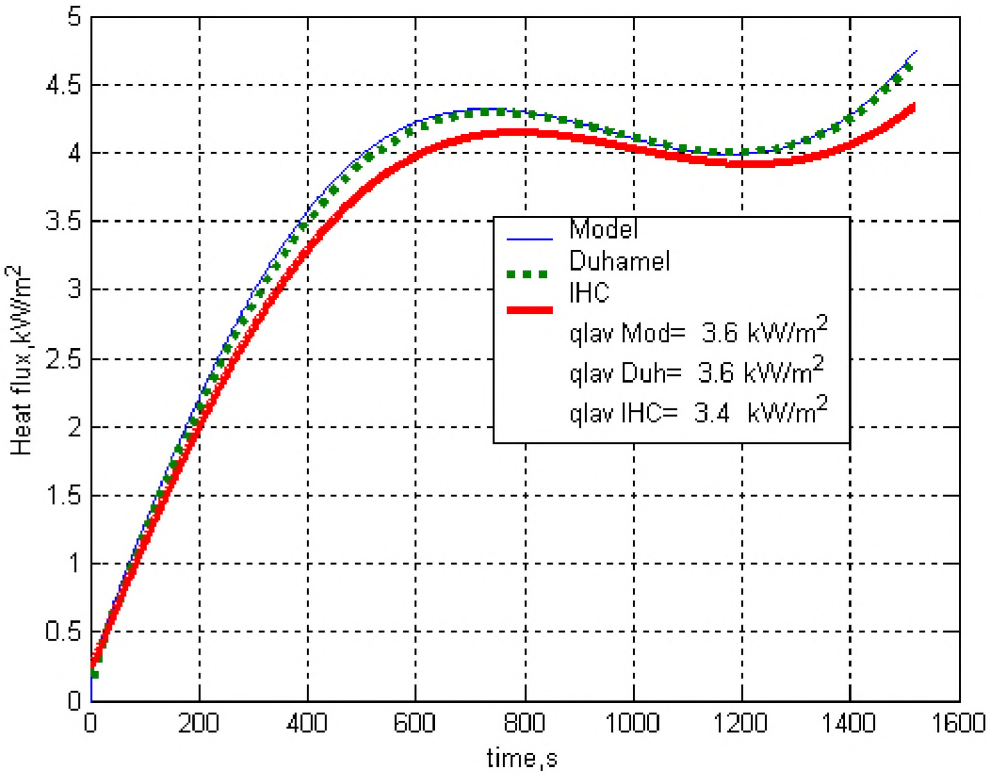

Figure 4.18. Heat flux at the PBX surface for test 8, electrical, 2002

The measured steel and PBX temperatures for test 9A are presented in Figure 4.19. Although the thermocouple at the top of the pipe was lost, the steel temperature seemed to be uniform around the container. The PBX temperature showed small differences (between 10 to 20 K) between the bottom and the top.

The heat flux at the explosive surface is presented in figure 4.20. The agreement is fairly good. The penetration of heat or diffusion length was estimated to be larger than the pipe radius and therefore, the semi-infinite assumption is not completely valid. However, the results of a 2-D version of the thermal-reaction model gave similar results. Thus, validating the 1-D approach. This is consistent with the work of others. An average of 0.8 kW/m^2 was computed. This represents 17 % of the heat supplied by the heater to the steel pipe.

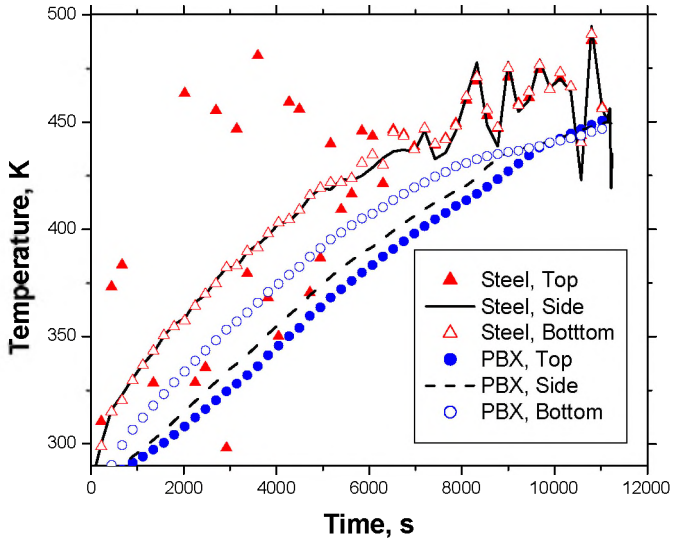

Figure 4.19. Measured temperatures for test 9A, electrical, 2002

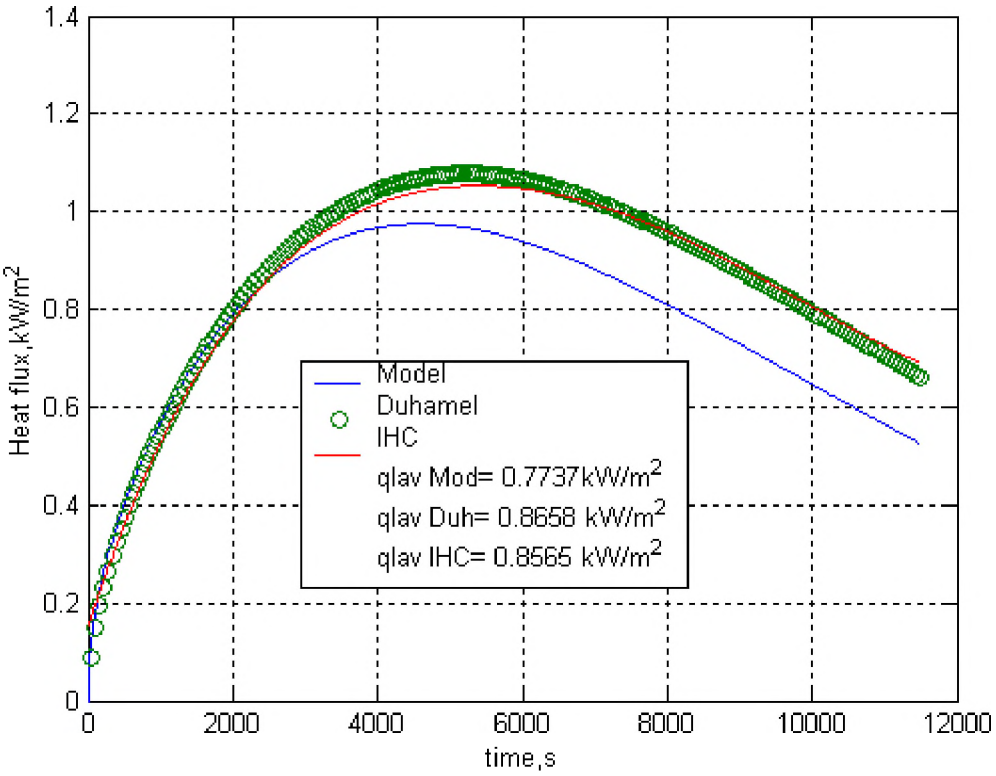

Figure 4.20. Heat flux at the at the PBX surface for test 9A, electrical, 2002 (No event)

The measured steel and PBX temperatures for test 9B are presented in Figure 4.21. Even though, the steel temperatures did not behave well, some uniformity in the temperatures can be appreciated for both materials. The temperatures at the PBX at the moment of the explosion were very comparable with the other tests.

The heat flux at the explosive surface is presented in Figure 4.22. The agreement, among the three different methods, is fairly good. The inverse heat conduction shows an overestimation, although, not very important if the average heat fluxes are compared. An average of 3 kW/m^2 was computed. This represents 16 % of the heat supplied by the heater to the steel pipe.

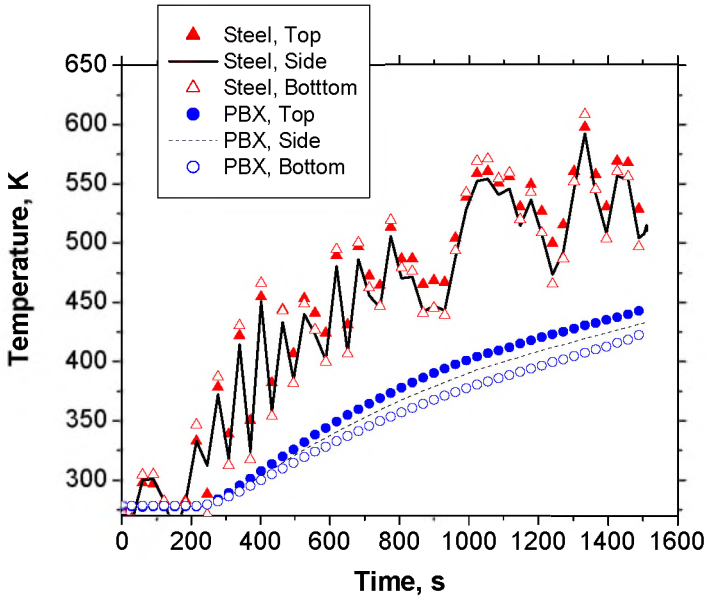

Figure 4.21. Measured temperatures for test 9B, electrical, 2002

4.2.5. TEST 10, ELECTRICAL, NOVEMBER, 2002

The main goal of test 10 was to explore the effects of no having a core in the explosive pellet. The voltage applied to this test was 110 Volts corresponding to a constant output of 19 kW/m^2. The explosion occurred after 1634 seconds (27.2 minutes), and was very comparable with test 6, 8, and 9B; however, the explosion was not nearly as violent.

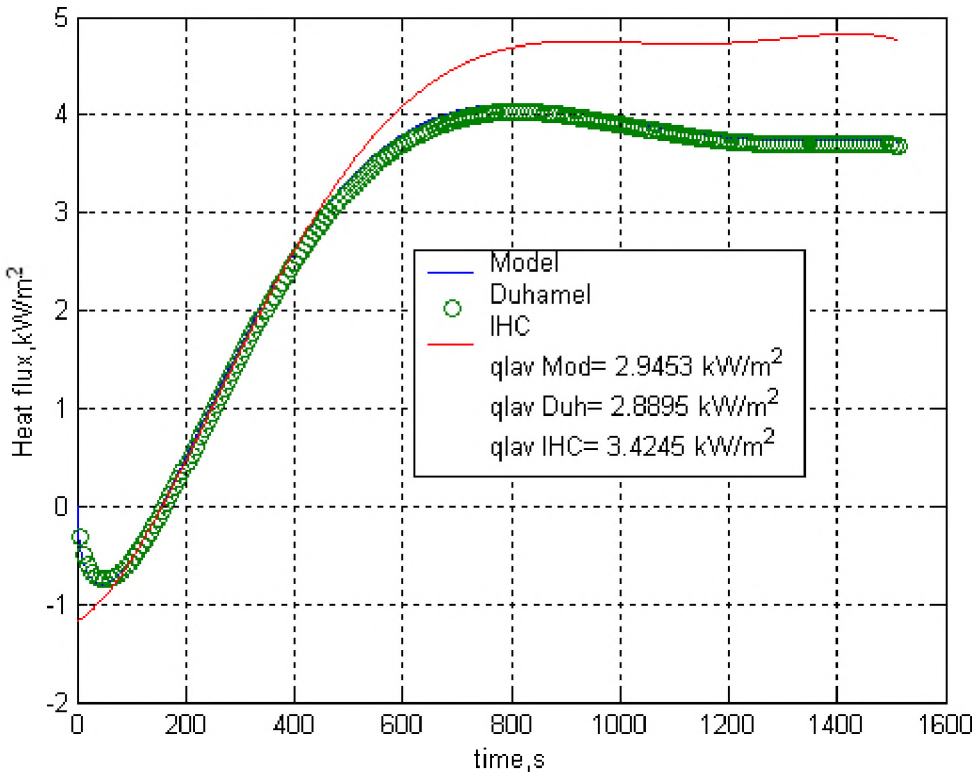

Figure 4.22. Heat flux at the PBX surface for test 9B, electrical, 2002

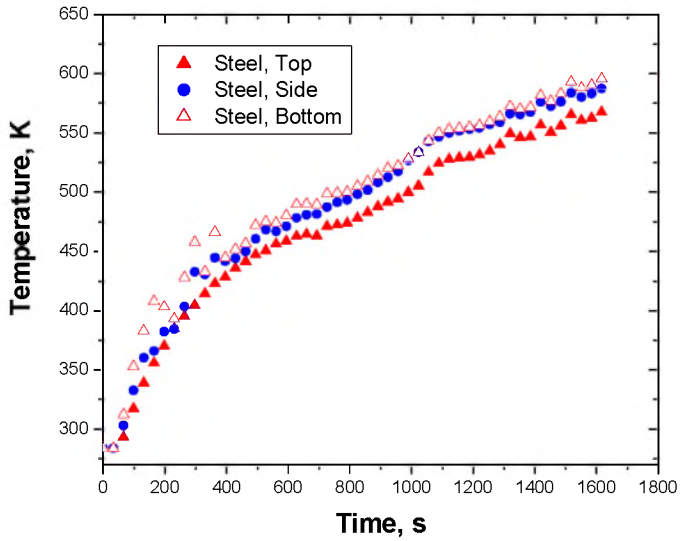

Figure 4.23. Experimental temperatures for test 10, electrical, 2002

The temperatures at the steel surface are presented in Figure 4.23. The steel temperatures were comparable to those obtained in test 9B. The similarities in steel temperatures and ignition time suggest that the heat flux at the explosive surface for this test must be also very close to that computed for test 9B.

4.2.6. THE IGNITION MODEL AND THE ELECTRICAL COOKOFF TESTS

The average of the computed heat fluxes and the experimental times to explosion for the electrical tests are compared in Table 4.2 and Figure 4.24 to those given by the ignition model for HMX-based explosives (Beckstead, 1994). It is important to mention again that the numerical ignition time is the value of time corresponding to the computed PBX heat flux in the ignition plot. It must not be confounded with the value predicted by the model proposed by Beckstead.

Table 4.2 Ignition times for the electrical cookoff tests

Test #	Steel Heat Flux, kW/m^2	PBX Heat Flux, kW/m^2	Time Experiment Ignition, min	Time from Ignition Plot, min	Error, %
6	18.9	3.6*	~30.0	32	6.7
7	75.8	9.4	3.2	5.0	56.2
8	18.9	3.6	25.3	32.0	26.4
9A**	4.7	0.8	192.4**	N/A	-
9B	18.9	3.0	25.2	45	78.5
10***	18.9	3.0***	27.2	45	65.4

*The heat flux for test 6 was assumed to be similar to that of test 8.

**There was not ignition for test 9A

***Test 10 did not have any internal instrumentation. The heat flux at the PBX was assumed to be similar to that of test 9B.

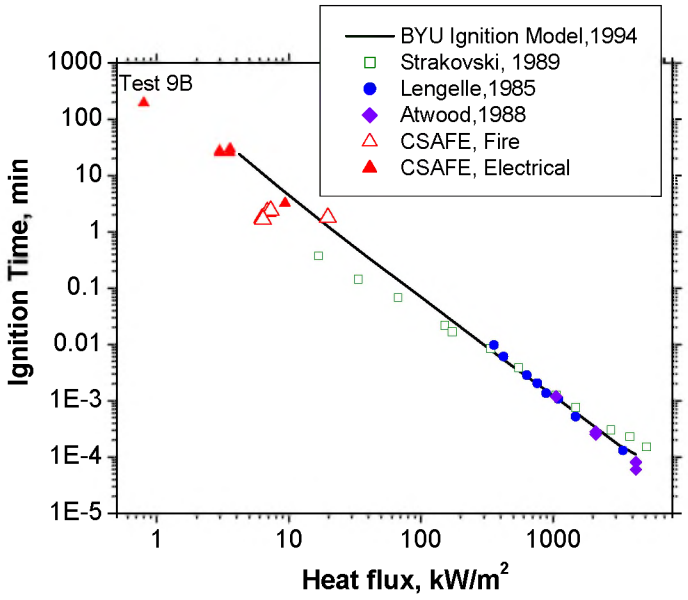

Figure 4.24. Experimental and numerical ignition times for HMX-based exposives.

Chapter 5

CONCLUDING REMARKS

A series of fast cookoff tests were carried out to represent an accident scenario where high-energy materials are exposed to a rapidly generated fire. The experiments were designed to develop a phenomenological understanding of the heat transfer in the overall system. Thermal boundaries at the fire/container and container/explosive interfaces were identified as critical for accomplishing the goals.

The initial experiments used propane burners but some uncertainties were found while measuring the steel surface temperatures. Then, it was identified that electrical heaters could provide heat fluxes in the same range of those found in fires with the additional advantage of a well-defined boundary at the steel surface. This helped to concentrate the efforts on the steel/explosive interface.

Three methods for heat transfer analysis were developed to study the thermal behavior of confined HMX-based explosives when heated by a fire or electricity. The first method used the Duhamel superposition principles to convert the measured surface temperature into heat flux. The second method used inverse heat equations to calculate the thermal boundaries at the surface from temperature measurement made within the explosive. The third method used a finite difference technique to model the overall system and thus, evaluate the relative importance of the different mechanisms of heat transfer.

The heat transfer analysis has demonstrated that there was a significant thermal contact resistance at the interface between the explosive material and the steel shell that resulted in a significant delay in the time to explosion. It was shown that an air gap could have been the responsible for this resistance.

The average heat flux at the explosive surface was between 12 and 20% of the heat flux applied to the steel surface. This confirms the effectiveness of the air gap and also the small diffusion length due to the insulating properties of the explosive

A comparison of the three numerical methods has revealed that conduction through the air gap may be the controlling mechanism of heat transfer across the steel/explosive interface.

The accuracy in the heat flux calculations is crucial in predicting the time to explosion with any suitable model. In this report, the numerical heat transfer results and the experimental times were compared with the ignition model proposed by Beckstead. An average heat flux was used because the current version of the ignition model assumes that the explosive is exposed to a constant heat flux.

A graphical comparison has shown that the data presented in this report follow the same trend of the ignition model. In general, a better agreement was found for the electrical tests than for the fire tests. Many reasons can be inferred from the differences between the tests. For instance, the fire tests used a cylindrical container that was 3 times longer or had 3 times more explosive than the one used in the electrical tests. Also, fire experiments are greatly influenced by weather conditions (i.e. wind influences non-uniform heating around the container).

Chapter 6

REFERENCES

1. Beck, J. B. Blackwell and St. Clair, Ch. 1985. *Inverse heat conduction: ill posed problems*, John Wiley Interscience publication, pp. 55.

2. Beckstead, M., 1994, "An Ignition Model for Modern Double Base Propellants," *31st JANNAF Combustion Meeting*, Sunnyvale, CA, pp. 163-180.

3. Burggraf, O. R., 1964, "An Exact Solution of the Inverse Problem in Heat Conduction. Theory and Applications," *ASME Journal of Heat Transfer*, 86, pp.373-382.

4. Buttsworth, D. R., and Jones, T. V., 1997, "Radial Conduction Effects in Transient Heat Transfer Experiments," *AIAA J.*, **101** (1005), pp. 209-212.

5. Carnahan, B., Luther, H. A., and Wilkes, J. O., 1969, *Applied Numerical Methods,* Krieger Publishing Company, pp. 429-530, Chap. 7.

6. Cook, W. and Felderman E., 1966, "Reduction of Data from Thin-Film Heat Transfer: A Concise Numerical Technique," *AIAA Journal*, 4 (3), pp.561-562.

7. Diller, T.E., 1996, "Methods of Determining Heat Flux from Temperature Measurements," *Proceedings of the International Instrumentation Symposium,* Instrument Society of America, pp. 251-262.

8. DiNenno, P., Appendix B, Property Data, in: The SFPE Handbook of Fire Protection Engineering, second edition, 1995, pp. A-26.

9. Gibbs, T. and Popolato, A., 1980, *LASL Explosive Property Data*, The University of California Press, Berkeley, CA, pp. 109-119.

10. Hills, R. G., and Hensel, Jr. E. C., 1986, "One-Dimensional Nonlinear Inverse Heat Conduction Technique," *Numerical Heat Transfer*, 10, pp. 369-393.

11. Kakac, S. and Yener, Y., 1993, *Heat Conduction*, Taylor & Francis, pp. 56-57, Chap. 3.

12. Online Material Property Data Sheet at www.matweb.com

13. McGuire, R. R., and Tarver, C. M., 1981, "Chemical Decomposition Models for the Thermal Explosion of Confined HMX, TATB, RDX and TNT Explosives," *Seventh International Symposium on Detonation*, Annapolis, MD, pp.56-64.

14. Menikoff, R. and Sewell, T., 2001, "Constituent Properties of HMX Needed for Meso-Scale Simulations," *Theoretical Division, Los Alamos National Laboratory*, Los Alamos, NM. Available online at: http://t14web.lanl.gov/Staff/rsm/Preprints/HMXmeso.pdf

15. Murry, R. L., 1998, "CSAFE Cookoff test #1", *Report TR11566, Thiokol Corporation*, Brigham City, November.

16. Murry, R. L., 1998, "CSAFE Cookoff Tests, Phase III," *Report TR12646, Thiokol Corporation,* Brigham City, September.

17. Murry, R. L., 1999, "CSAFE Cookoff Tests CY1999," *Report TR11996, Thiokol Corporation*, Brigham City, December.

18. Pershing, D., 2000, Center for the Simulation of Accidental Fires and Explosions, Annual Report, 2000, University of Utah, Salt Lake City, Ut., Available online at http://www.csafe.utah.edu/documents/FY01annual.pdf

19. Eddings, E., and Sarofim, A., 1999, CSAFE Validation, Available online at http://www.combustion.utah.edu/main.html?http://www.combustion.utah.edu/programs.html

APPENDIX A AND OTHER FILES INCLUDED IN THE CD

The CD contains three major folders: Data, Pictures, Report.

DATA: This folder contains all the data in Excel and Origin files. There are two different origin files; one contains the original data and the other all the plots. For convenience, the plots are then collected in a single file (see Appendix A files)

PICTURES: This folder contains all the pictures taken at the experimental site. They are ordered by subfolders according to the test.

REPORT: This folder contains the electronic version of each chapter, the full report, and the appendixes.

APPENDIX A: This appendix contains all the plots from the cookoff tests. Due to its extension, only the electronic files have been included. For convenience, different formats of the files are saved in the CD. Here is an explanation of them.

APPENDIXA.doc: Large file. Contains the plot pasted as Origin objects. Allows modification of the plots.

APPENDIXA.pdf: Small file, it corresponds to APPENDIXA.doc.

APPENDIXA_pict.doc: Small file. Contains the plots pasted as pictures.

APPENDIXA_pict.pdf: Small file, corresponding to APPENDIXA_pict.doc

APPENDIX B: This appendix was included in the report for the sake of the discussion. It contains all the plots from the tests in a comparison form. That is, multiple temperatures are included in the same plot in order to easily see or comment about the particular behavior in one test.

APPENDIX B

PLOTS, TEST 1, FIRE, NOVEMBER 1998

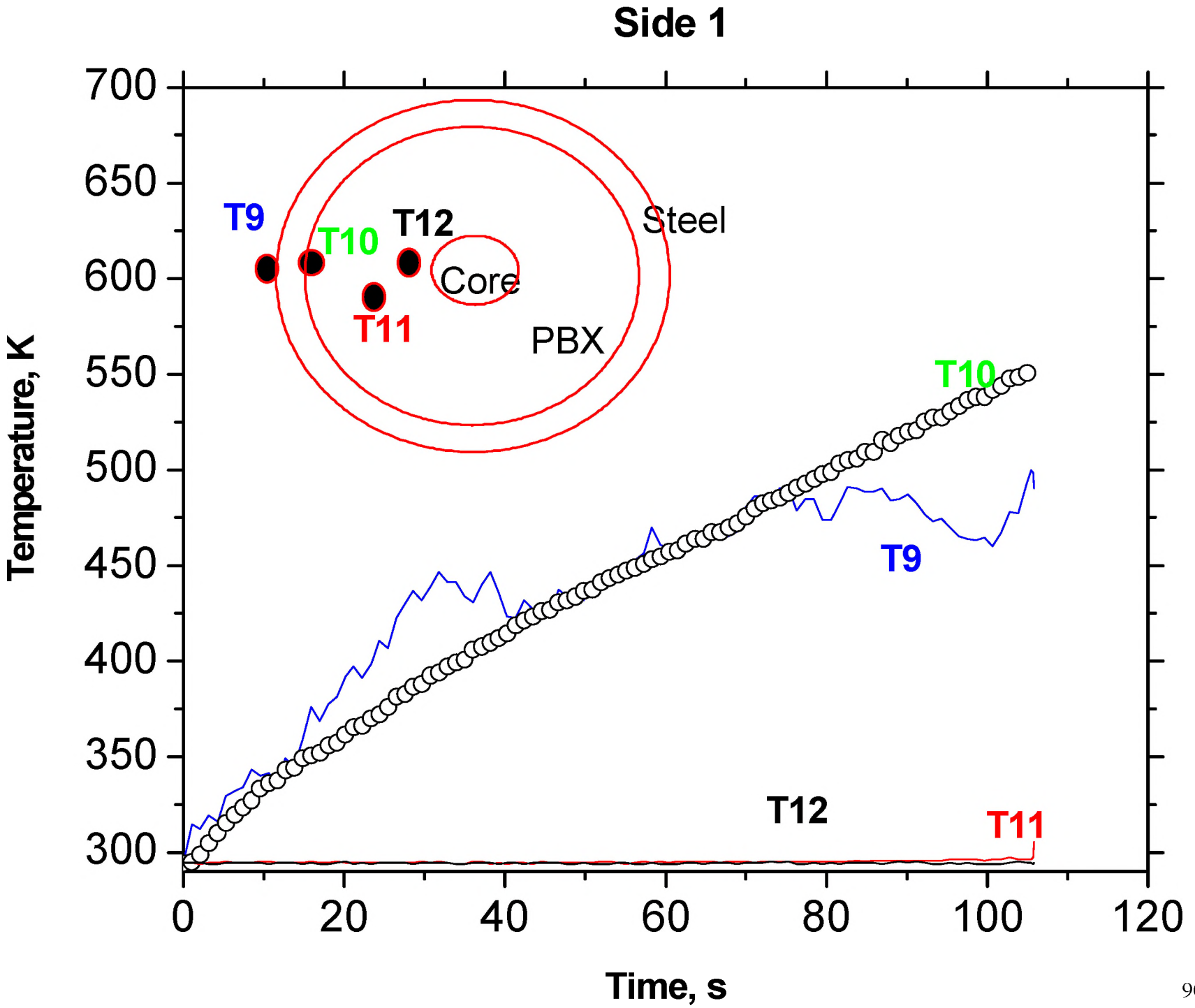
Side 1
Temperature, K
Time, s
700
650
600
550
500
450
400
350
300
0
20
40
60
80
100
120
T9
T10
T12
T11
Steel
Core
PBX

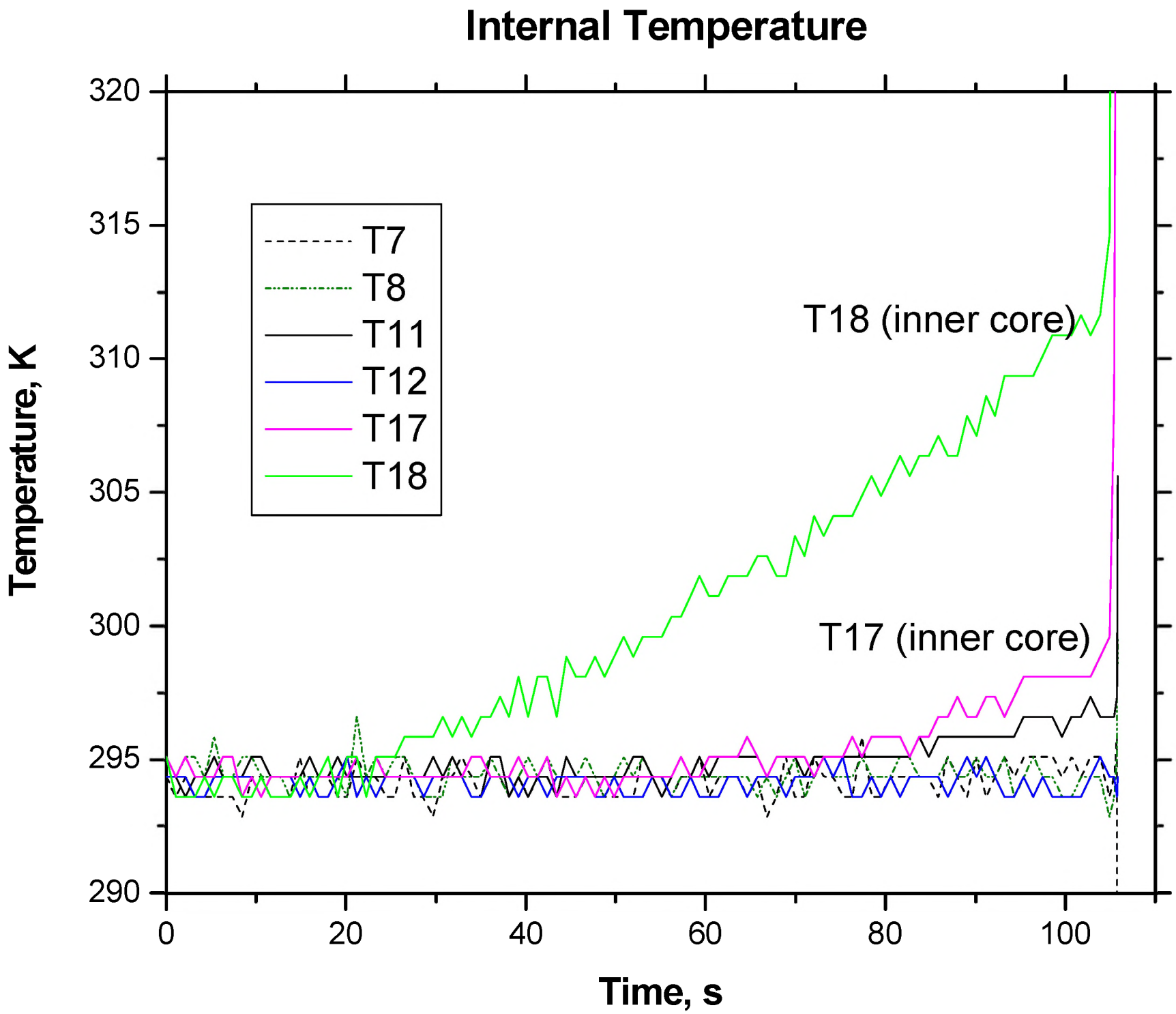
Internal Temperature
Temperature, K
Time, s
320
315
310
305
300
295
290
0
20
40
60
80
100
T7
T8
T11
T12
T17
T18
T18 (inner core)
T17 (inner core)

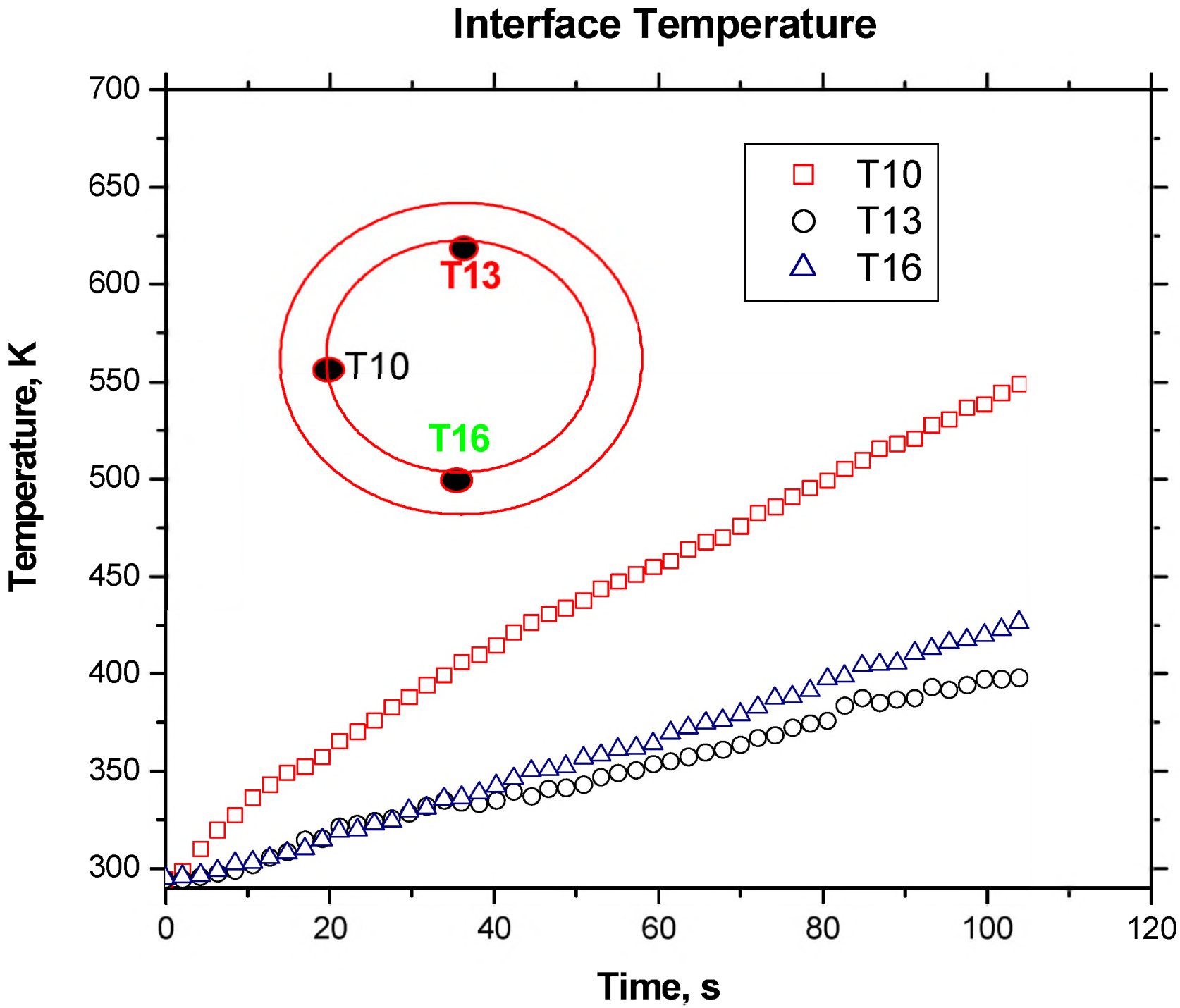
Interface Temperature
Temperature, K
Time, s
700
650
600
550
500
450
400
350
300
0
20
40
60
80
100
120
T10
T13
T16
T13
T10
T16

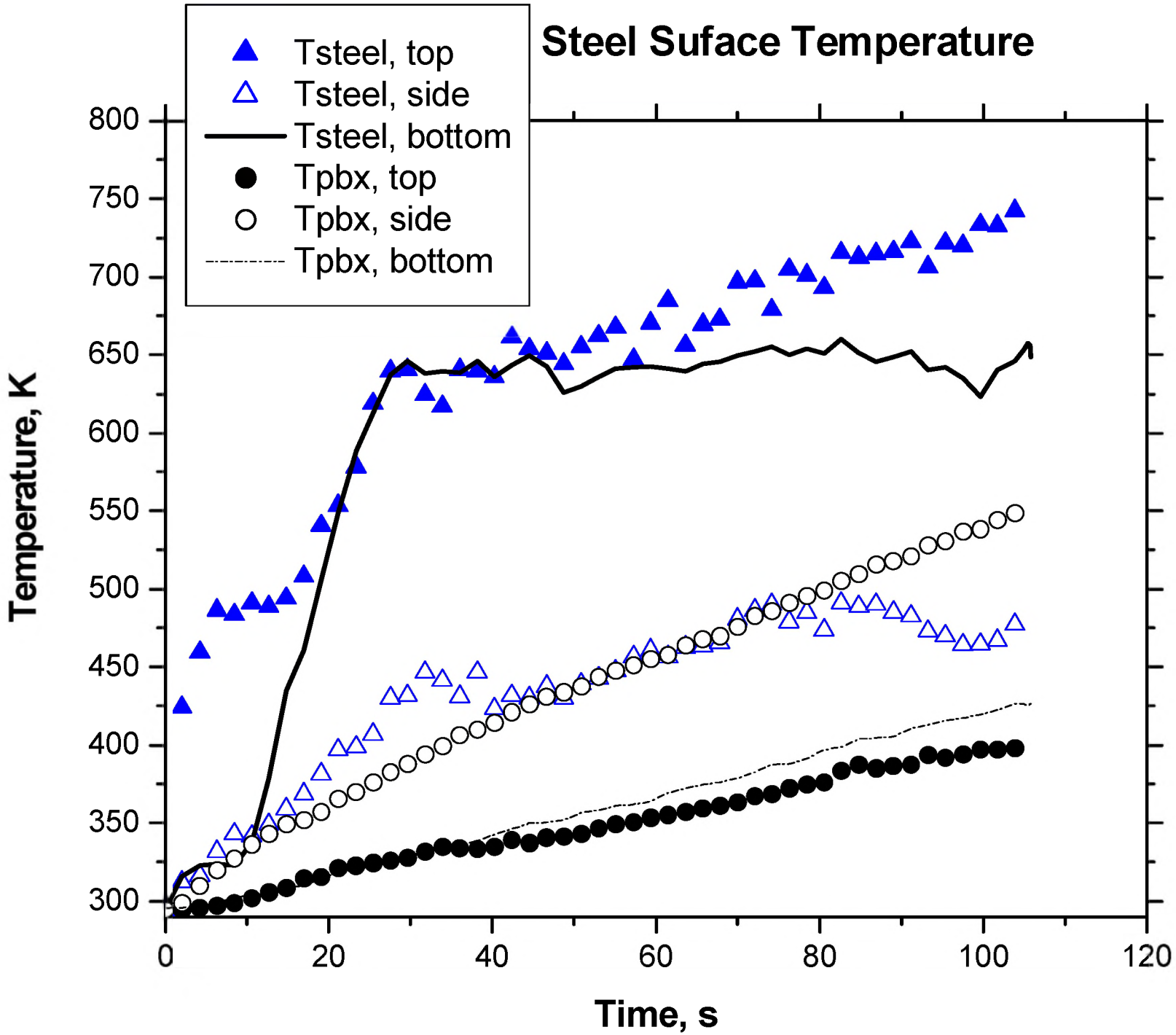
Steel Suface Temperature
Tsteel, top
Tsteel, side
Tsteel, bottom
Tpbx, top
Tpbx, side
Tpbx, bottom
Temperature, K
Time, s
800
750
700
650
600
550
500
450
400
350
300
0
20
40
60
80
100
120

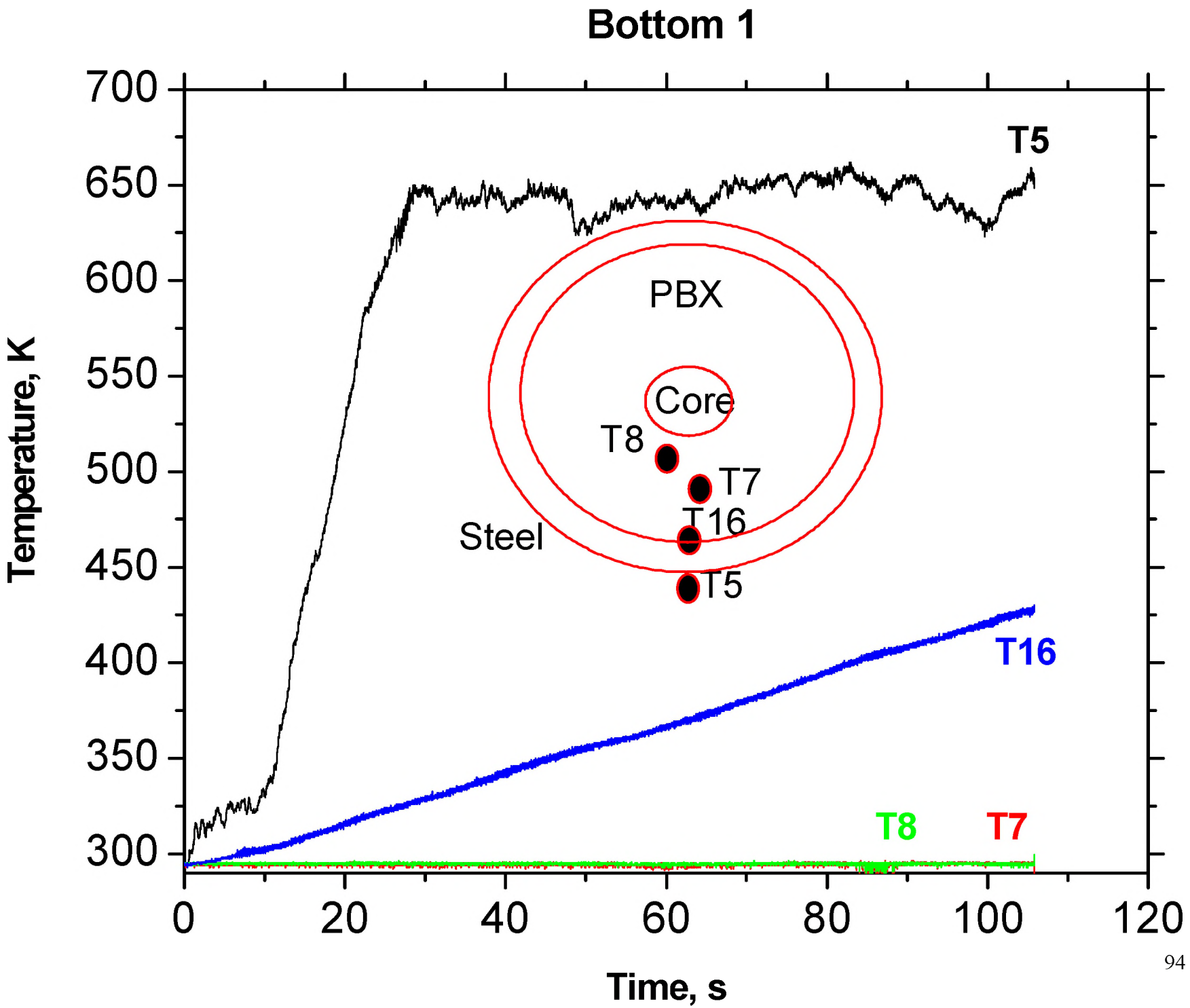
Bottom 1
Temperature, K
Time, s
700
650
600
550
500
450
400
350
300
0
20
40
60
80
100
120
T5
PBX
Core
T8
T7
T16
Steel
T5
T16
T8
T7

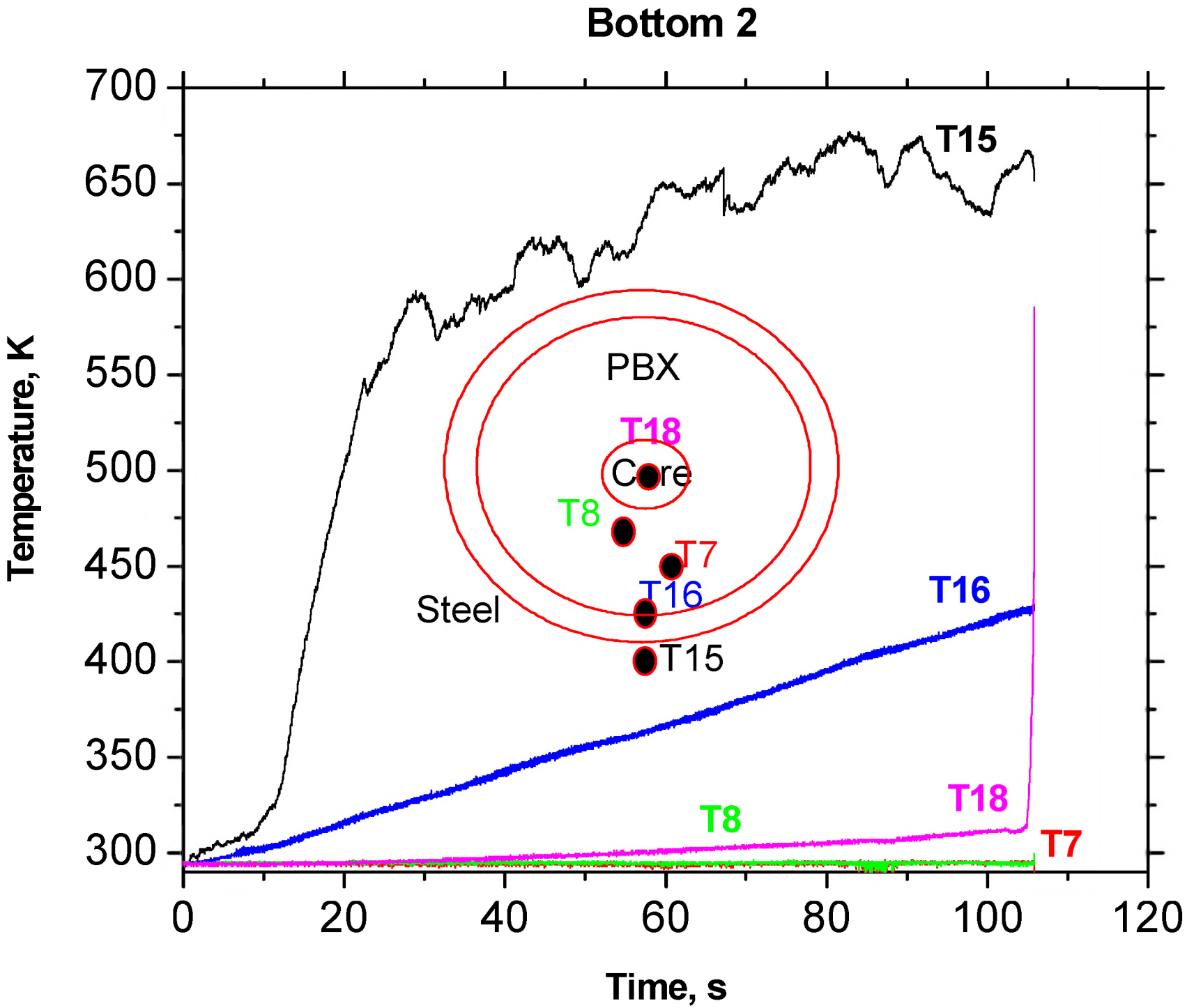
Bottom 2
Temperature, K
Time, s
700
650
600
550
500
450
400
350
300
0
20
40
60
80
100
120
T15
PBX
T18
Core
T8
T7
T16
Steel
T15
T16
T18
T8
T7

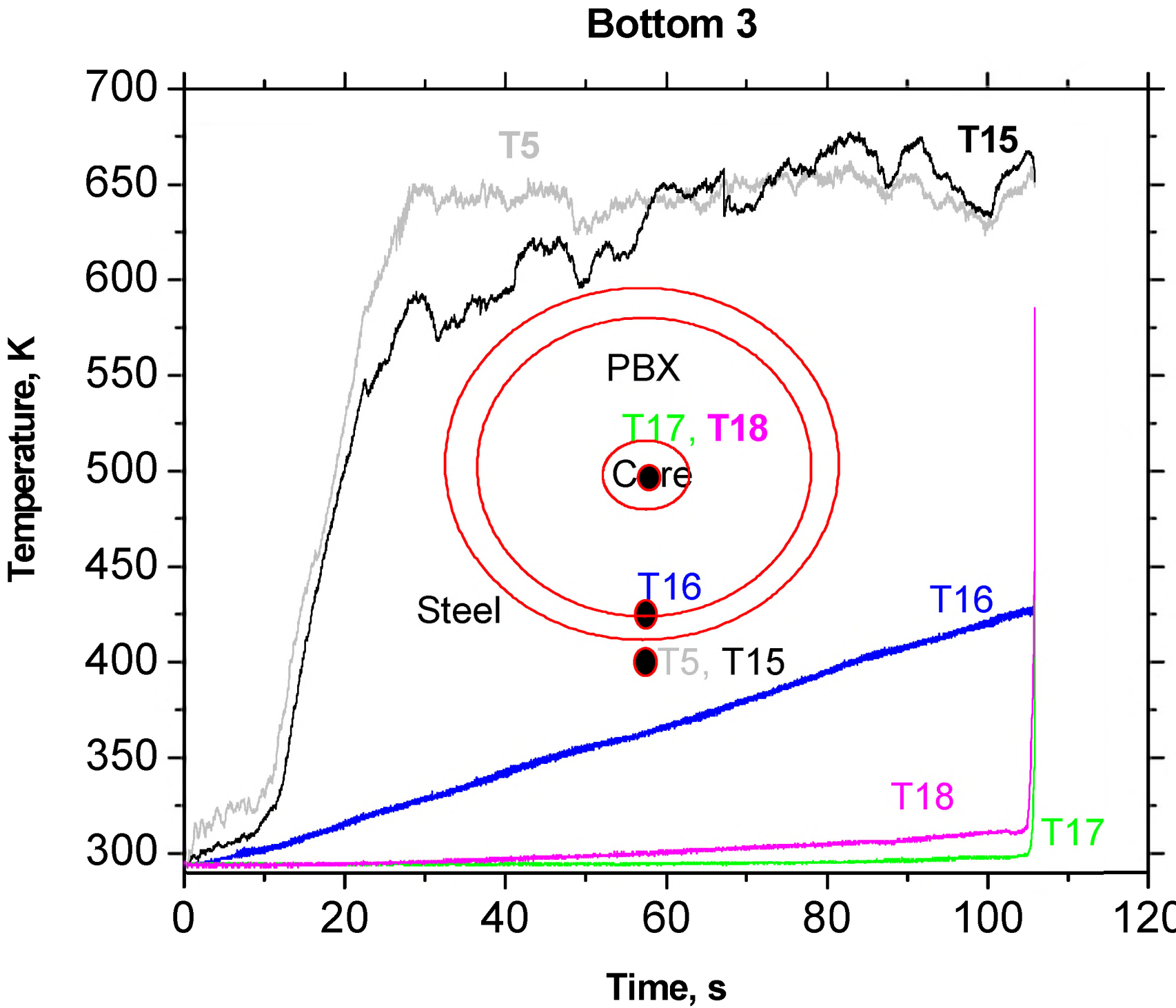
Bottom 3
Temperature, K
Time, s
700
650
600
550
500
450
400
350
300
0
20
40
60
80
100
120
T5
T15
PBX
T17, T18
Core
T16
Steel
T5, T15
T16
T18
T17

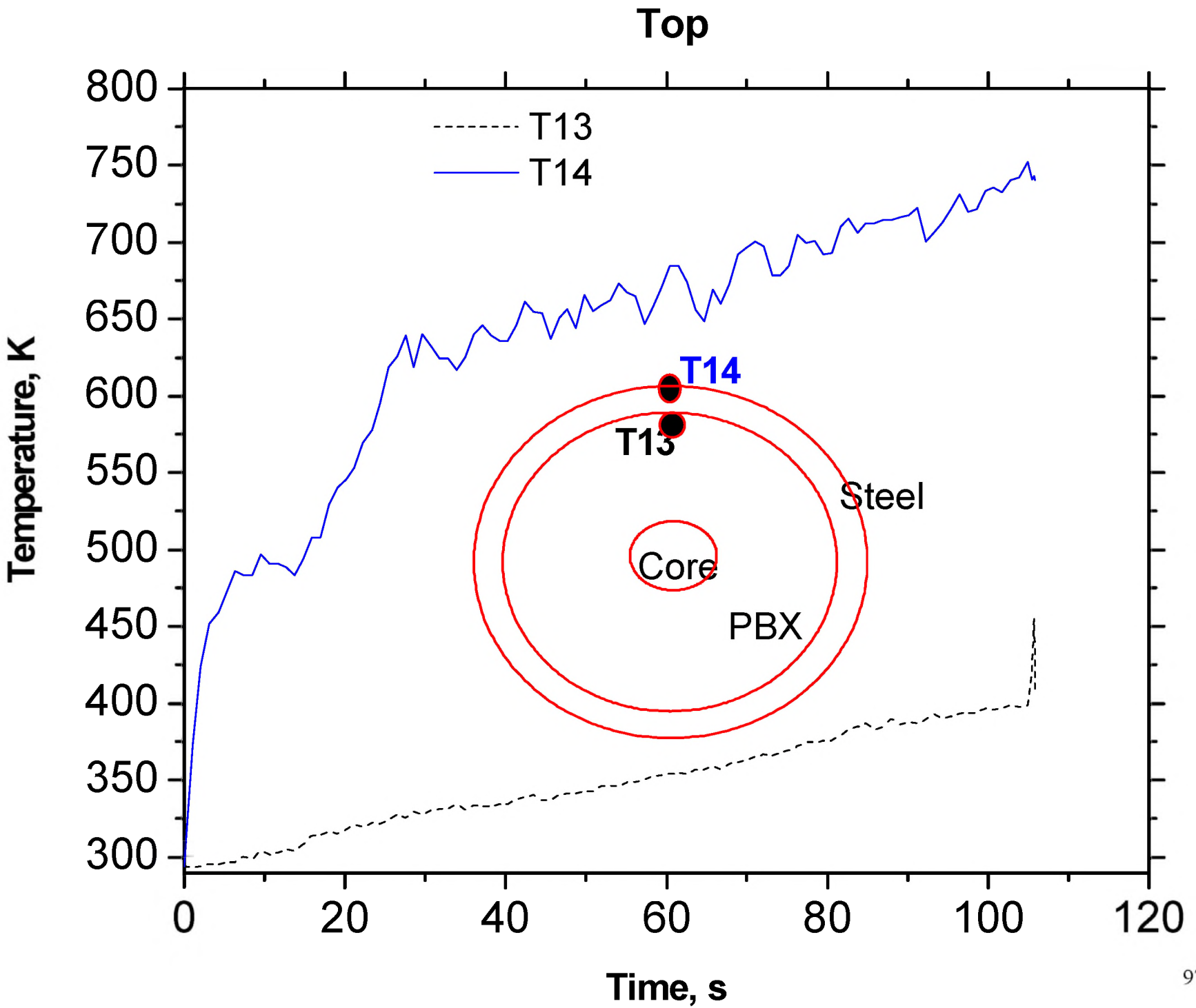
Top
T13
T14
T14
T13
Steel
Core
PBX
Temperature, K
Time, s
800
750
700
650
600
550
500
450
400
350
300
0
20
40
60
80
100
120

PLOTS, TEST 2, FIRE, OCTOBER 1999

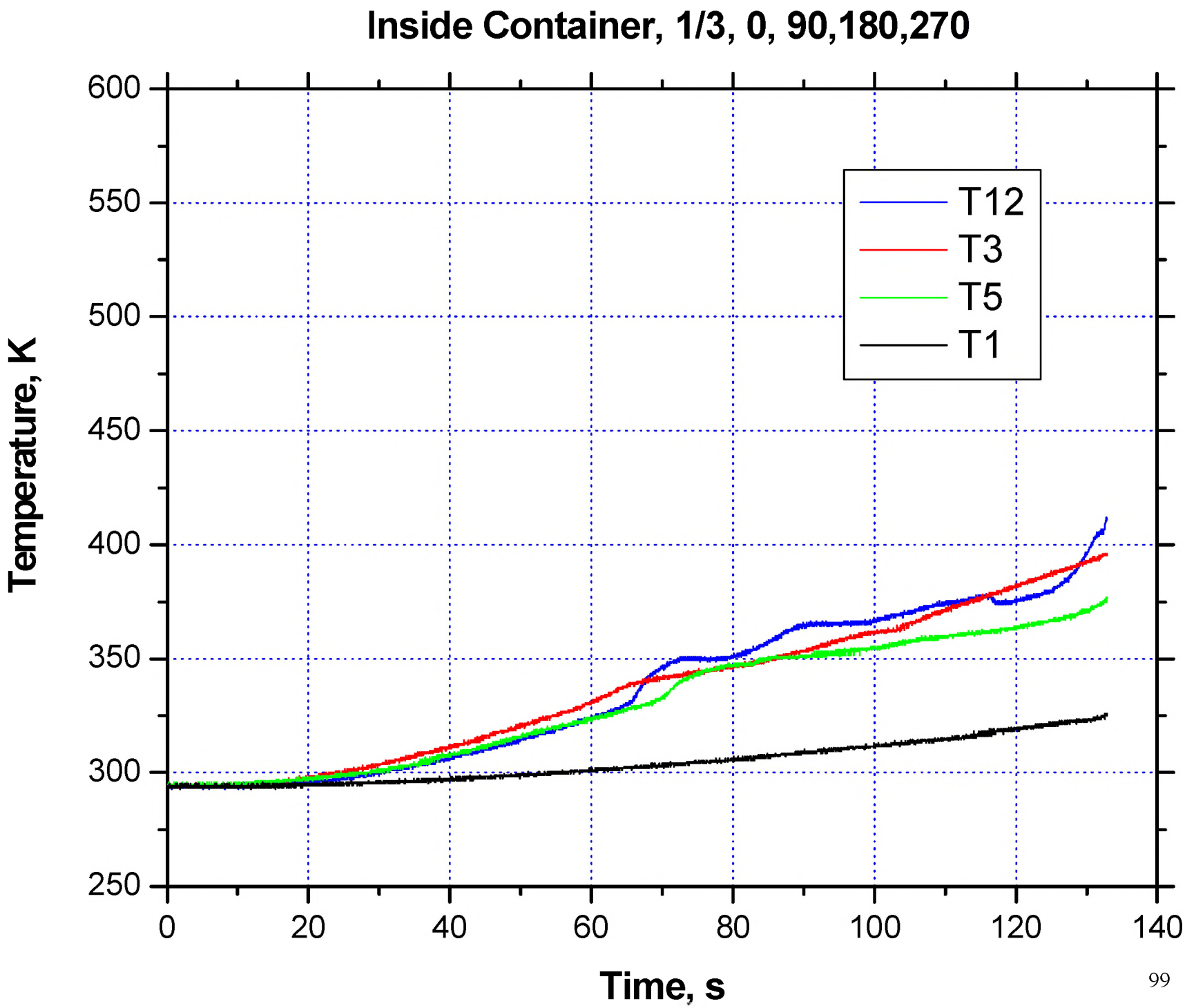
Inside Container, 1/3, 0, 90,180,270
Temperature, K
Time, s
T12
T3
T5
T1
600
550
500
450
400
350
300
250
0
20
40
60
80
100
120
140

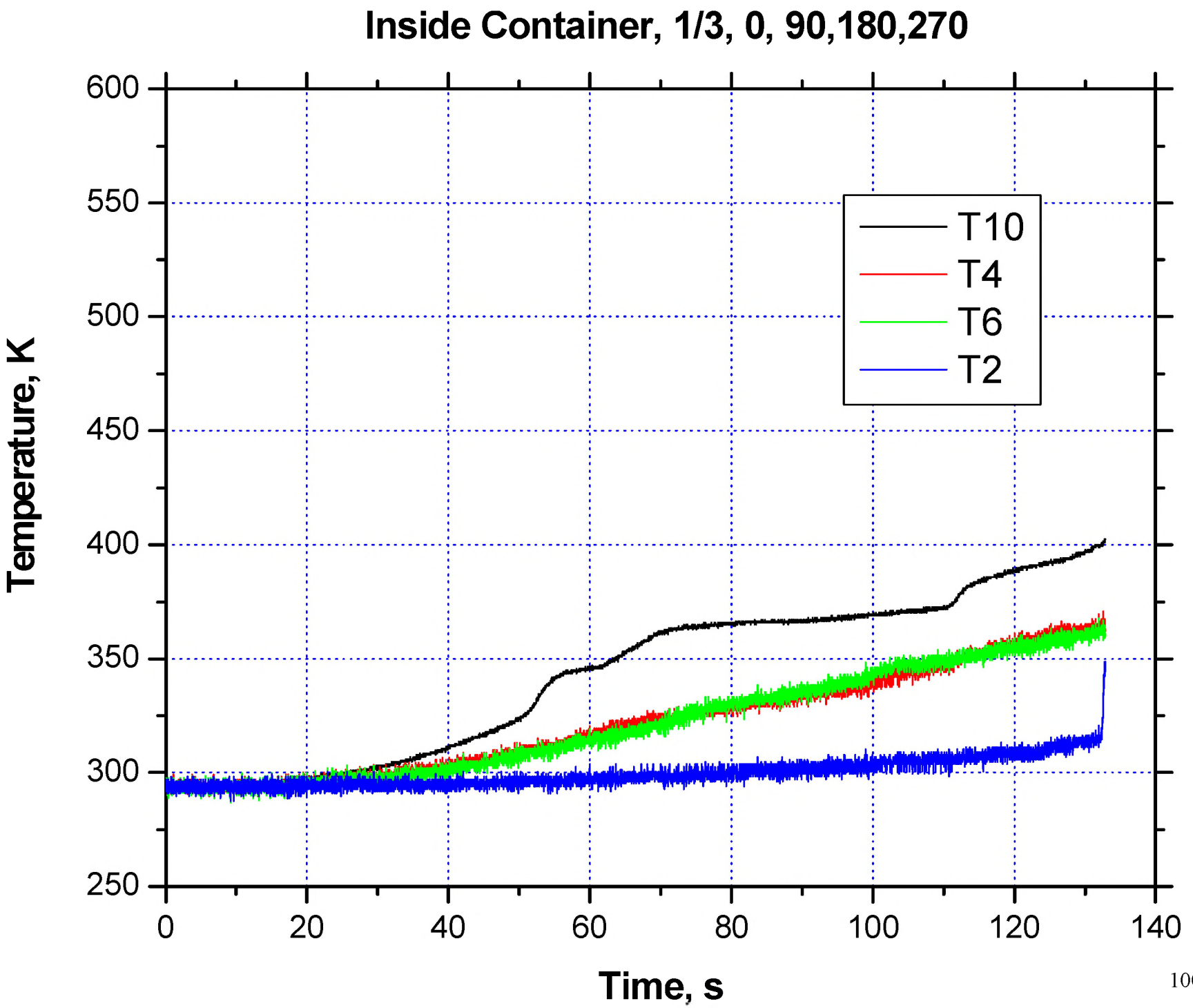
Inside Container, 1/3, 0, 90,180,270
Temperature, K
Time, s
T10
T4
T6
T2
600
550
500
450
400
350
300
250
0
20
40
60
80
100
120
140

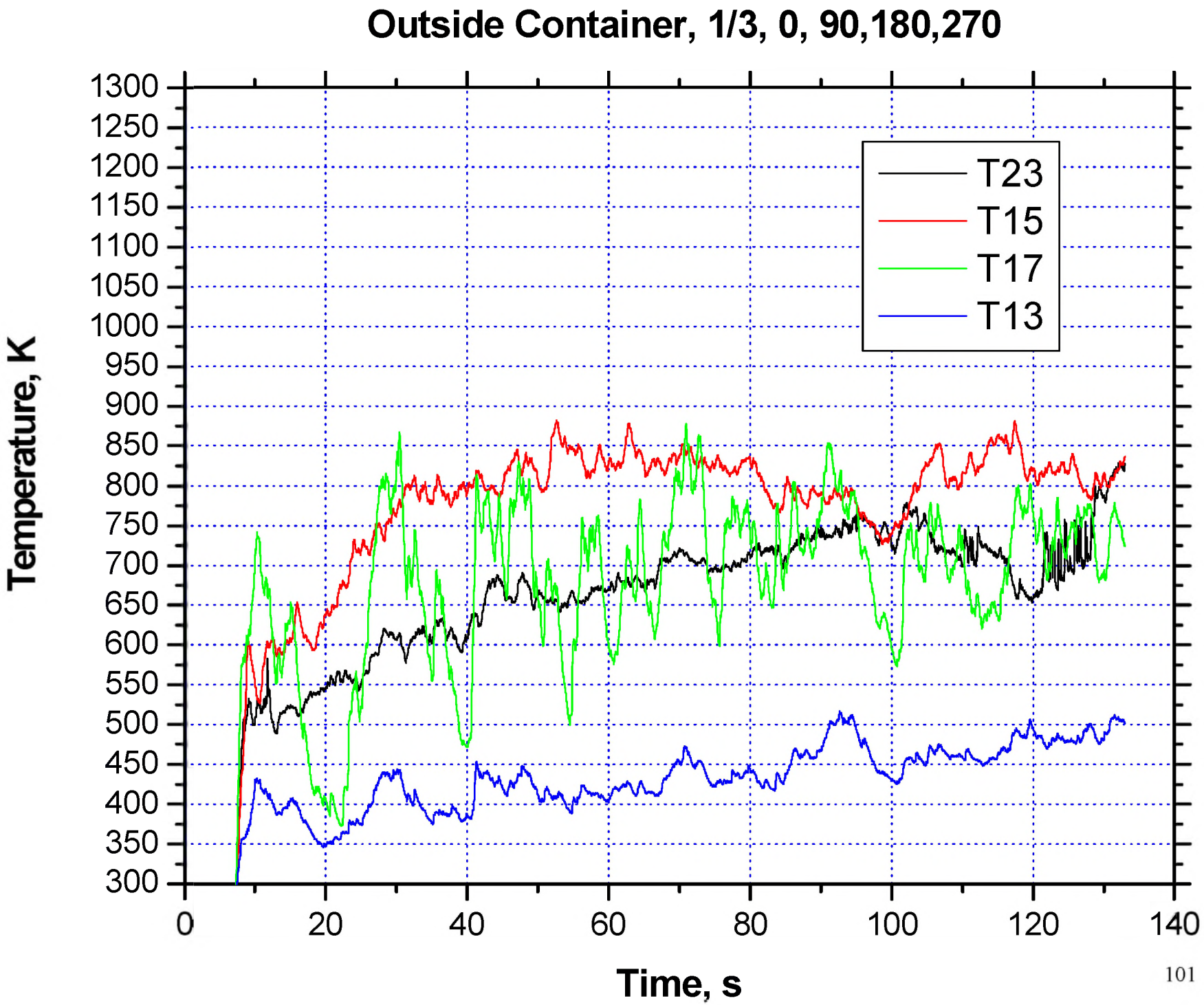
Outside Container, 1/3, 0, 90,180,270
Temperature, K
Time, s
T23
T15
T17
T13
1300
1250
1200
1150
1100
1050
1000
950
900
850
800
750
700
650
600
550
500
450
400
350
300
0
20
40
60
80
100
120
140

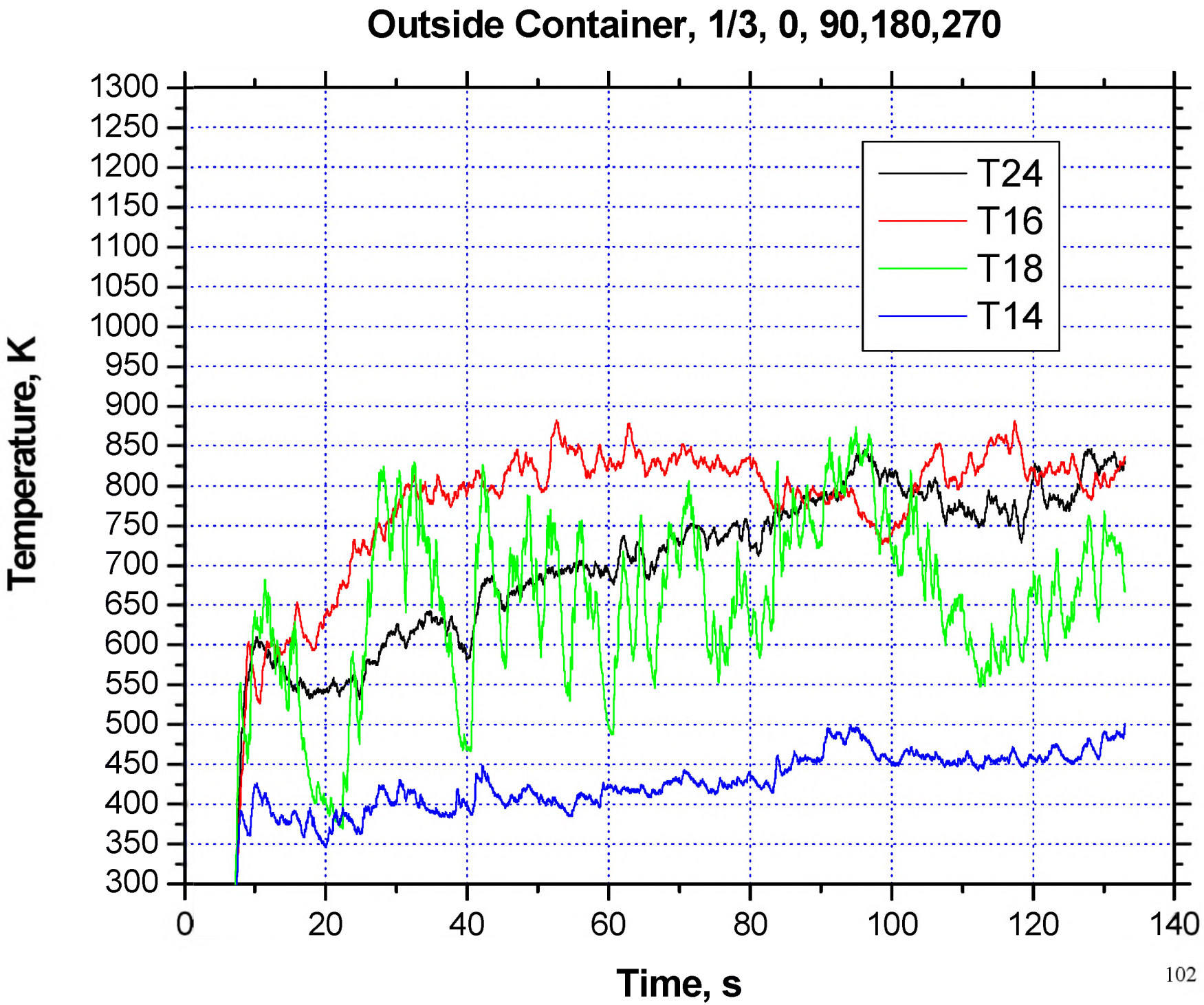
Outside Container, 1/3, 0, 90,180,270
Temperature, K
Time, s
T24
T16
T18
T14
1300
1250
1200
1150
1100
1050
1000
950
900
850
800
750
700
650
600
550
500
450
400
350
300
0
20
40
60
80
100
120
140

PLOTS, TEST 3, FIRE, OCTOBER 1999

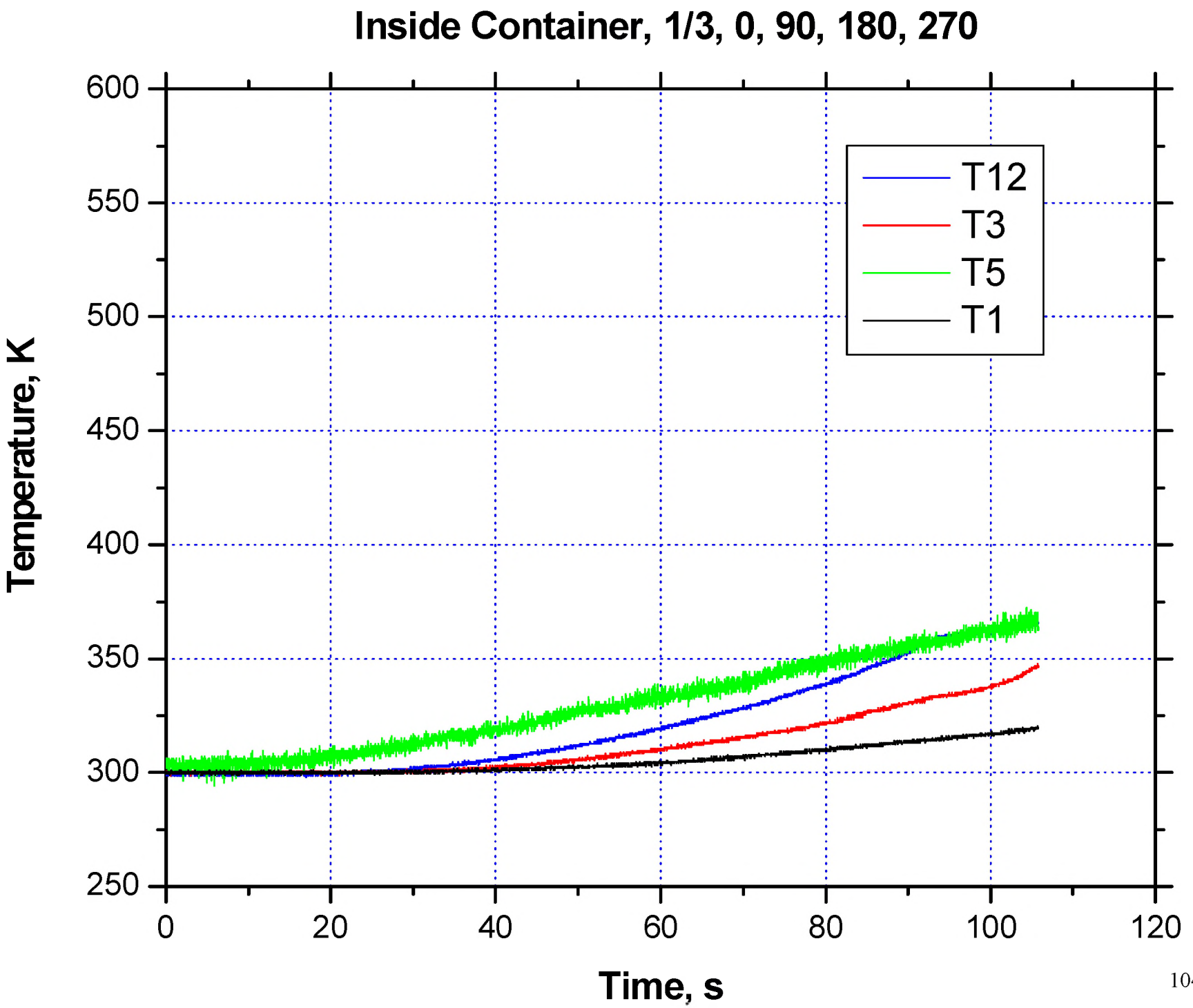
Inside Container, 1/3, 0, 90, 180, 270
Temperature, K
Time, s
600
550
500
450
400
350
300
250
0
20
40
60
80
100
120
T12
T3
T5
T1

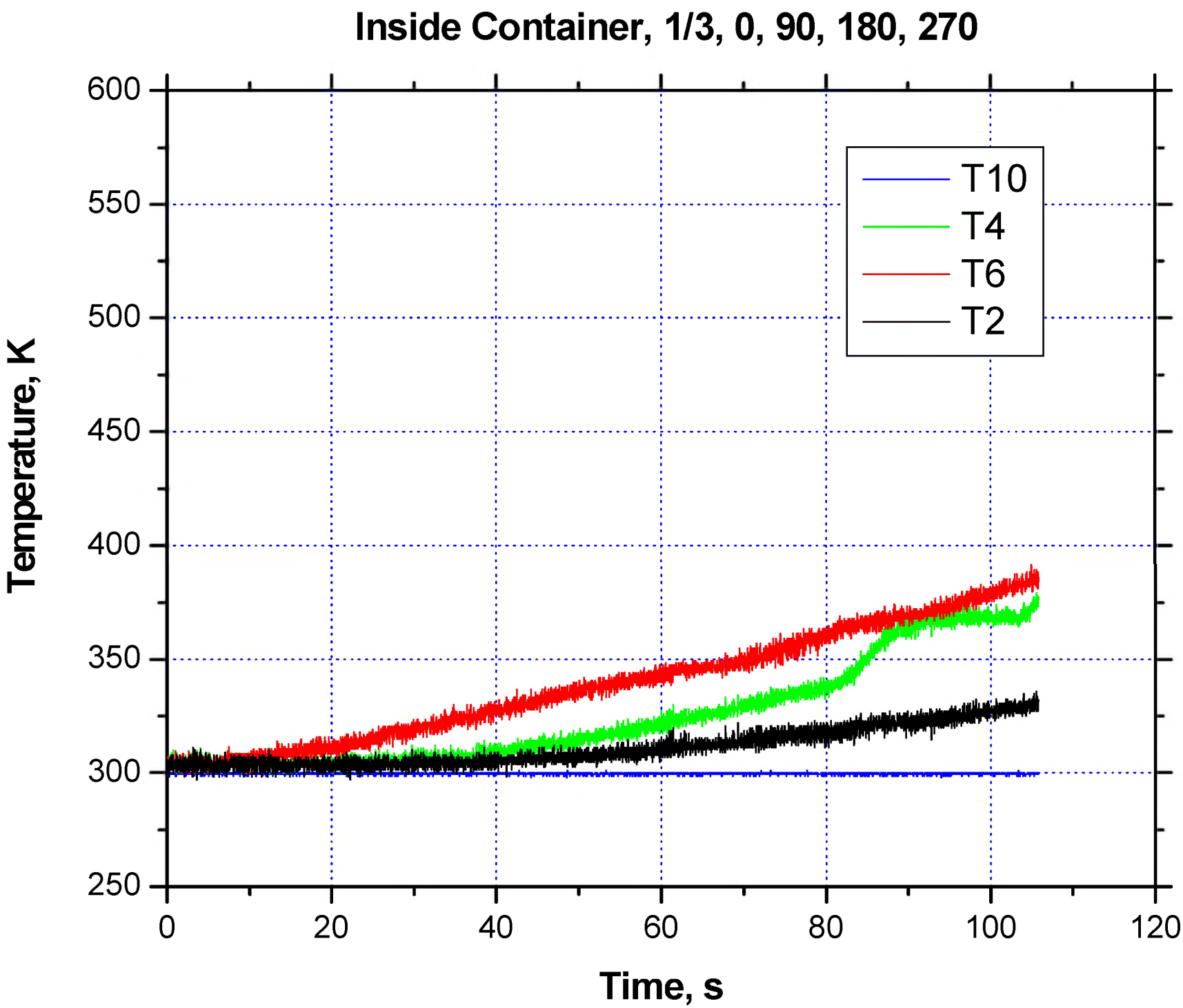
Inside Container, 1/3, 0, 90, 180, 270
Temperature, K
Time, s
600
550
500
450
400
350
300
250
0
20
40
60
80
100
120
T10
T4
T6
T2

PLOTS, TEST 4, FIRE, OCTOBER 1999

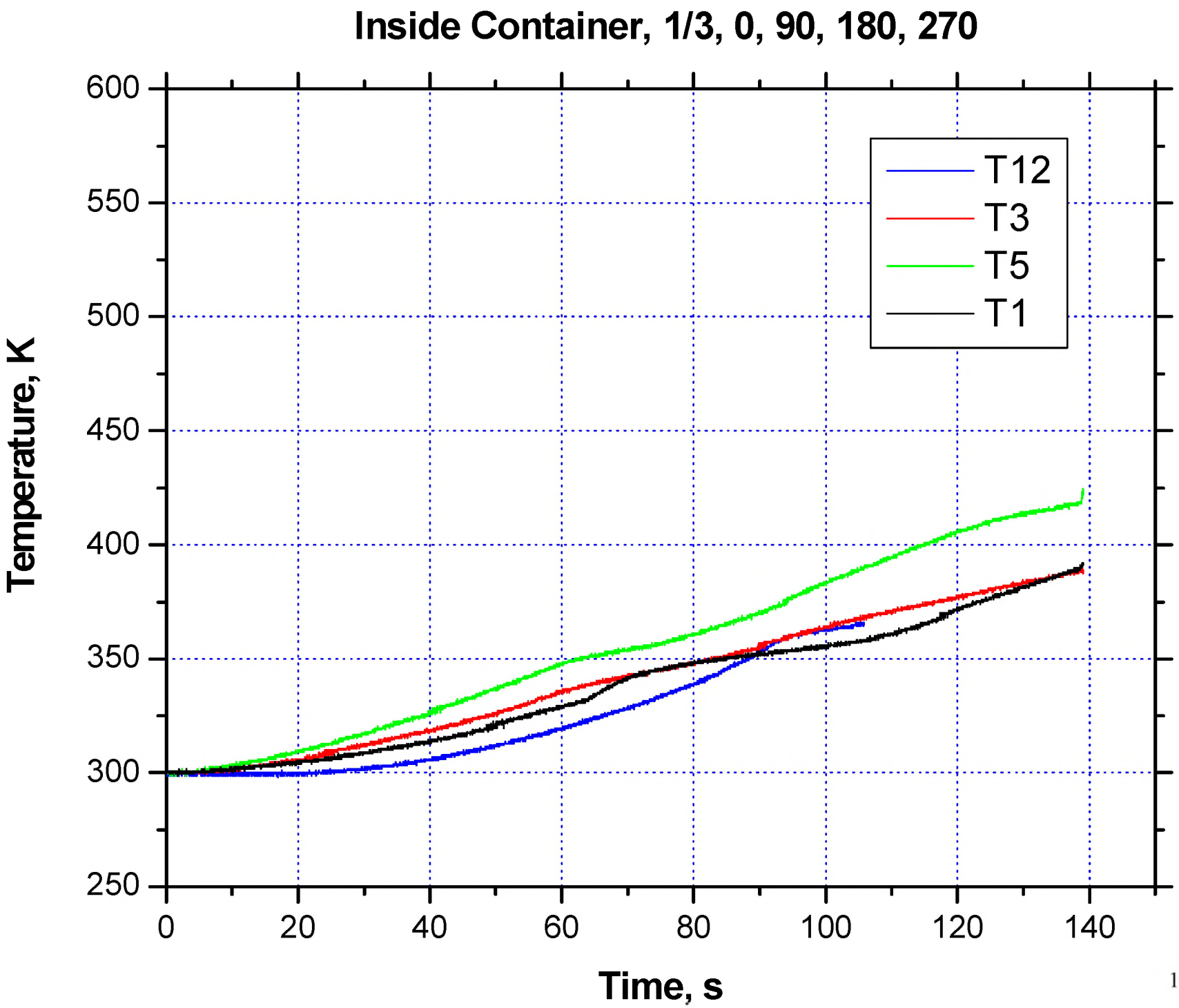
Inside Container, 1/3, 0, 90, 180, 270
Temperature, K
Time, s
600
550
500
450
400
350
300
250
0
20
40
60
80
100
120
140
T12
T3
T5
T1

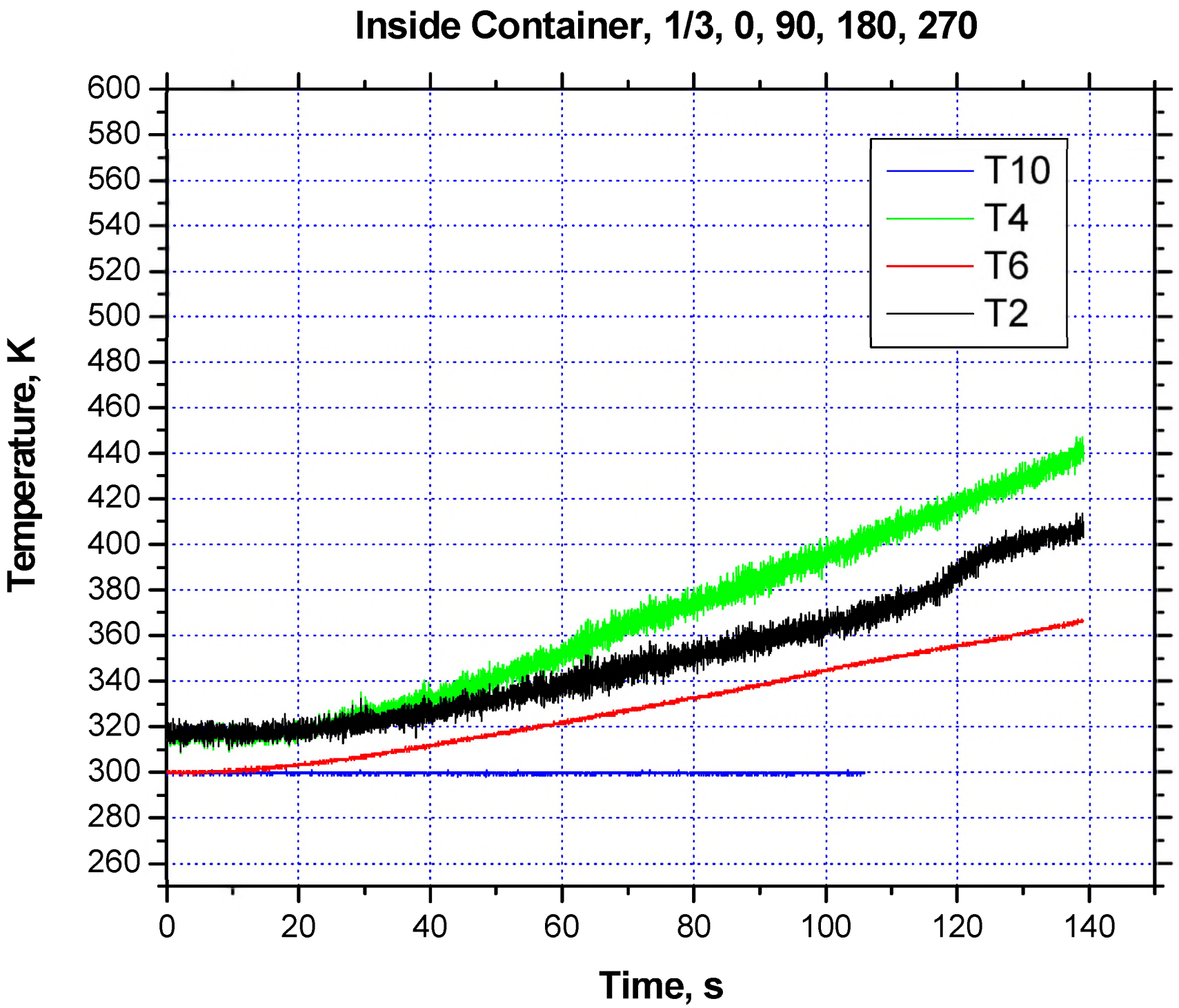
Inside Container, 1/3, 0, 90, 180, 270
Temperature, K
600
580
560
540
520
500
480
460
440
420
400
380
360
340
320
300
280
260
0
20
40
60
80
100
120
140
Time, s
T10
T4
T6
T2

PLOTS, TEST 5, FIRE, OCTOBER 1999

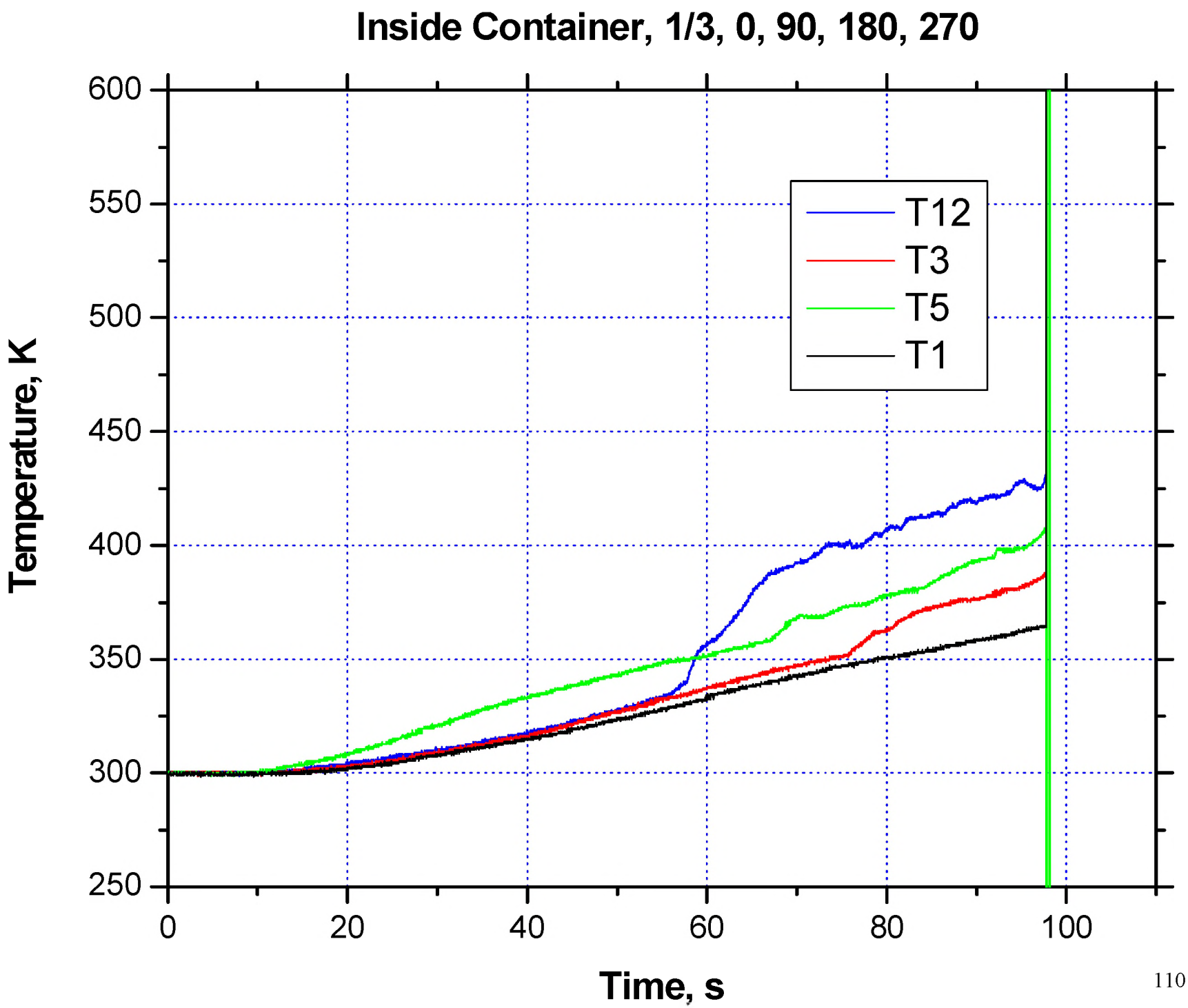
Inside Container, 1/3, 0, 90, 180, 270
Temperature, K
Time, s
600
550
500
450
400
350
300
250
0
20
40
60
80
100
T12
T3
T5
T1

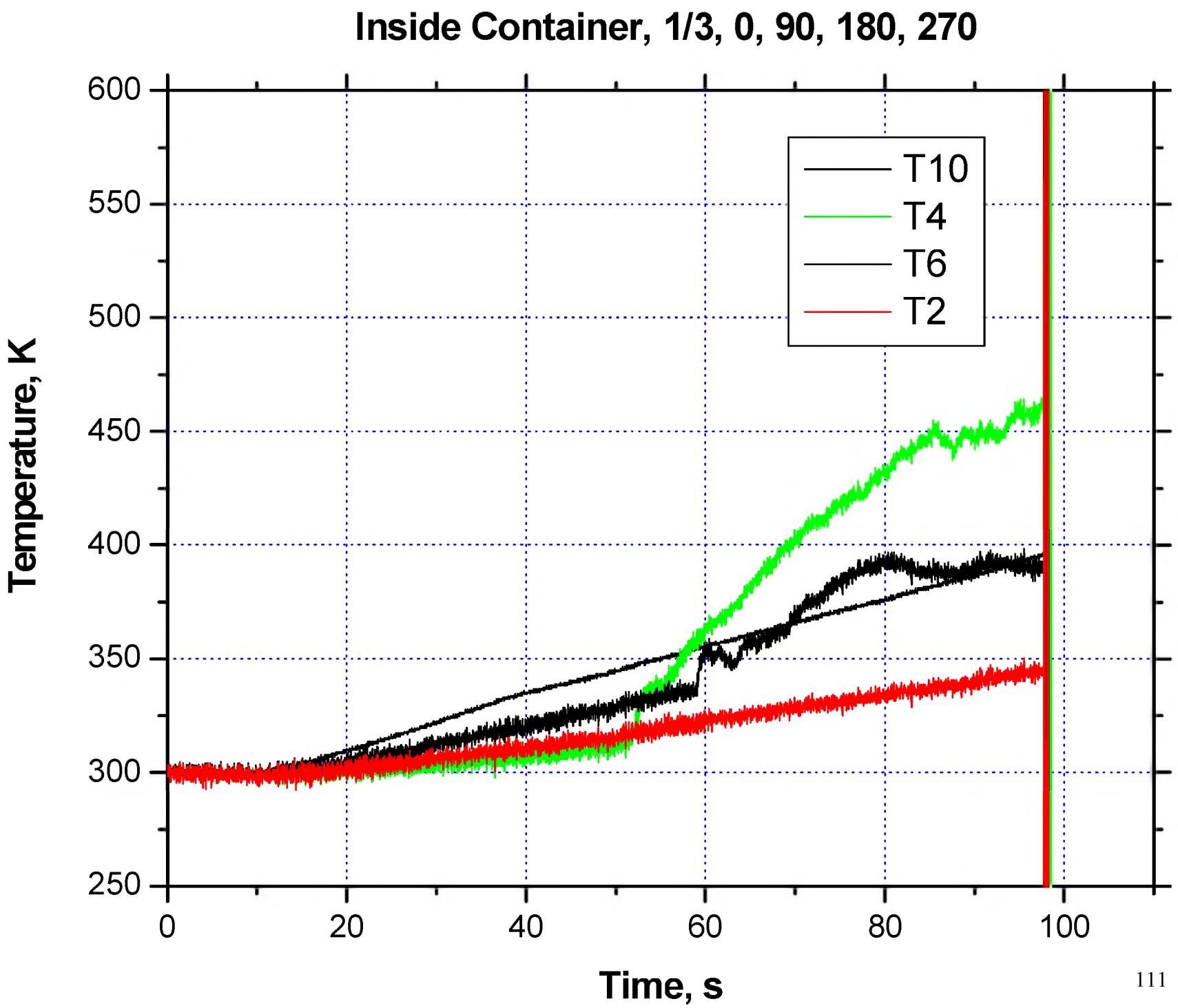
Inside Container, 1/3, 0, 90, 180, 270
Temperature, K
Time, s
600
550
500
450
400
350
300
250
0
20
40
60
80
100
T10
T4
T6
T2

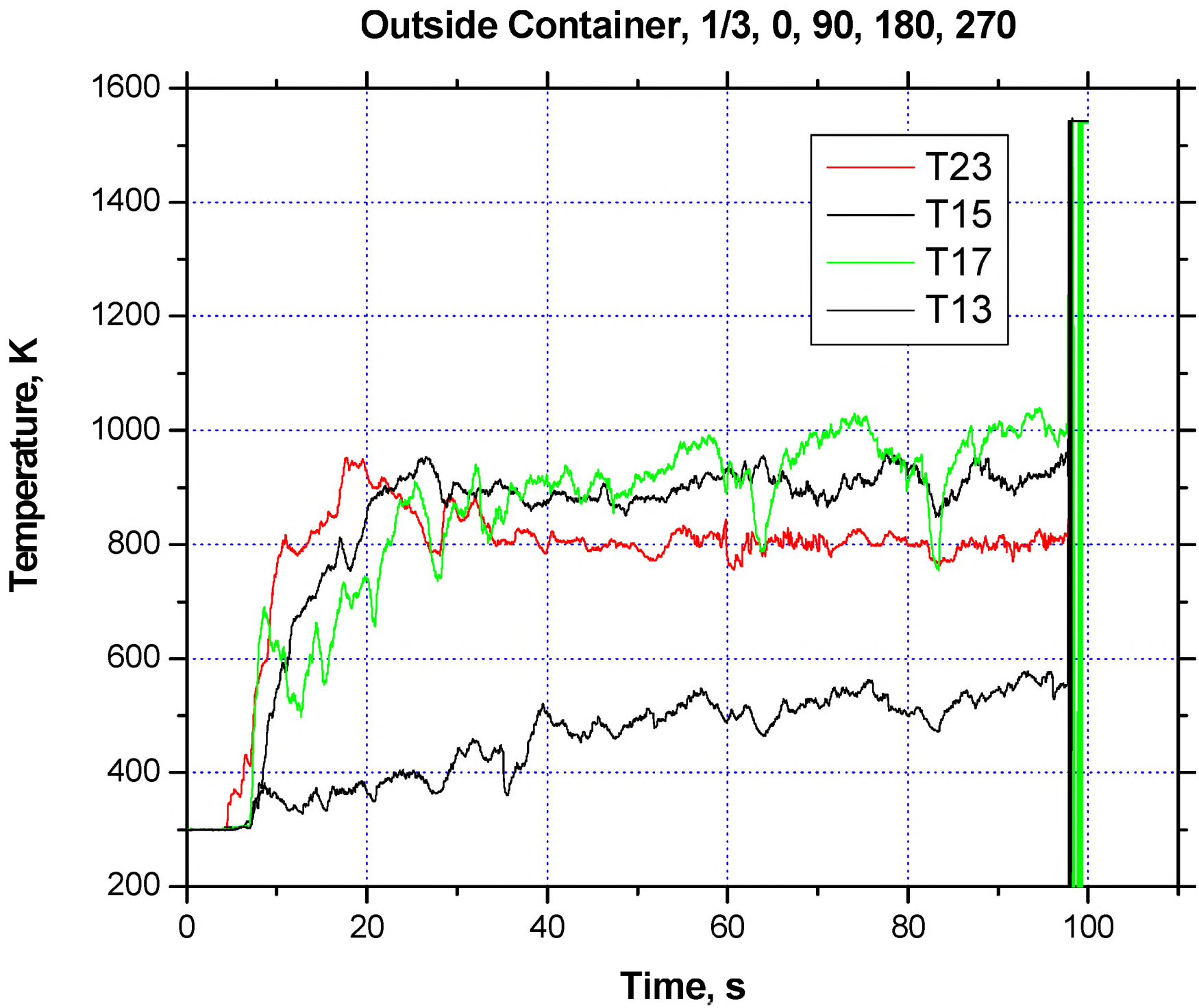
Outside Container, 1/3, 0, 90, 180, 270
Temperature, K
Time, s
T23
T15
T17
T13
1600
1400
1200
1000
800
600
400
200
0
20
40
60
80
100

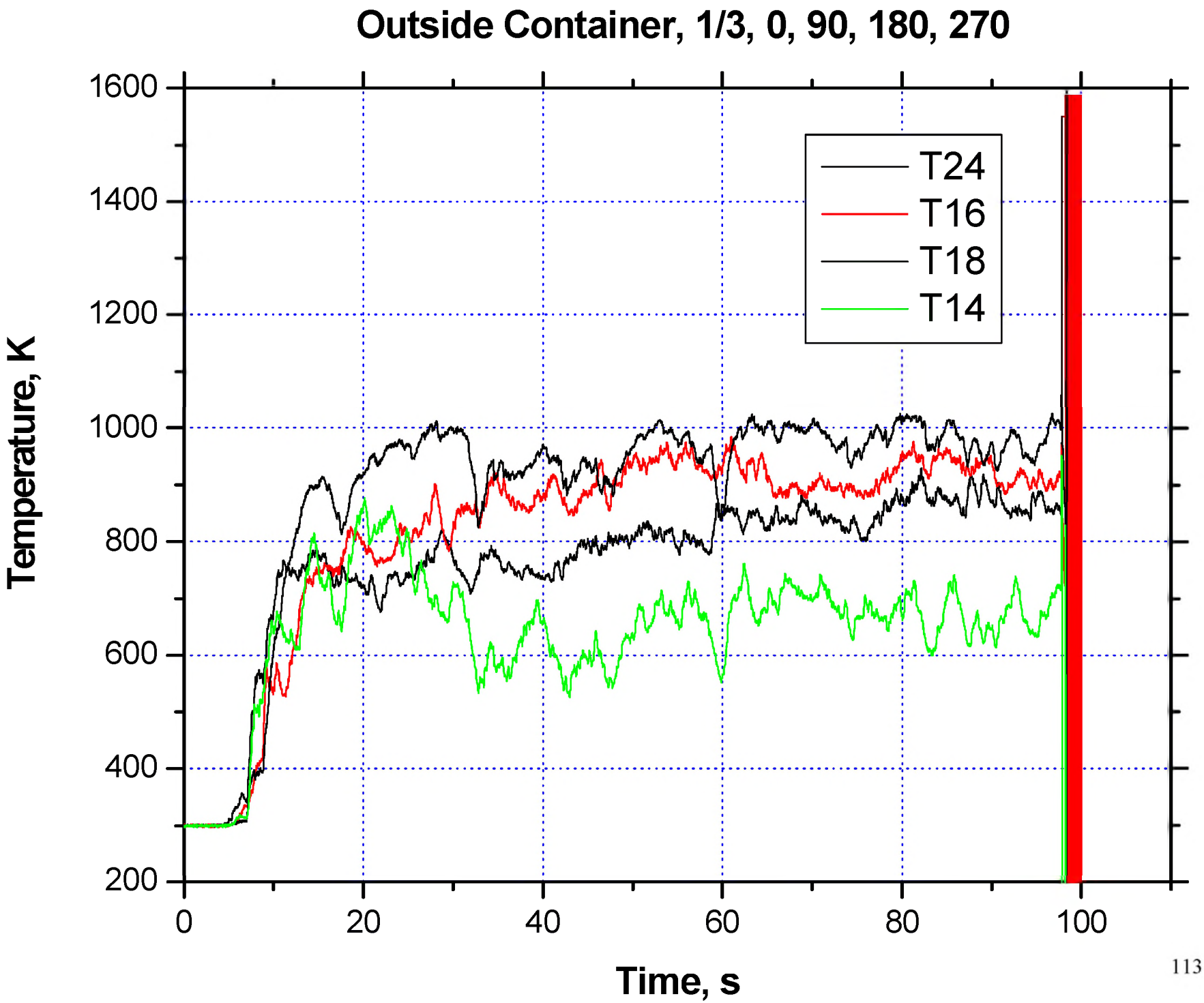
Outside Container, 1/3, 0, 90, 180, 270
Temperature, K
Time, s
T24
T16
T18
T14
1600
1400
1200
1000
800
600
400
200
0
20
40
60
80
100

PLOTS, TEST 6, ELECTRICAL, JULY 2002

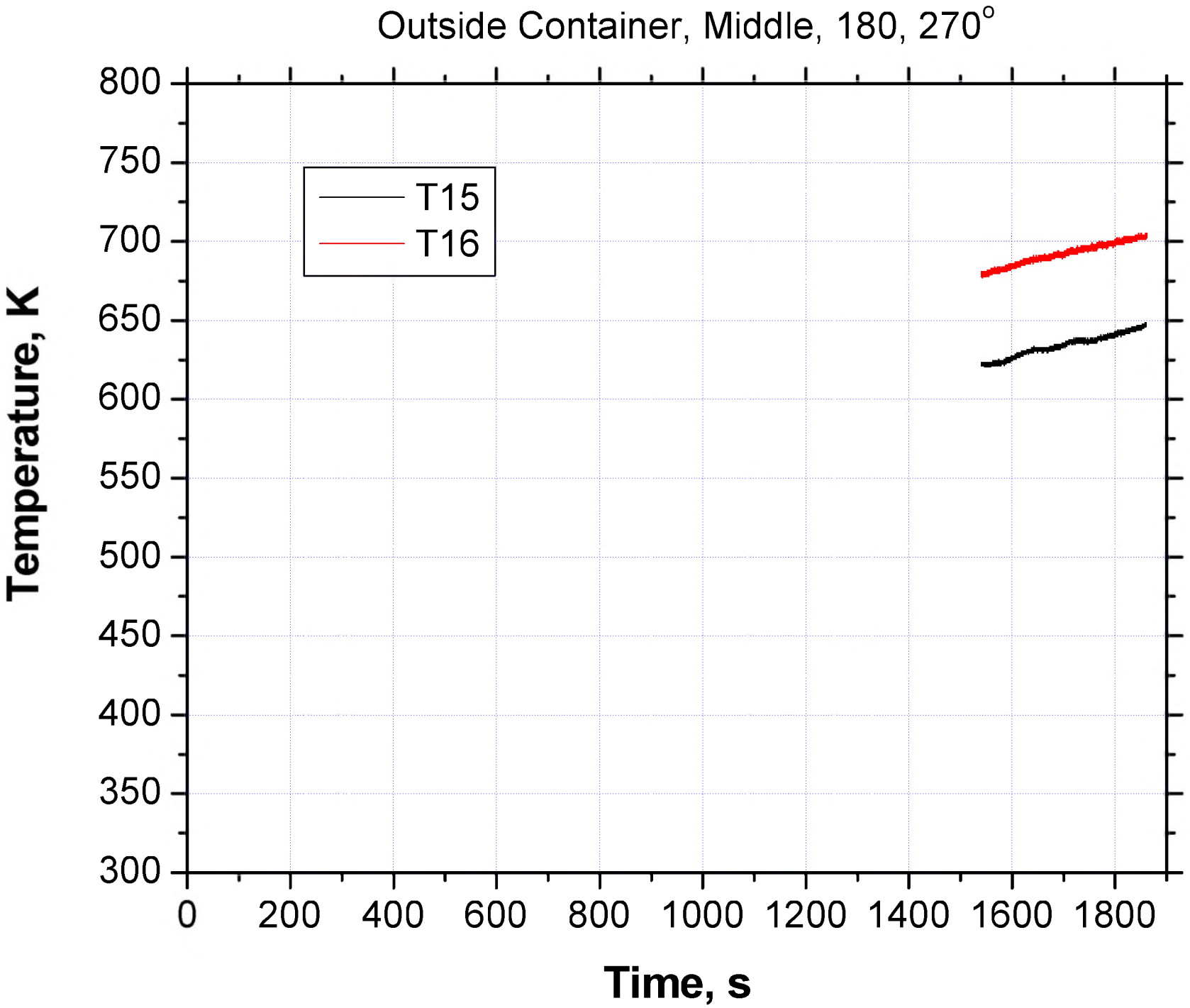
Outside Container, Middle, 180, 270°
T15
T16
Temperature, K
Time, s
800
750
700
650
600
550
500
450
400
350
300
0
200
400
600
800
1000
1200
1400
1600
1800

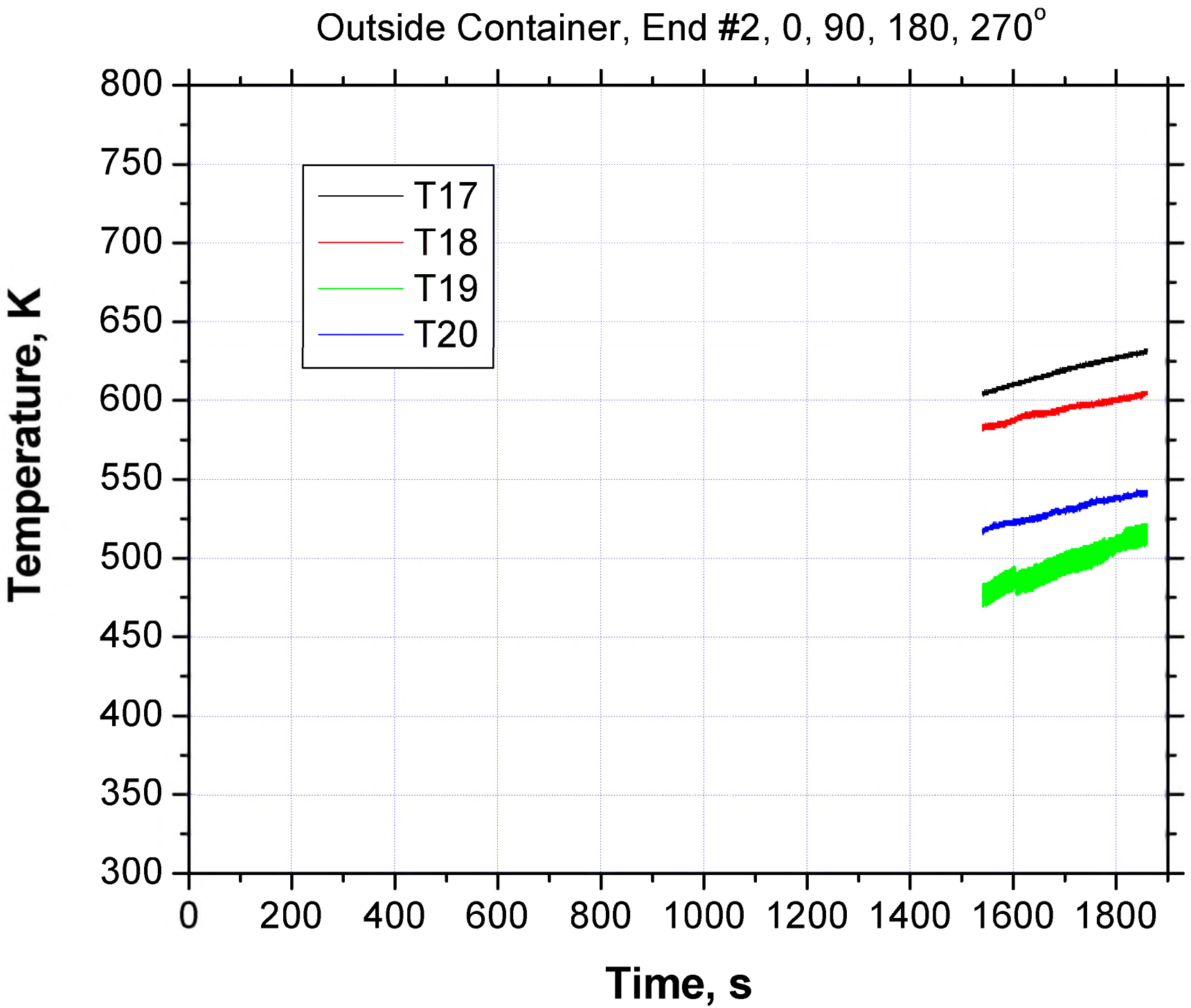
Outside Container, End #2, 0, 90, 180, 270°
Temperature, K
Time, s
T17
T18
T19
T20
800
750
700
650
600
550
500
450
400
350
300
0
200
400
600
800
1000
1200
1400
1600
1800

PLOTS, TEST 7, ELECTRICAL, AUGUST 2001

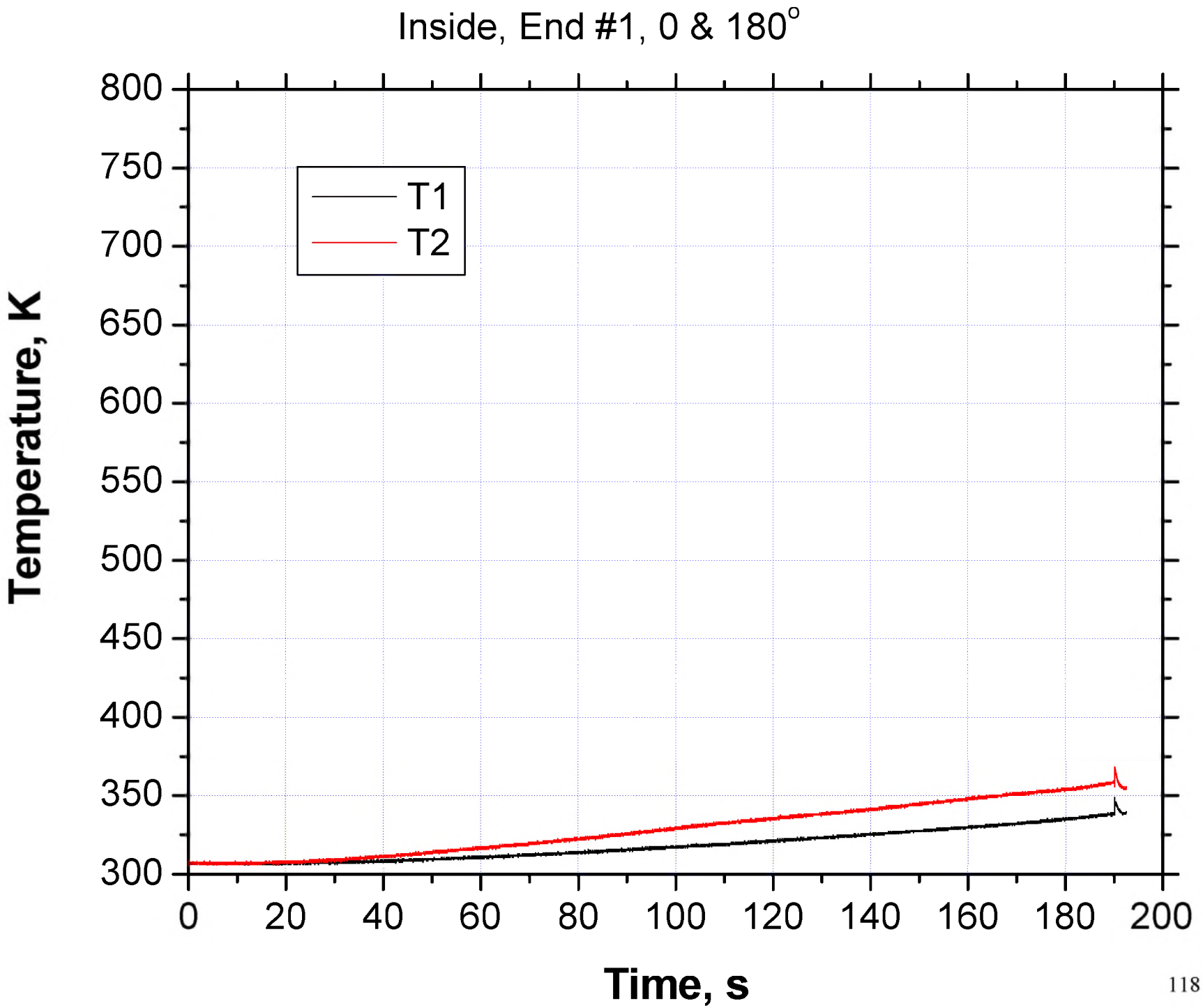
Inside, End #1, 0 & 180°
T1
T2
Temperature, K
Time, s
800
750
700
650
600
550
500
450
400
350
300
0
20
40
60
80
100
120
140
160
180
200

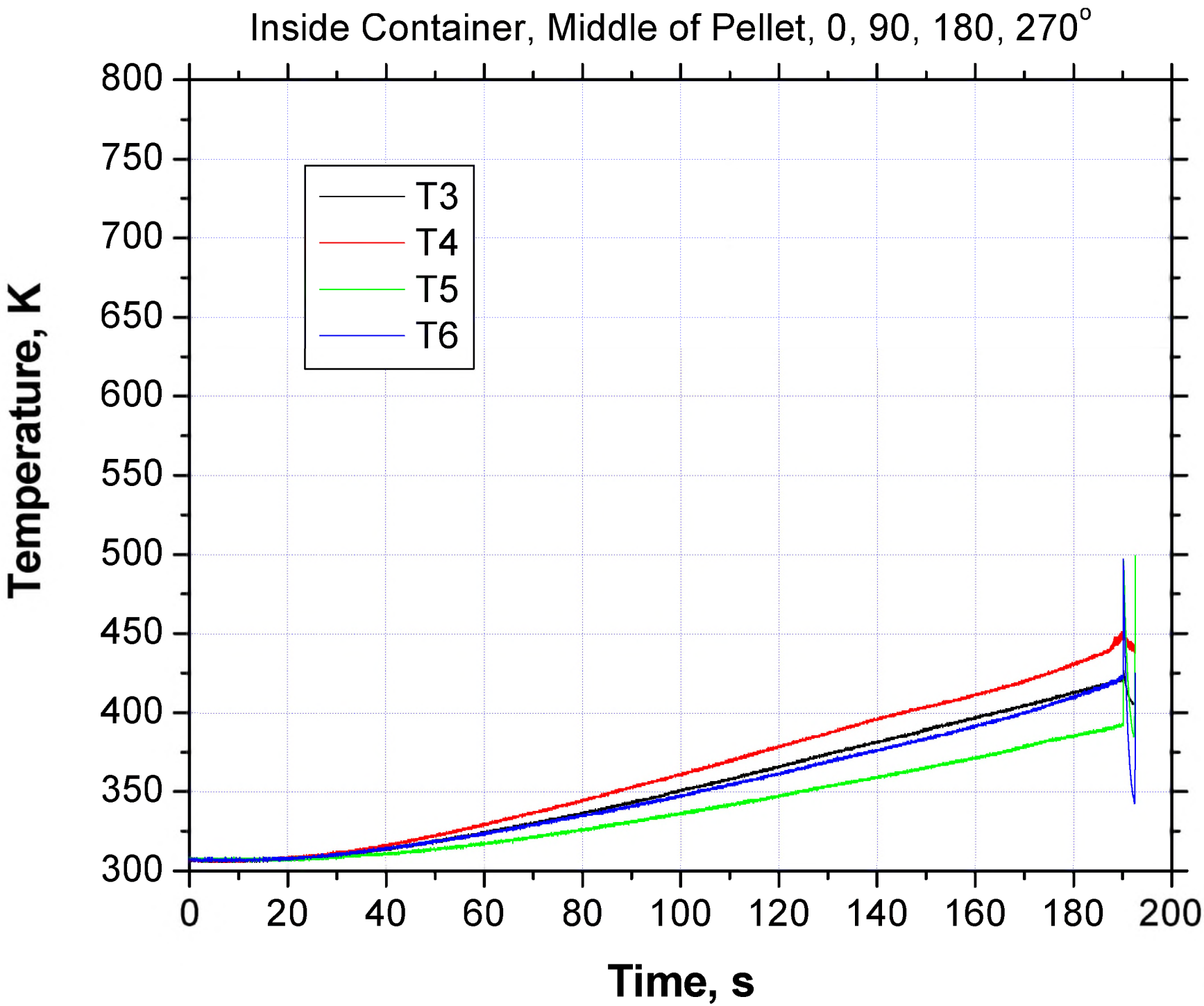
Inside Container, Middle of Pellet, 0, 90, 180, 270°
Temperature, K
Time, s
T3
T4
T5
T6
800
750
700
650
600
550
500
450
400
350
300
0
20
40
60
80
100
120
140
160
180
200

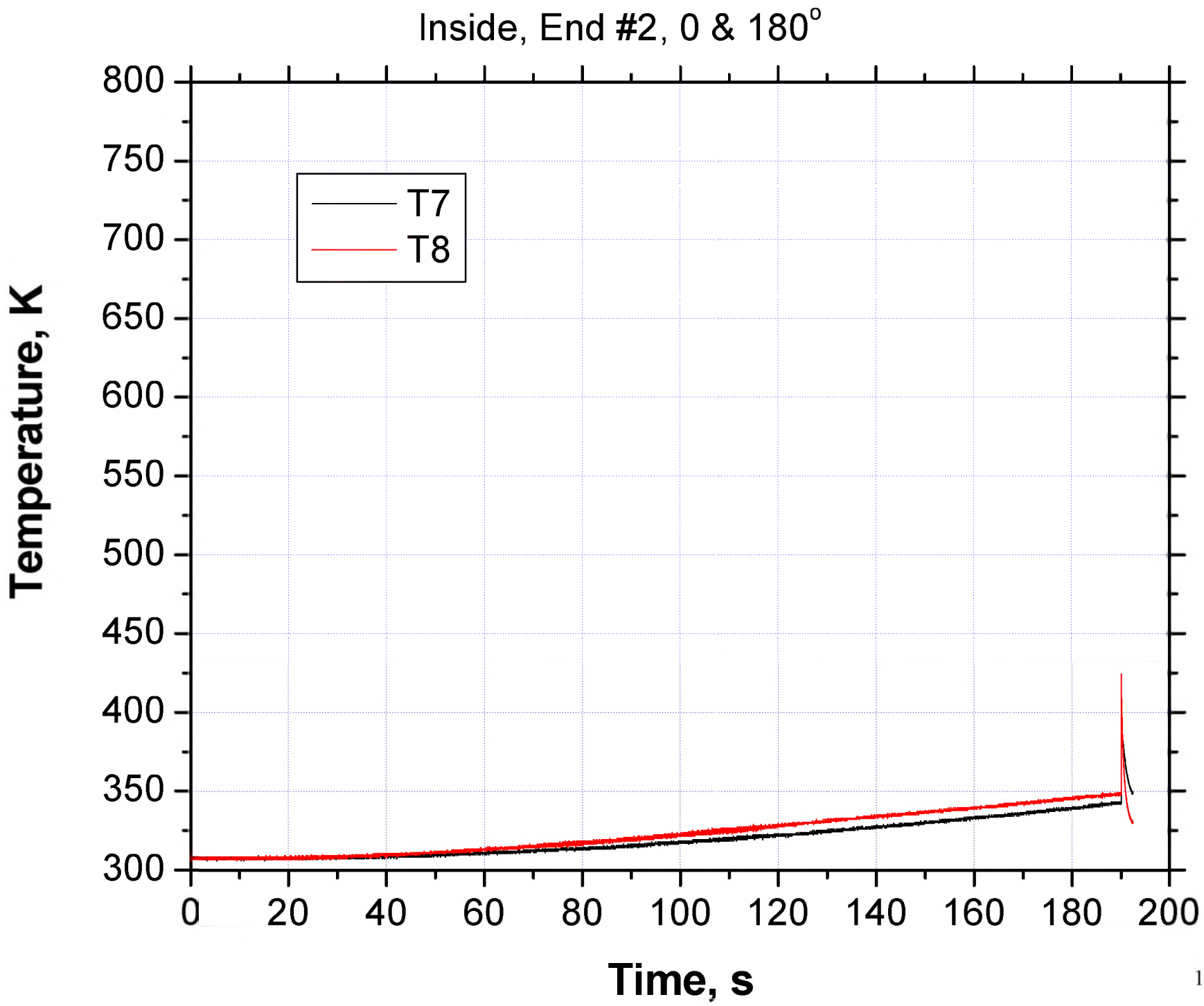
Inside, End #2, 0 & 180°
T7
T8
Temperature, K
Time, s
800
750
700
650
600
550
500
450
400
350
300
0
20
40
60
80
100
120
140
160
180
200

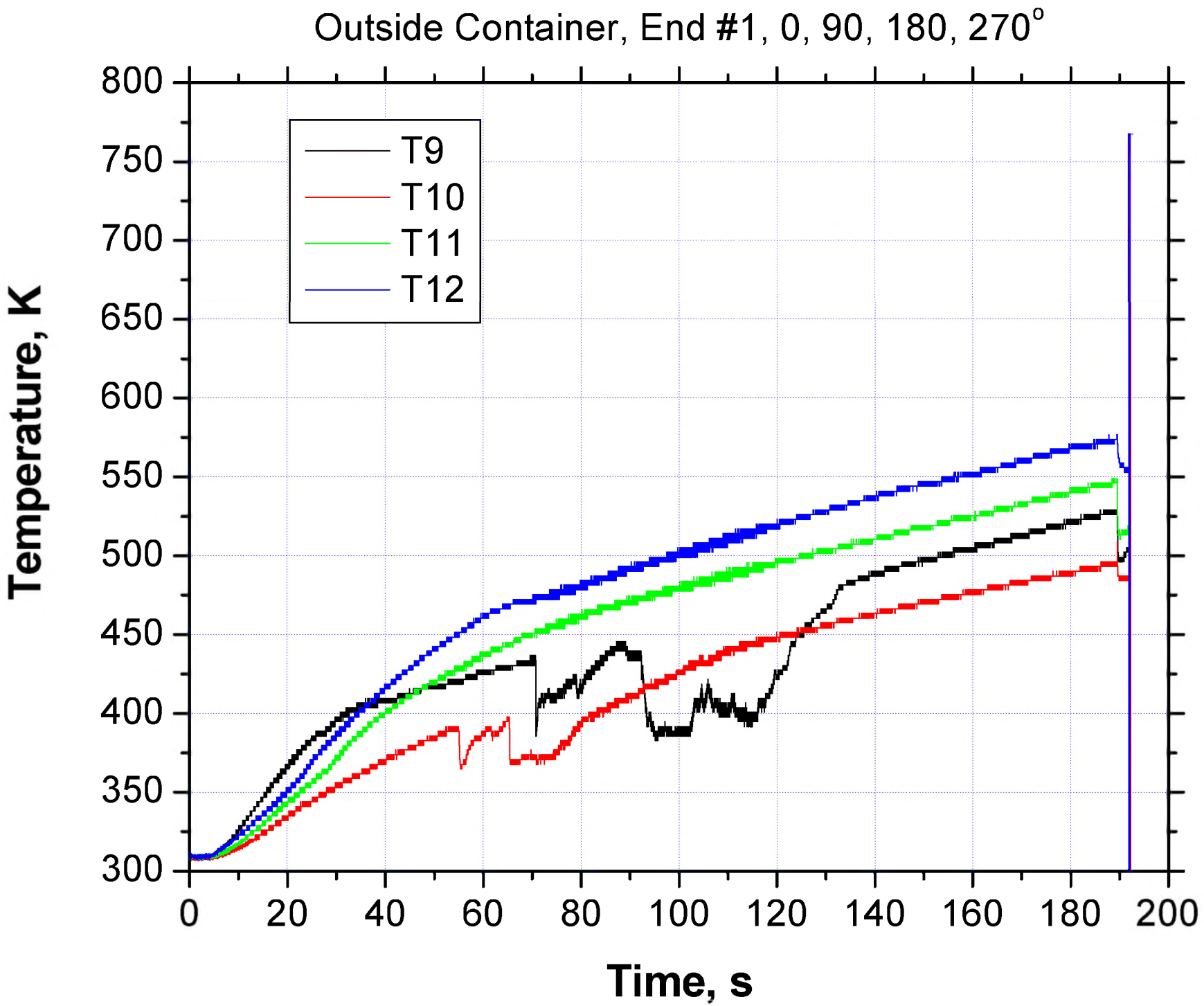
Outside Container, End #1, 0, 90, 180, 270°
T9
T10
T11
T12
Temperature, K
Time, s
800
750
700
650
600
550
500
450
400
350
300
0
20
40
60
80
100
120
140
160
180
200

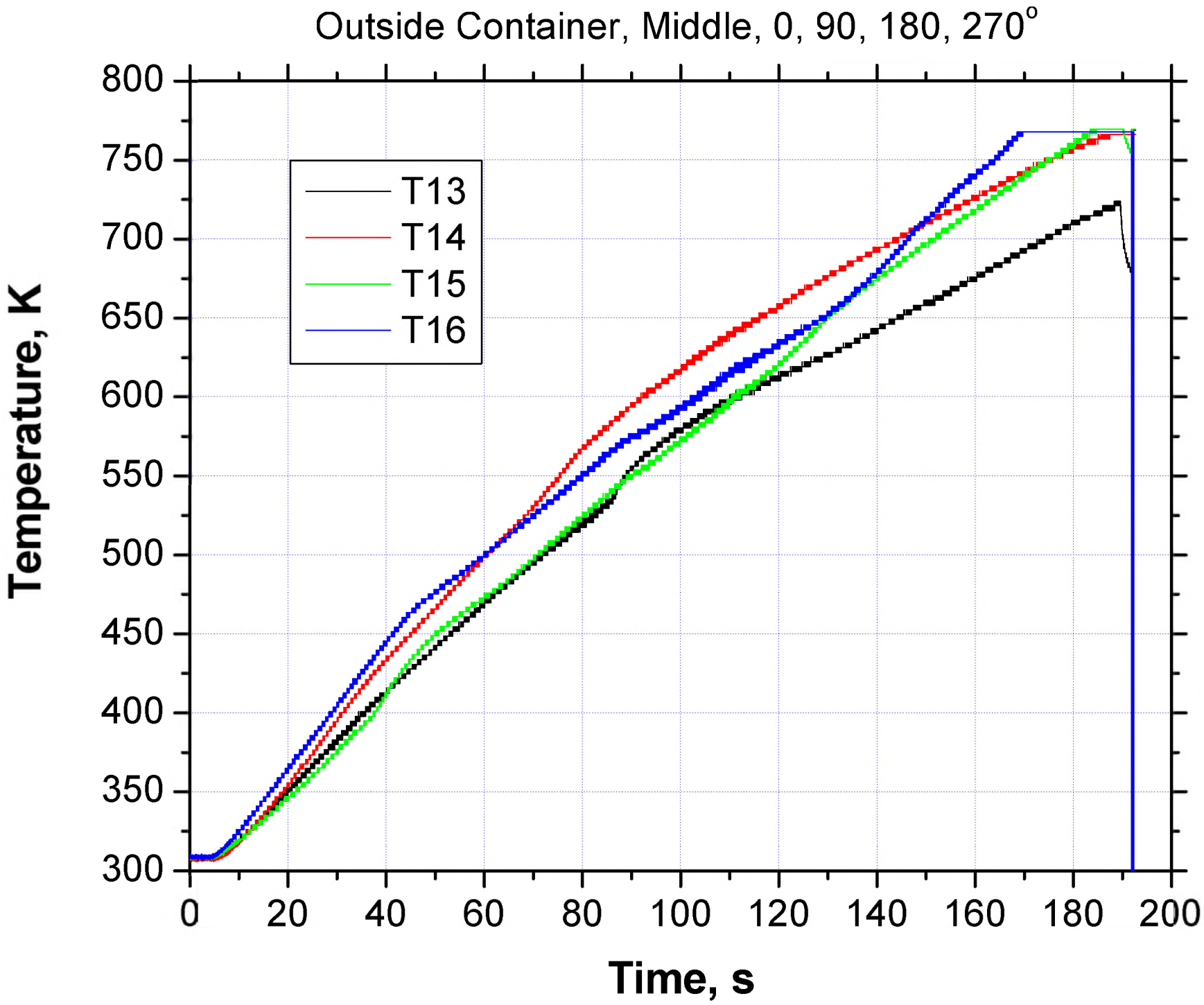
Outside Container, Middle, 0, 90, 180, 270°
T13
T14
T15
T16
Temperature, K
Time, s
800
750
700
650
600
550
500
450
400
350
300
0
20
40
60
80
100
120
140
160
180
200

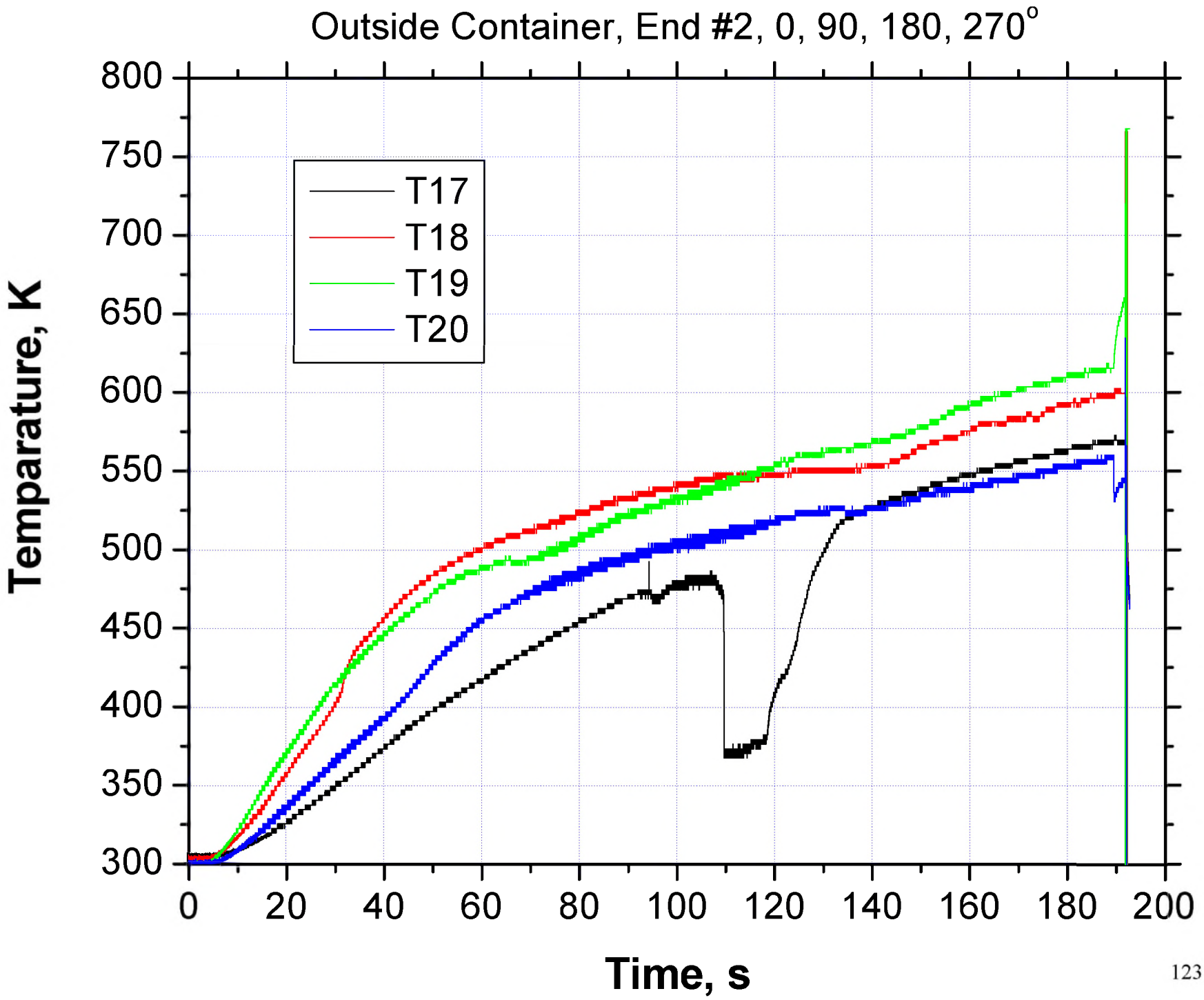
Outside Container, End #2, 0, 90, 180, 270°
T17
T18
T19
T20
Temparature, K
Time, s
800
750
700
650
600
550
500
450
400
350
300
0
20
40
60
80
100
120
140
160
180
200

PLOTS, TEST 8, ELECTRICAL, SEPTEMBER 2002

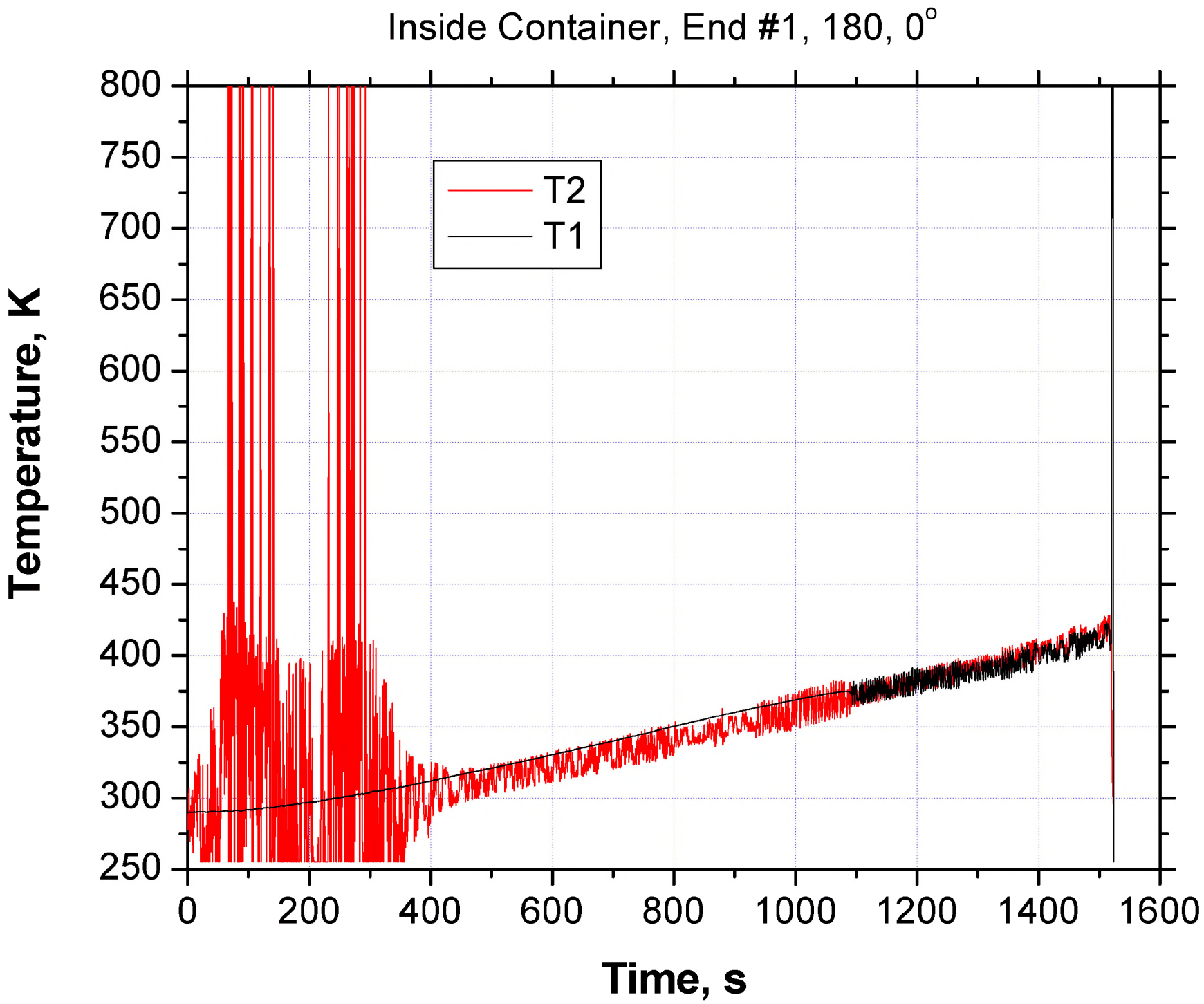
Inside Container, End #1, 180, 0°
T2
T1
Temperature, K
Time, s
800
750
700
650
600
550
500
450
400
350
300
250
0
200
400
600
800
1000
1200
1400
1600

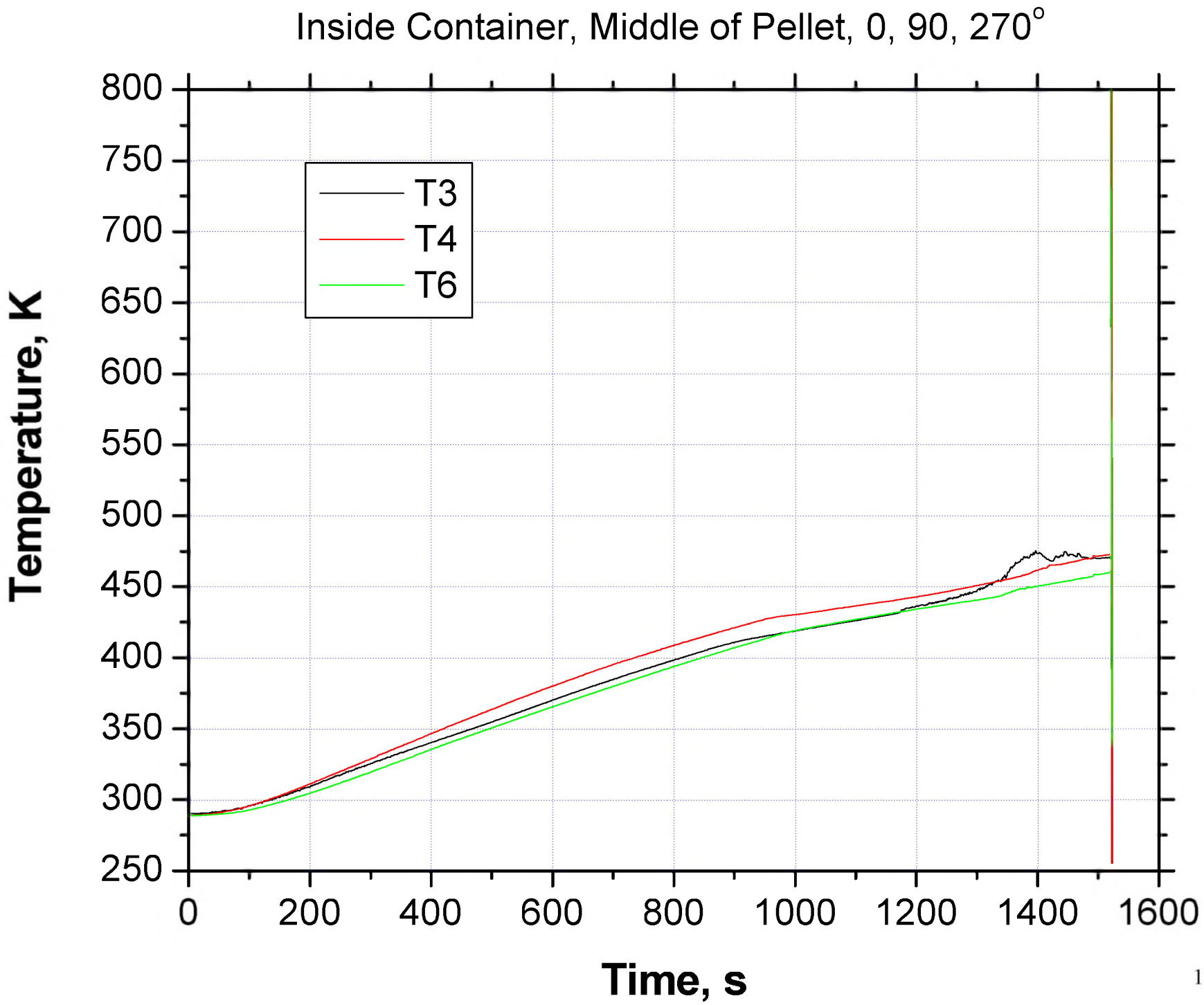
Inside Container, Middle of Pellet, 0, 90, 270°
T3
T4
T6
Temperature, K
Time, s
800
750
700
650
600
550
500
450
400
350
300
250
0
200
400
600
800
1000
1200
1400
1600

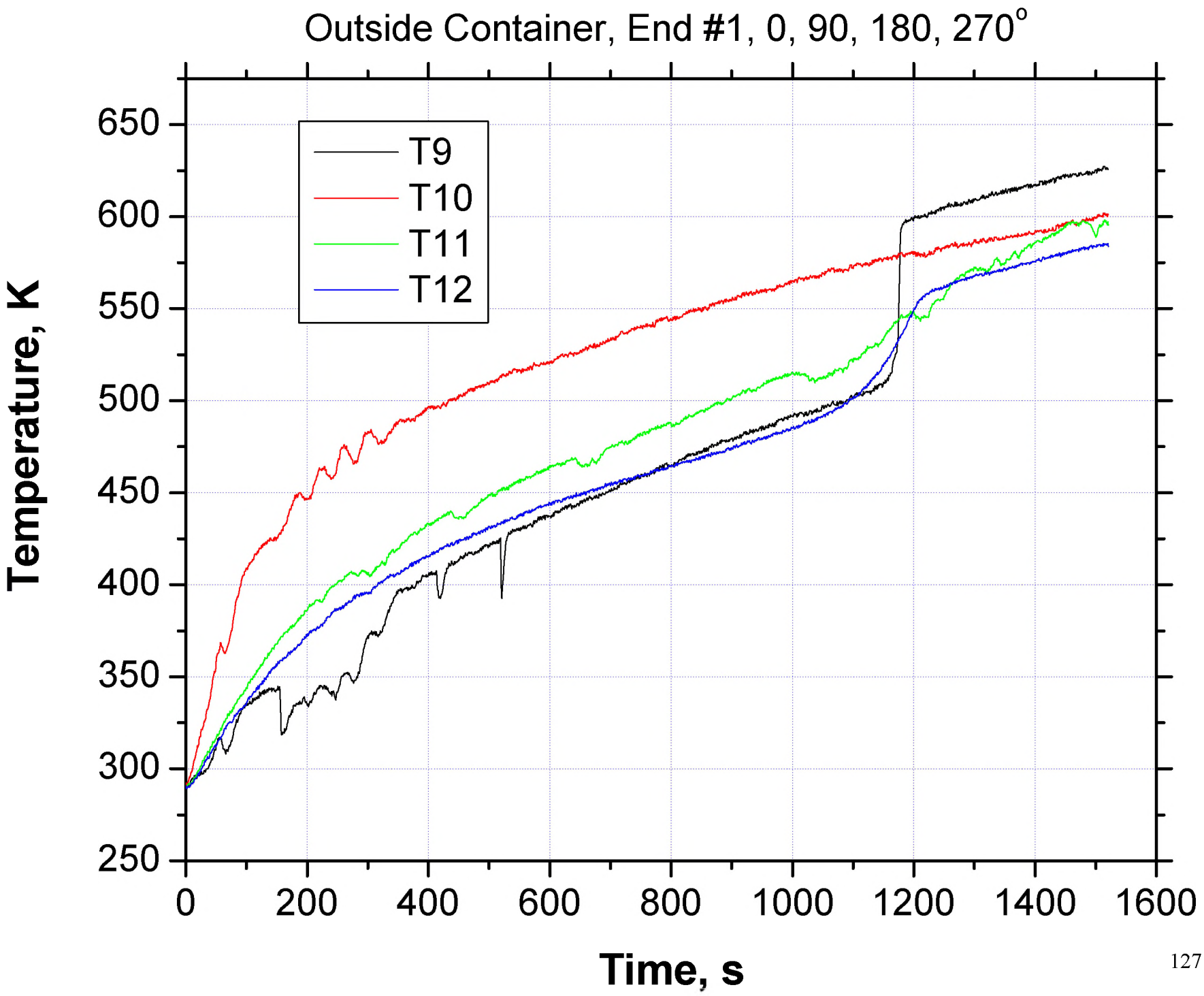
Outside Container, End #1, 0, 90, 180, 270°
T9
T10
T11
T12
Temperature, K
650
600
550
500
450
400
350
300
250
0
200
400
600
800
1000
1200
1400
1600
Time, s

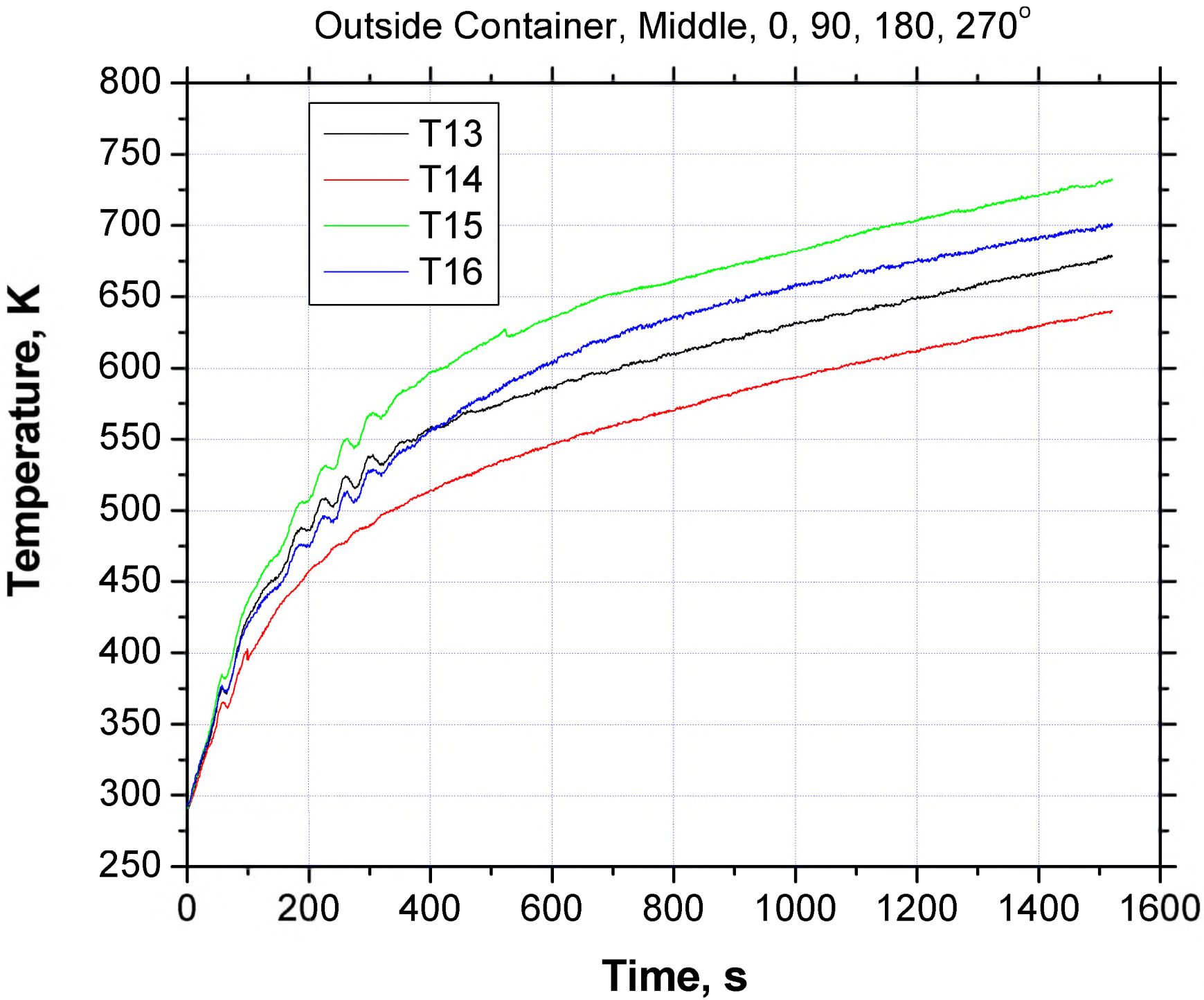
Outside Container, Middle, 0, 90, 180, 270°
T13
T14
T15
T16
Temperature, K
Time, s
800
750
700
650
600
550
500
450
400
350
300
250
0
200
400
600
800
1000
1200
1400
1600

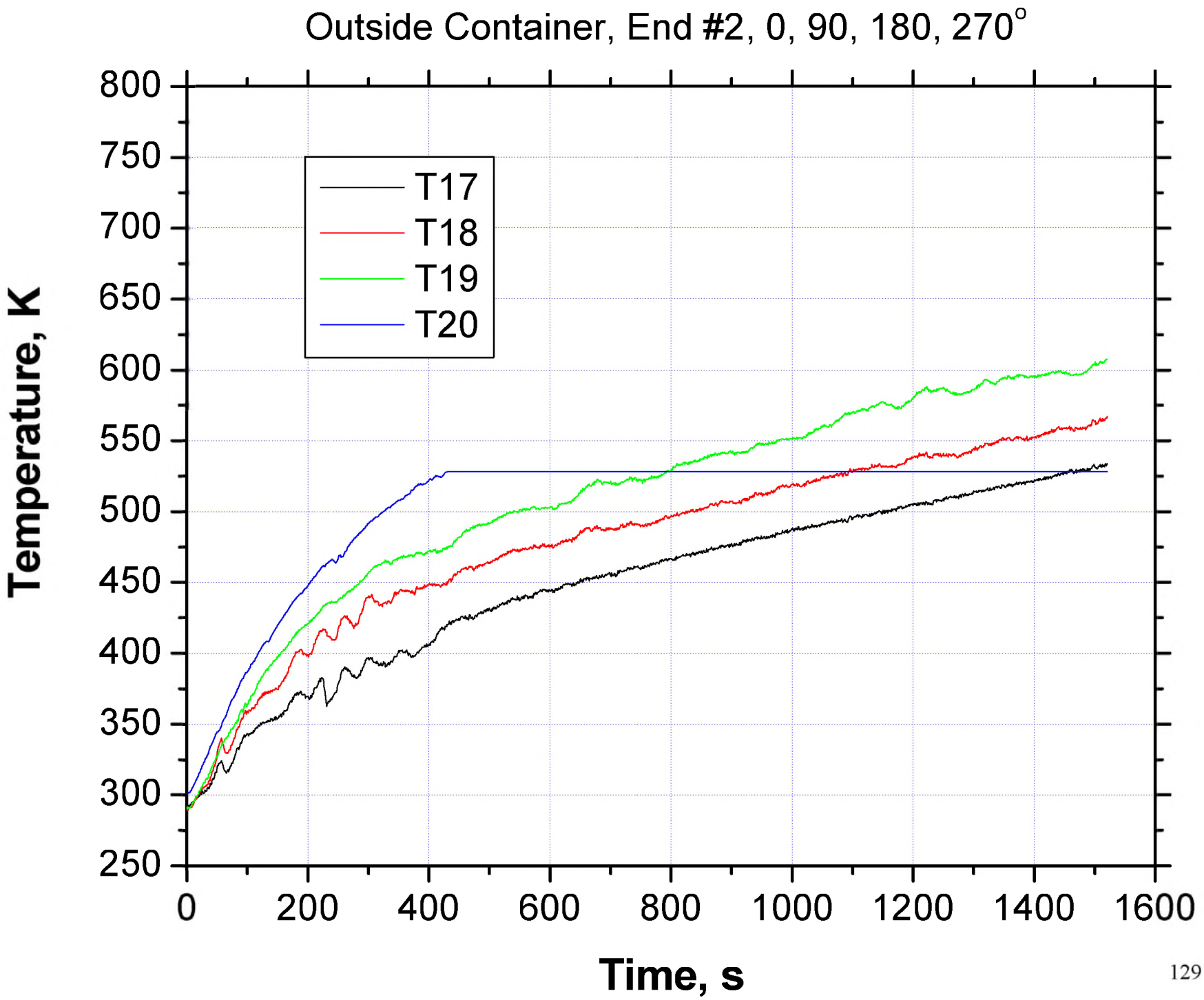
Outside Container, End #2, 0, 90, 180, 270°
T17
T18
T19
T20
Temperature, K
Time, s
800
750
700
650
600
550
500
450
400
350
300
250
0
200
400
600
800
1000
1200
1400
1600

PLOTS, TEST 9A, ELECTRICAL, NOVEMBER 2002

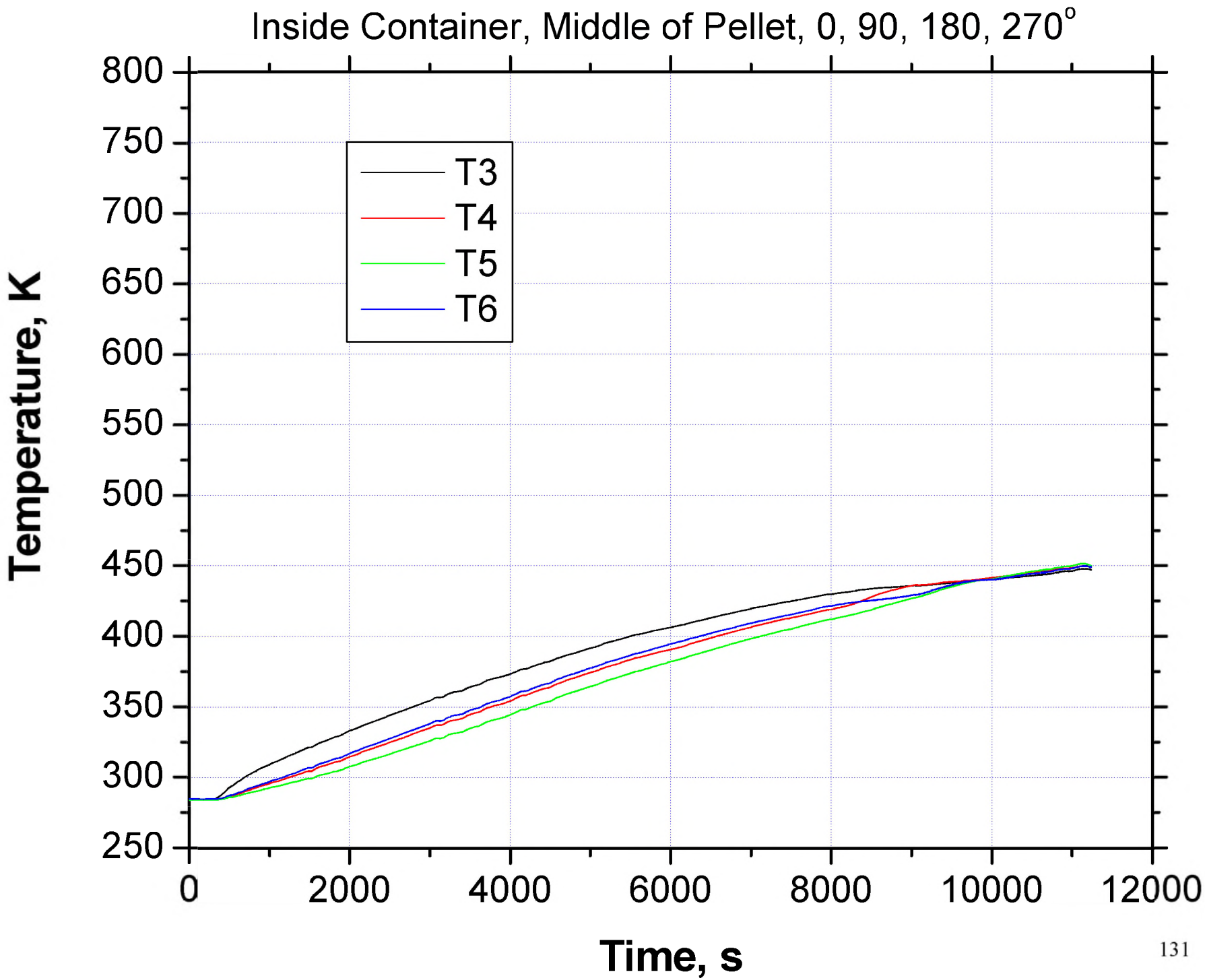
Inside Container, Middle of Pellet, 0, 90, 180, 270°
T3
T4
T5
T6
Temperature, K
Time, s
800
750
700
650
600
550
500
450
400
350
300
250
0
2000
4000
6000
8000
10000
12000

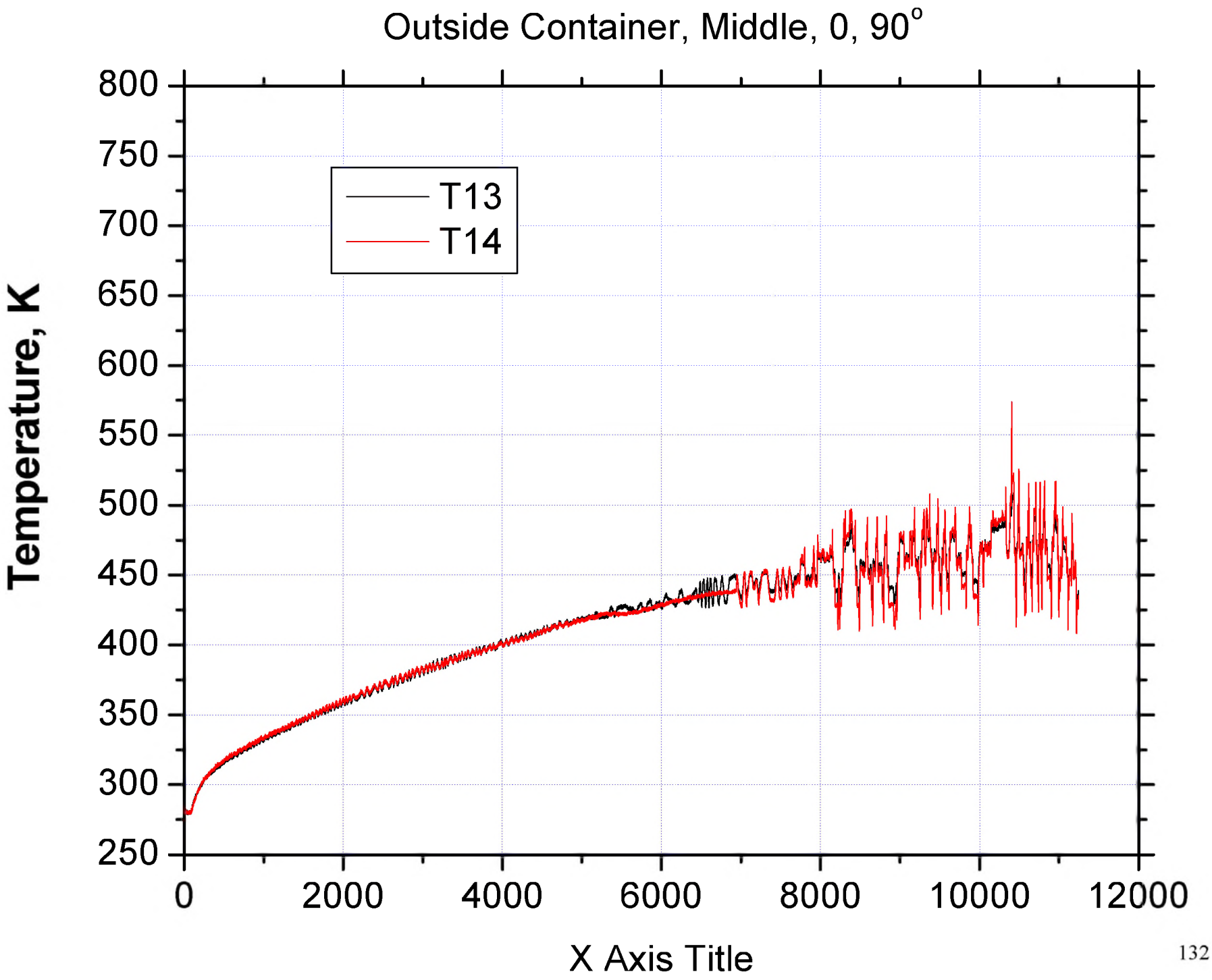
Outside Container, Middle, 0, 90°
T13
T14
Temperature, K
800
750
700
650
600
550
500
450
400
350
300
250
0
2000
4000
6000
8000
10000
12000
X Axis Title

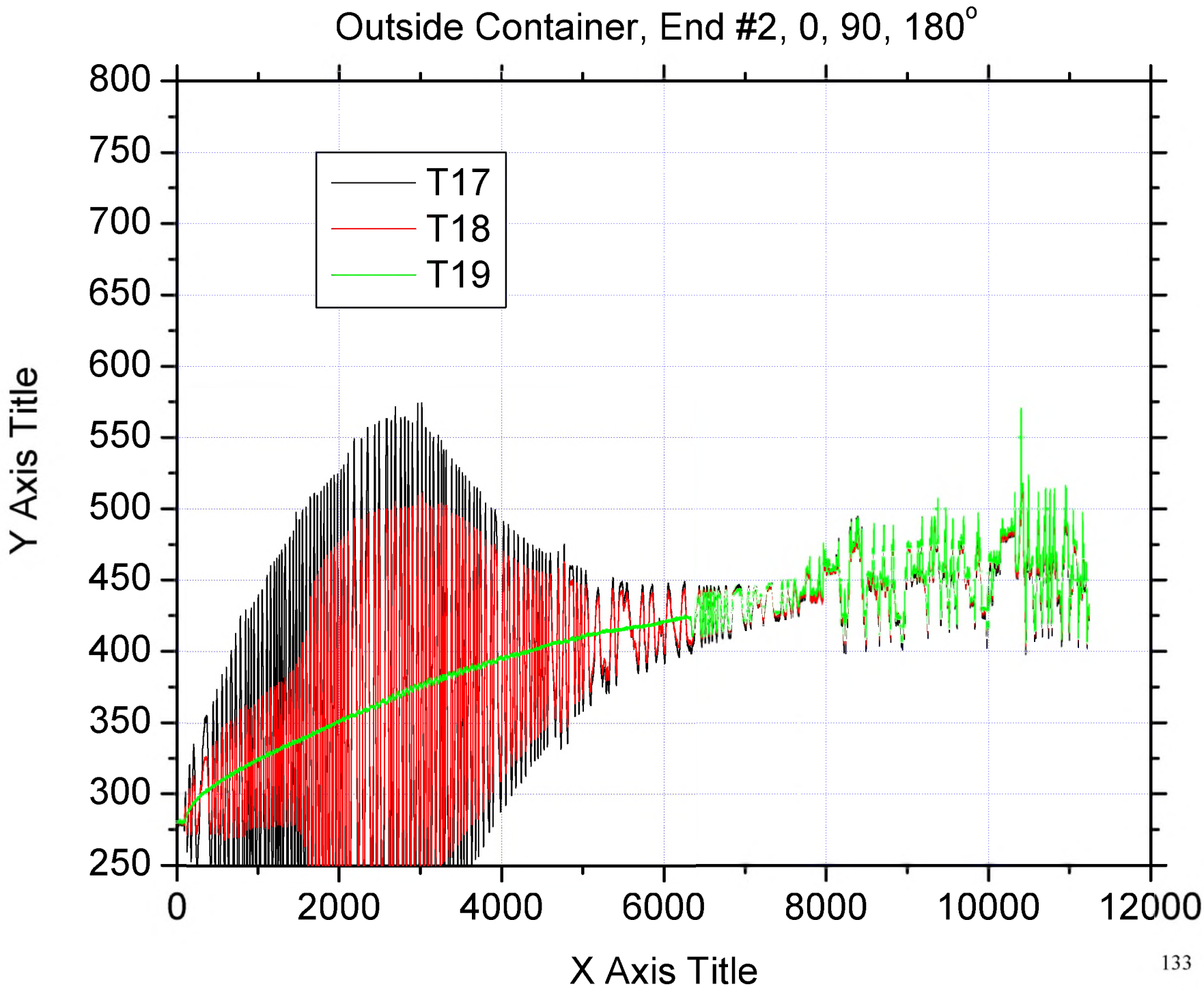
Outside Container, End #2, 0, 90, 180°
T17
T18
T19
Y Axis Title
X Axis Title
800
750
700
650
600
550
500
450
400
350
300
250
0
2000
4000
6000
8000
10000
12000

PLOTS, TEST 9B, ELECTRICAL, NOVEMBER 2002

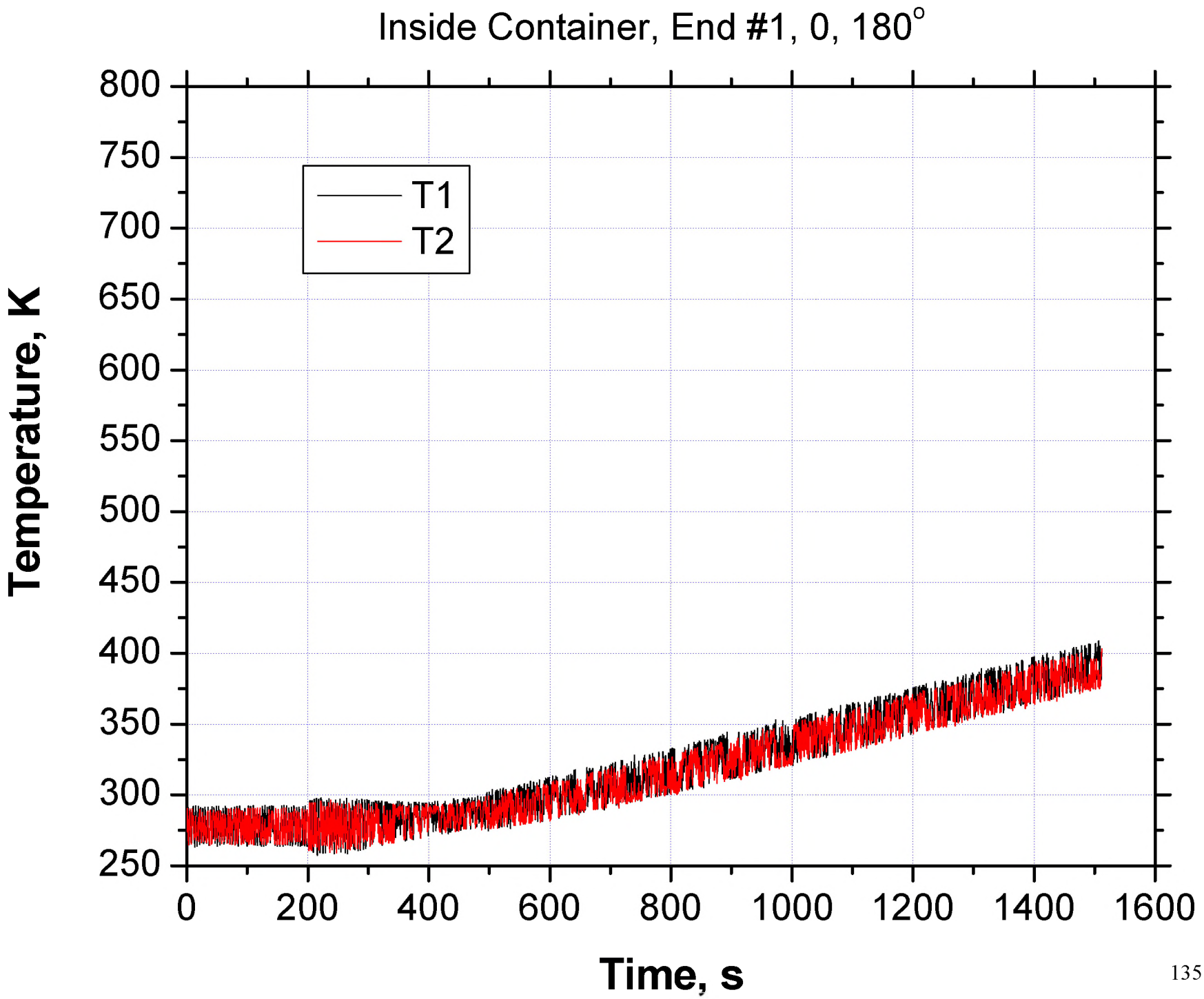
Inside Container, End #1, 0, 180°
T1
T2
Temperature, K
Time, s
800
750
700
650
600
550
500
450
400
350
300
250
0
200
400
600
800
1000
1200
1400
1600

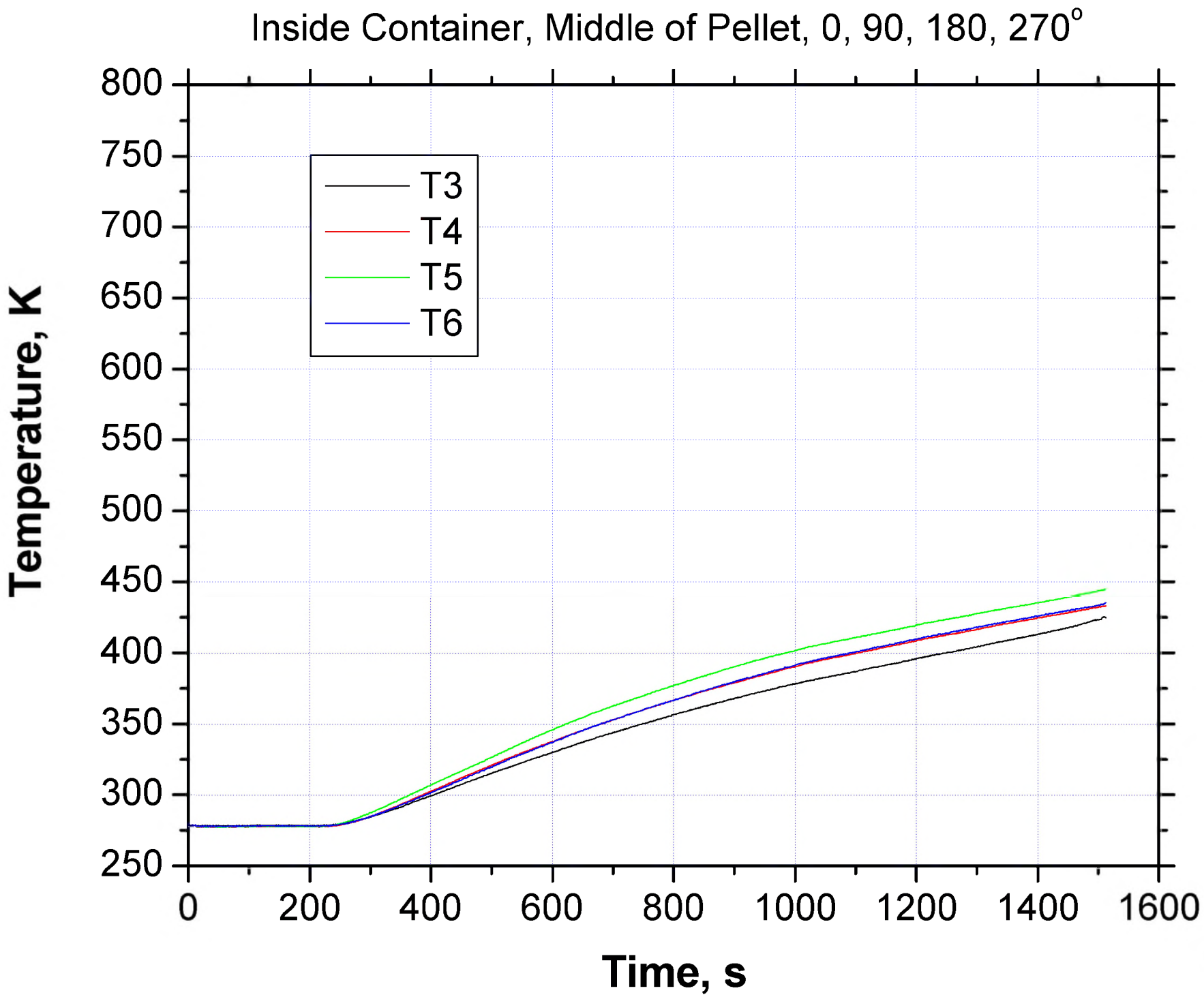
Inside Container, Middle of Pellet, 0, 90, 180, 270°
Temperature, K
Time, s
T3
T4
T5
T6
800
750
700
650
600
550
500
450
400
350
300
250
0
200
400
600
800
1000
1200
1400
1600

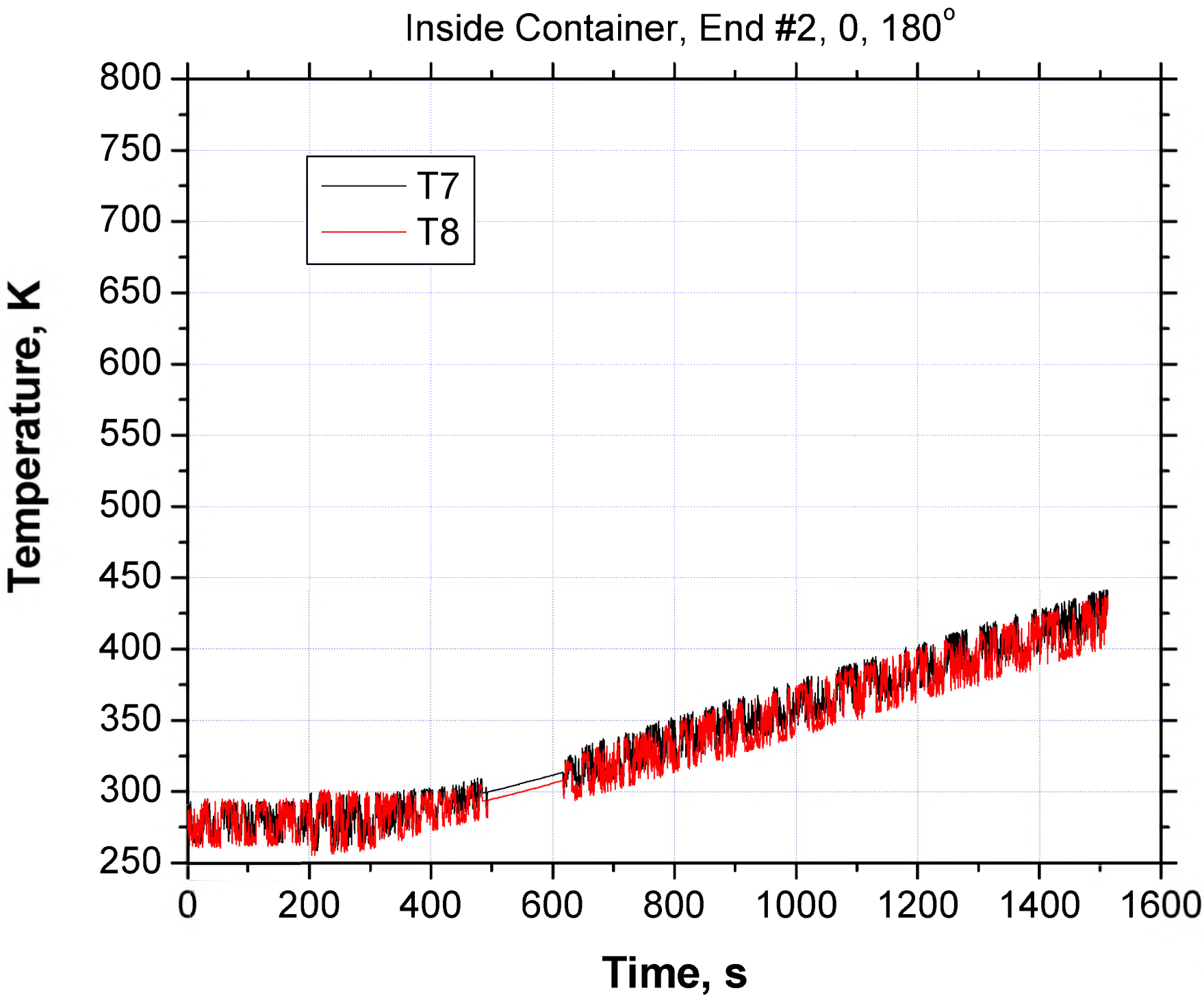
Inside Container, End #2, 0, 180°
T7
T8
Temperature, K
Time, s
800
750
700
650
600
550
500
450
400
350
300
250
0
200
400
600
800
1000
1200
1400
1600

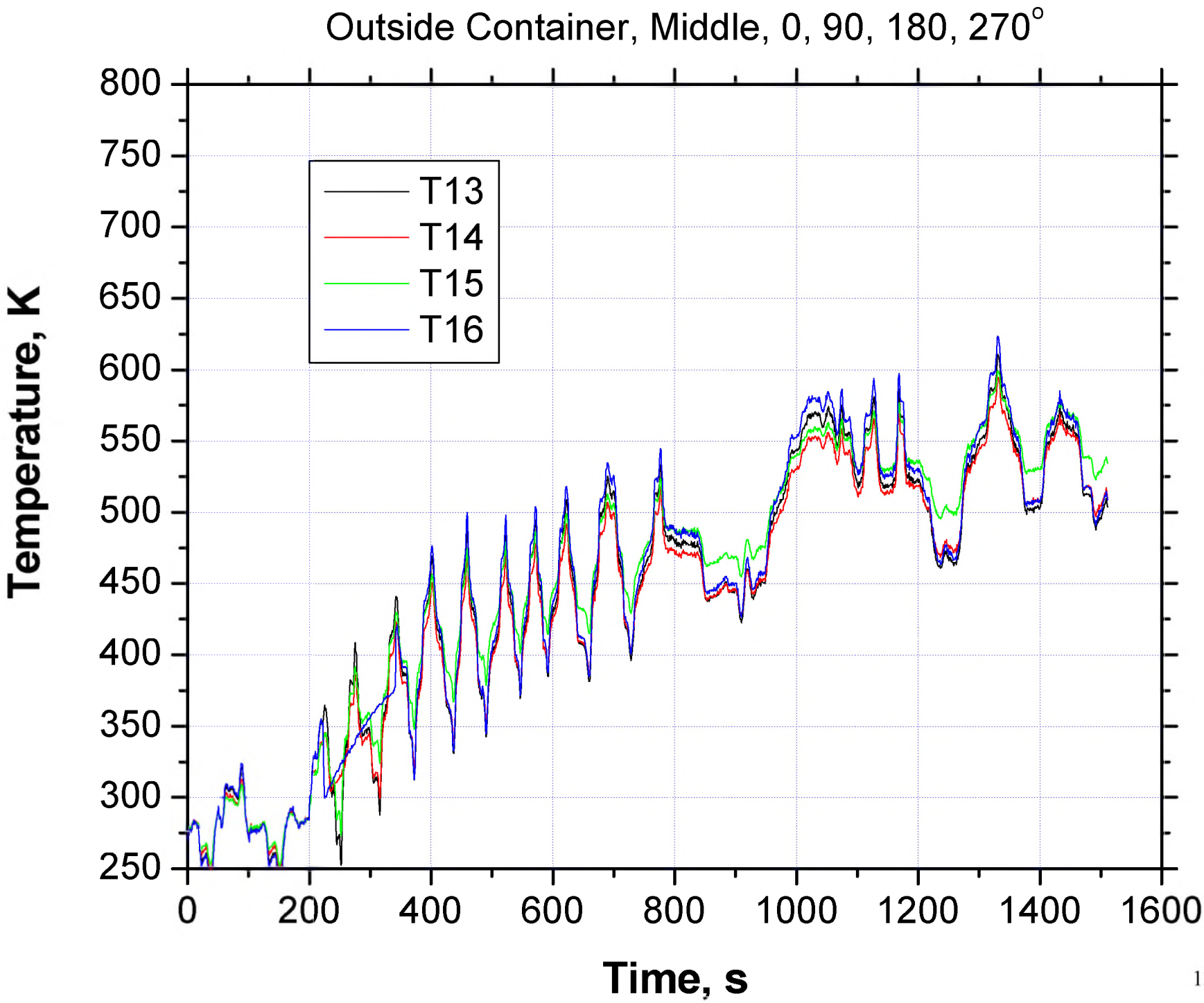
Outside Container, Middle, 0, 90, 180, 270°
Temperature, K
Time, s
T13
T14
T15
T16
800
750
700
650
600
550
500
450
400
350
300
250
0
200
400
600
800
1000
1200
1400
1600

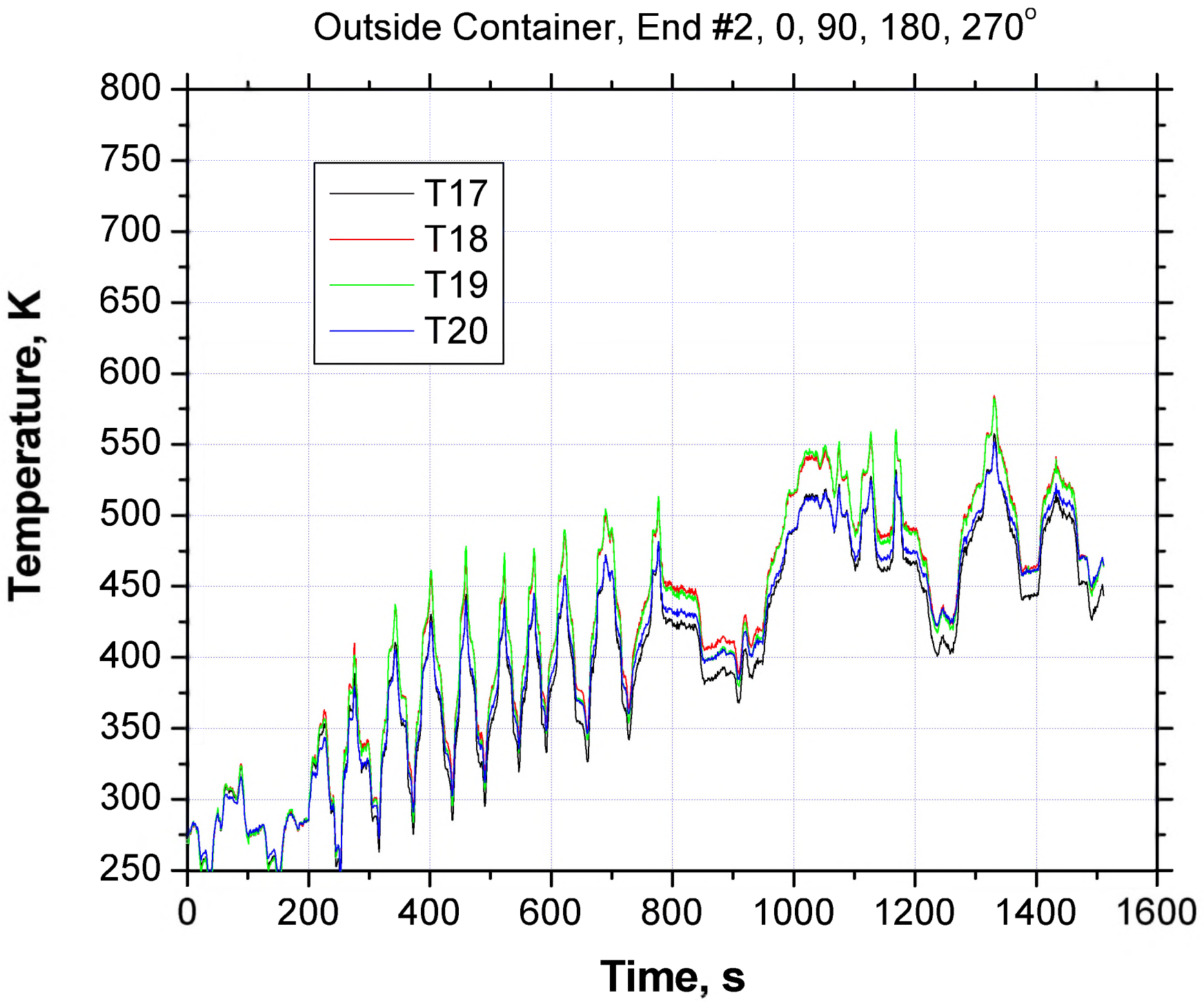
Outside Container, End #2, 0, 90, 180, 270°
T17
T18
T19
T20
Temperature, K
Time, s
800
750
700
650
600
550
500
450
400
350
300
250
0
200
400
600
800
1000
1200
1400
1600

PLOTS, TEST 10, ELECTRICAL, NOVEMBER 2002

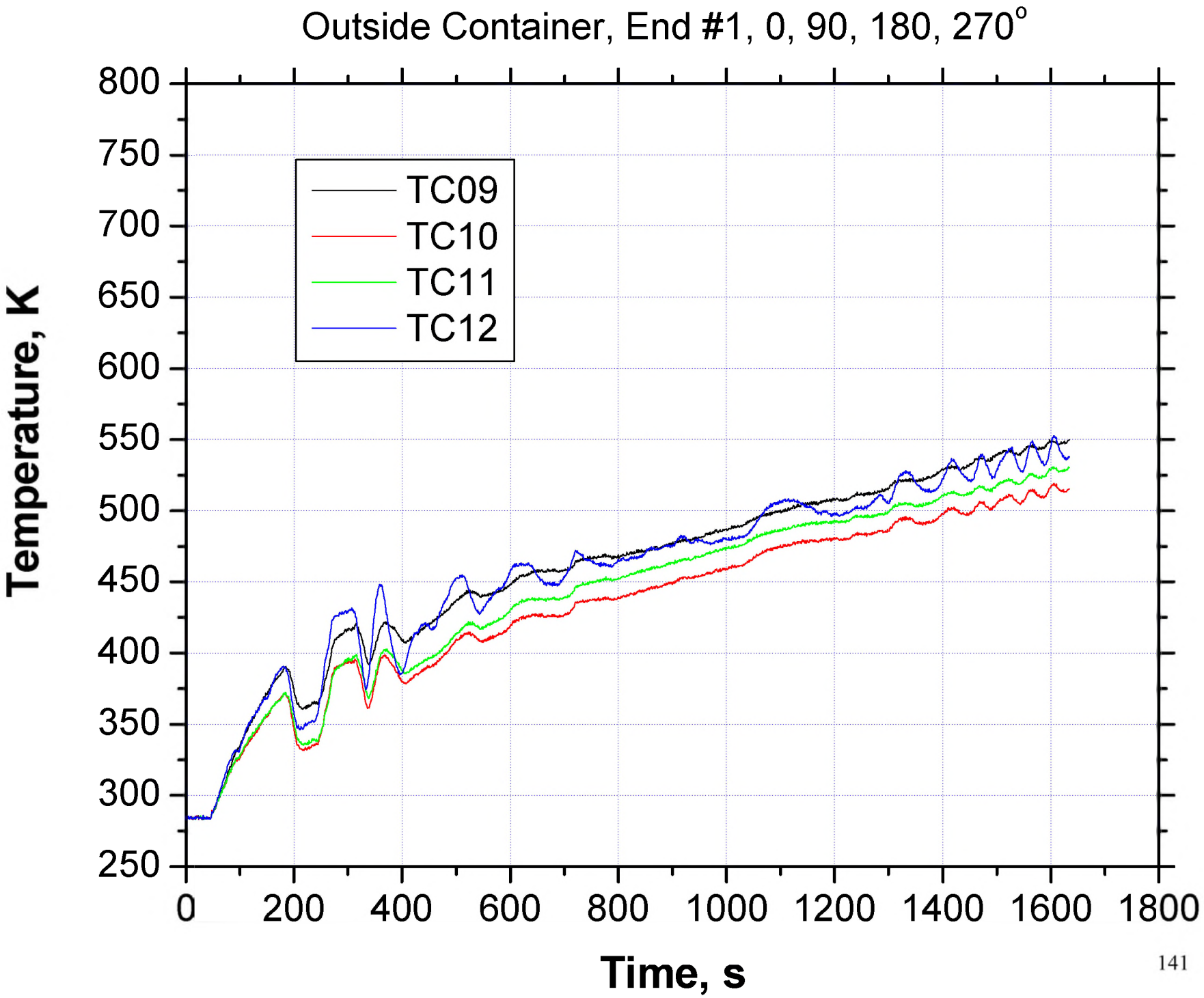
Outside Container, End #1, 0, 90, 180, 270°
TC09
TC10
TC11
TC12
Temperature, K
Time, s
800
750
700
650
600
550
500
450
400
350
300
250
0
200
400
600
800
1000
1200
1400
1600
1800

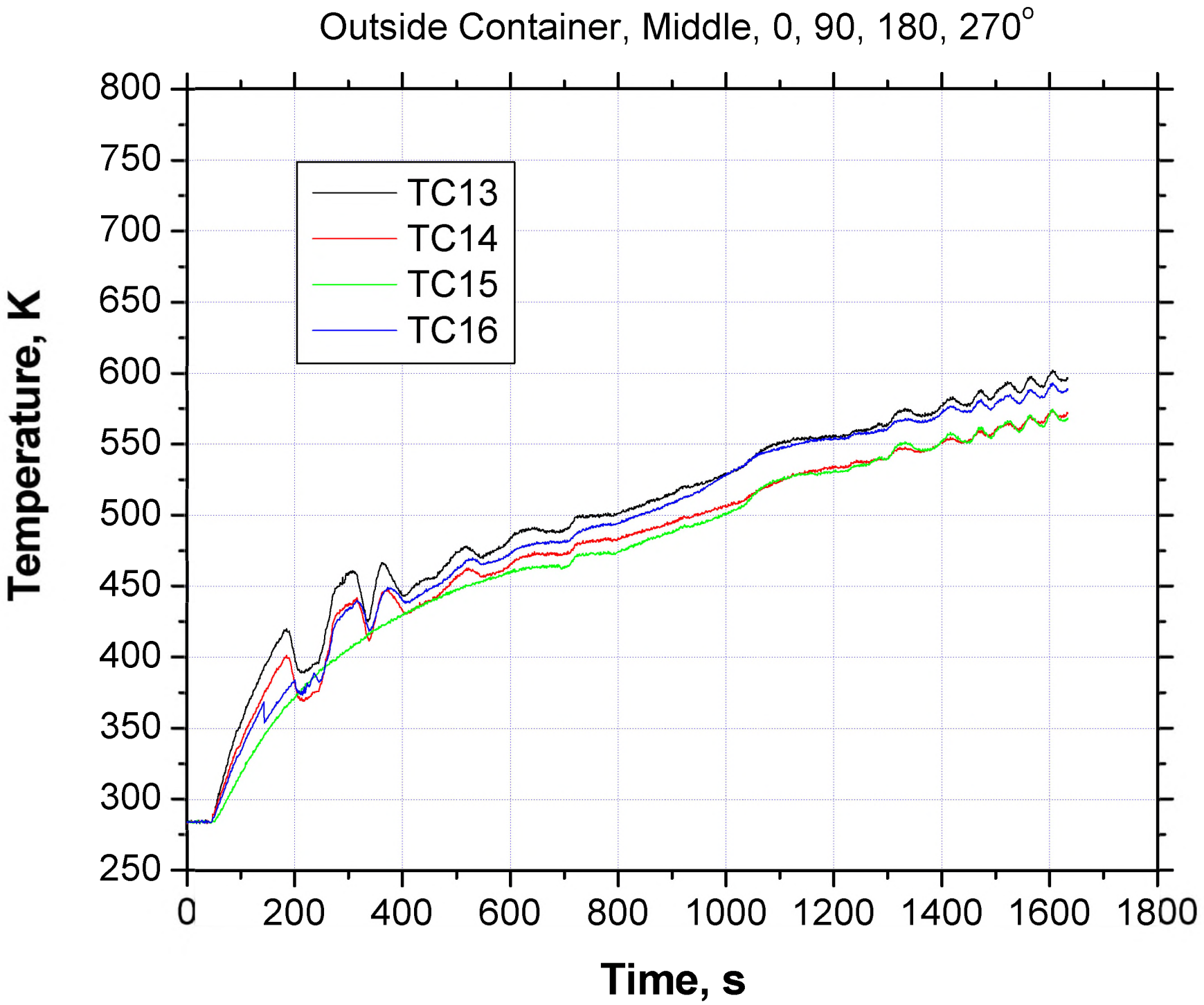
Outside Container, Middle, 0, 90, 180, 270°
TC13
TC14
TC15
TC16
Temperature, K
Time, s
800
750
700
650
600
550
500
450
400
350
300
250
0
200
400
600
800
1000
1200
1400
1600
1800

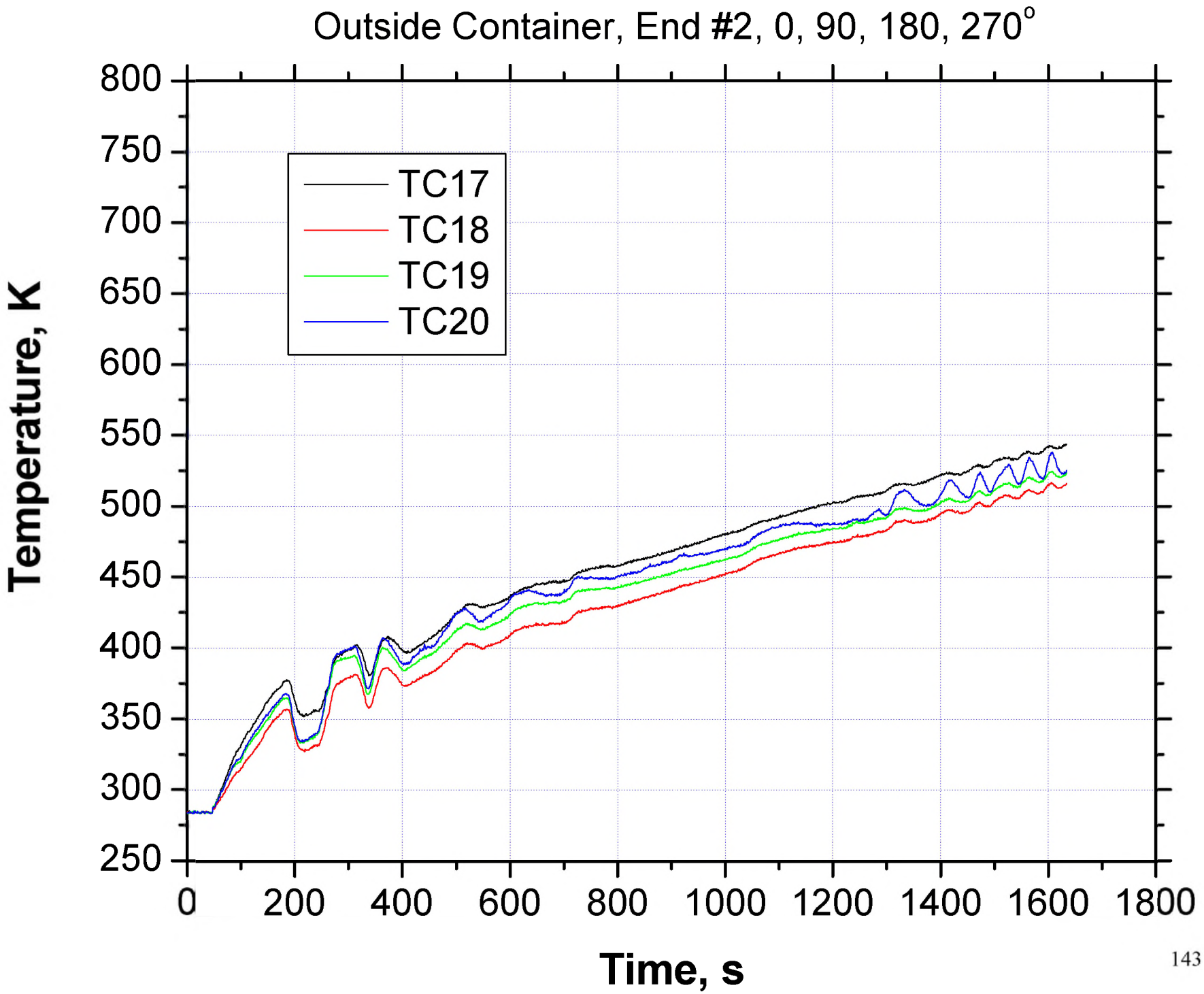
Outside Container, End #2, 0, 90, 180, 270°
TC17
TC18
TC19
TC20
Temperature, K
Time, s
800
750
700
650
600
550
500
450
400
350
300
250
0
200
400
600
800
1000
1200
1400
1600
1800